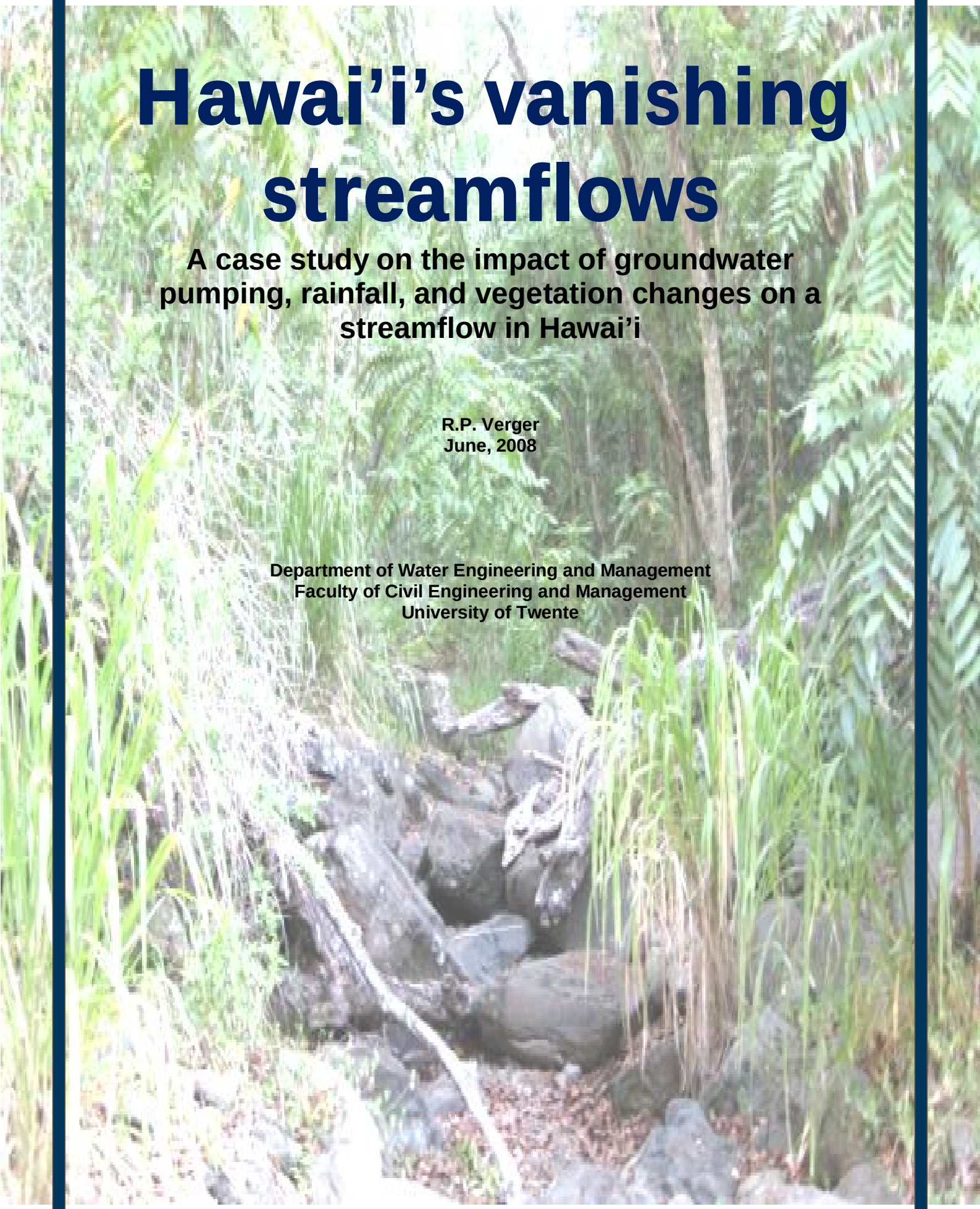

Hawai'i's vanishing streamflows

A case study on the impact of groundwater pumping, rainfall, and vegetation changes on a streamflow in Hawai'i

R.P. Verger

June, 2008

Department of Water Engineering and Management
Faculty of Civil Engineering and Management
University of Twente

Hawai'i's vanishing streamflows

Document:	M. Sc. thesis
Date:	June 18, 2008
Assigned by:	University of Twente Department of Water Engineering and Management (WEM)
In association with:	University of Hawai'i at Mānoa Department of Natural Resources and Environmental Management (NREM)
Author:	R.P.Verger
Graduation Committee:	Dr. ir. D.C.M. Augustijn (University of Twente) Dr. ir. M.J. Booij (University of Twente)
External advisor:	Assoc. Professor Dr. A. Fares (University Hawai'i at Mānoa)

Preface

Writing this report was an effort which took 7.5 months. During this period I have learnt too many things to mention here, but at least I have to be very grateful to those people who contributed directly and indirectly to this work. First, I want to thank all my advisors from Hawai'i and the Netherlands. Thank you, Dr. Fares, for accepting me as an exchange visitor's student to the University of Hawai'i and for giving me this great opportunity. I am also very grateful to my Dutch advisors, Mr. Augustijn and Mr. Booij, who assigned me in first instance this project. They provided me with very useful help and extensive comments during the whole process and of course for their patient during sometimes difficult times.

My time spending in Hawai'i would not have been so nice and instructive without the people working at the Hydrology Lab. It was such a great experience hiking with Tran through Mākaha Valley. The useful discussions, provided help, and moreover, a very nice time I had with Sanjit, Safeeq, Amjad, Alan, Dr. Abbas, and Samira as my colleagues, are things I will always remember when I look back to this period.

Finally, I like to thank my family (dad, mom, brother) who are always supportive to me in whatever I do. The fact that we are together as a family during my graduation ceremony in good health is the most precious thing. Thank you my friends (Remco, Thomas), (former) flat mates and people from the afstudeerkamer for such a nice time during all these years. Noëlle, thank you so much for just being you.

Robert Verger

Enschede
June, 2008

Summary

An important component of Hawaiian water resources is drinking water obtained from groundwater. For Hawai'i groundwater accounts 45% of the state's water needs and 99% of its drinking water. Due to increasing water needs, trends in rainfall, and changes in vegetation, groundwater storages are decreasing. These causes are believed to be the reason for the long term downward trend in base flow of Hawaiian streams in several islands resulting in dry streams. More research is required to determine the exact causes for the observed trends in streamflow and groundwater resources. Therefore, a case study was setup to study the reduction of streamflow in Mākaha Valley (Fares et al., 2004). The objective of this study is to investigate the impact of groundwater pumping, decreasing rainfall, and vegetation changes on streamflow in a subwatershed of Mākaha Valley. This is done by 1) investigating the spatial distribution of infiltration rates across the study area, and 2) assessing an integral watershed model in describing streamflow of the watershed.

The infiltration rate is often an important parameter in hydrological modeling since it determines the division between runoff and drainage into a soil profile. It is often constitutes a highly uncertain variable across a watershed. The large spatial variability makes it difficult to quantify. A tension infiltrometer was used to measure saturated hydraulic conductivity which provides an indication for infiltration under saturated conditions. Saturated hydraulic conductivity is an important input parameter for hydrological models. In addition, soil core samples were taken to calculate dry bulk density and porosity to provide supportive data concerning soil hydraulic properties. Conventional statistics and geostatistics were used to determine and analyze the spatial distribution of saturated hydraulic conductivity. Conventional statistics comprised descriptive statistics, analysis of variances (ANOVA), and linear correlation. Geostatistics implied calculating semivariances for possible geospatial interpolation.

Results showed a very large variability in values of saturated hydraulic conductivity, very low values of dry bulk density, and high values for porosity. A lognormal distribution has been confirmed for saturated hydraulic conductivity, which was required for ANOVA. ANOVA was applied to topographical characteristics. Only the observed distinction between stream, on ridges, and in gulches to appeared to have significant different means for saturated hydraulic conductivity. Dry bulk density showed significantly different means for different elevations and between hydrologic soil groups. Porosity also showed a significant difference between areas nearby the stream, on ridge, and in gulches. Pair wise comparison of means (Fisher's LSD) for significant ANOVA showed a significantly different mean for saturated hydraulic conductivity and porosity between stream and gulch. Dry bulk density showed a significantly different mean for elevations lower than 525 m and higher than 525 m. No correlations were found between saturated hydraulic conductivity and other variables which implied that geospatial interpolation by cokriging is not relevant.

Semivariogram analysis showed that there is no spatial correlation for saturated hydraulic conductivity confirming that geospatial interpolation is irrelevant.

By combining results from ANOVA and Fisher's LSD, a spatial distribution of saturated hydraulic conductivity was obtained. Based on these results a spatial map of saturated hydraulic conductivity was constructed by dividing the subwatershed in three topographical areas: stream area, ridges, and gulches. A GIS extraction method was used to extract these three topographical elements out of the study area. From observations, slope and flow accumulation were appropriate indicators to distinguish stream areas, ridges, and gulches in the Mākaha Valley. It should be noted that this method only provides an indication of ranges in which saturated hydraulic conductivity can vary at a particular location in the study area. It relies on accuracy of available and aggregated GIS data. This method can be expanded when other field data in relation with other topographical data are available. When using this map as a model input map, mean values from Fisher's LSD of saturated hydraulic conductivities should be taken as indicators.

In the second part of this study, the Distributed Hydrological Vegetation Model (DHSVM) was used to study the effects of groundwater pumping, rainfall, and vegetation changes on streamflow. A modified version was used to deal with a geological framework. This model requires meteorological data, a digital elevation model (DEM), a watershed boundary, a flow network, terrain shadowing, percent open sky, vegetation data, soil (depth)data, and geological data. For soil data, the spatial distributed map of saturated hydraulic conductivity can possibly be used as model input data. Finally, observed stream gage data were used for calibration and validation.

Calibration was done by first determining the parameters for which streamflow was most sensitive. Streamflow appeared to be sensitive to some soil parameters and geology parameters but not for saturated hydraulic conductivity as first was expected. Two calibration methods were used: univariate calibration and a multi/bivariate calibration. Univariate calibration was conducted by adjusting iteratively soil depth, base layer conductivity, and maximum infiltration rate until a good model performance was obtained. Model performance did not improve by varying lateral hydraulic conductivity and its exponential decrease when soil depth and base layer conductivity were optimized. Univariate calibration provided a reasonable model performance. Multi/bivariate calibration was performed by finding the optimal value between lateral hydraulic conductivity and exponential decrease of depth. A slightly better model performance was obtained here. Results of univariate calibration seemed more representative for Mākaha streamflow because there was no baseflow flowing. However, model performance was less good. Both calibrations did not show a clear solution for finding an optimal way to calibrate DHSVM due to likely interdependency between parameters and uncertainty in groundwater storages. Validation was done by using both calibrations and provided for another year for both calibrations poor model performance.

By using the best model performance from bivariate calibration results (no pumping) for the calibration period, a scenario analysis was performed to determine the impact of groundwater pumping, changing rainfall, and vegetation changes on streamflow. To illustrate a significant effect on streamflow, base layer conductivity was varied so that deep losses to groundwater were simulated equally to mean and maximum values of

groundwater pumping. Only during high pumping, both peakflow and baseflow become very sensitive to this change. This groundwater abstraction term confirmed that groundwater pumping likely has an impact on streamflow. Although the uncertainty in groundwater storages still must be resolved. No rainfall trends were available, but decreasing and increasing hourly rainfall data with 15% showed that large sensitivity was only noticeable in peakflows. Groundwater storages were likely less affected, and subsequently, baseflow too. By changing vegetation into all bare landcover or evergreen forest, almost no sensitivity was found for change in streamflow. However, both scenarios increased evapotranspiration. This is common for evergreen forest. In case of bare landcover, DHSVM probably increased evaporation when the soil water content is near saturation. From this study it can be concluded that only groundwater pumping influences baseflow and changed rainfall only contributed to a change in peakflow. Changes in vegetation or land cover have little effect on streamflow. DHSVM is a suitable hydrological model when there are sufficient data available (geological) and an integrated watershed approach is desired.

Future research should focus on verification of high values of saturated hydraulic conductivity by using different field methods. Taking measurements at the restricted upper part of the study area would be useful because of a different soil type and expected higher conductivities. Also the possible correlation between vegetation and infiltration rates should be studied further. Model performance can be improved by further optimizing the calibration parameters. This involves studying the interdependency of parameters which have an impact on streamflow. Decreasing lack of geological field data, which limited initial calibration and verification due to expansion of the modified model, should also contribute to a better model performance. This possibly implies gaining geological data regarding water tables and the temporal impact of groundwater pumping by using hourly or daily pumping data. To determine the impact of groundwater pumping and changing rainfall, it would be useful to study these factors in a more detailed manner related to streamflow. Using a groundwater model, which can deal with this complex type of geology subject to groundwater abstraction, can provide more insight in the uncertainty of groundwater storages in the Mākaha Valley. Further studying rainfall trends to provide a more detailed scenario analysis gives more information about the impact of changing rainfall on streamflow. Although streamflow was not sensitive to vegetation changes, a proper evapotranspiration simulation by studying vegetation parameters is still necessary. Rainfall interception by vegetation is an example of an important process related to evapotranspiration and the total water balance.

Abbrevations

ANOVA	Analyses of Variances
DEM	Digital Elevation Model
DHSVM	Distributed Hydrological Soil Vegetation Model
DR	Double Ring infiltrometer
GIS	Geographical Information System
HBWS	Honolulu Board of Water Supply
LSD	Least Significant Difference
NOAA	National Oceanic and Atmosperic Association
NRCS	Natural Resources Conservation Service
NS	Nash-Sutcliff coefficient
RE	Relative Volume Error
TI	Tension Infiltrometer
USDA	U.S. Department of Agriculture
USDI	U.S. Department of Interior
USGS	U.S. Geological Survey
Y	Multi-objective function

Contents

Chapter 1
Introduction

1.1 Hawaiian water resources

Water resource supplies are subject to continuous changes by both natural causes and by human interventions. This includes, among others, alterations in trends of climate and land use changes. Water resource supplies primarily depend on climate. Land use, subject to deforestation, affects the water resource supplies indirectly by changing the distribution of infiltration, runoff, and evapotranspiration. This affects the water resource supply for several purposes such as groundwater abstraction, industry, and agriculture.

When it concerns Hawai'i's water resources, it is not differently. Hawai'i is concerned with a high degree of spatial and temporal variability in both climate and land use, and this is believed to have an impact on water resources in Hawai'i. The water resource supplies are under pressure, as there are experienced more cycles of droughts (Fares et al., 2004). Dynamic changes in land use are a result of cultivation of the agricultural sector, impact of mass tourism, and urbanization, and these involve more pressure by increasing water needs. This is further complicated by change in vegetation due to proliferation of invasive species that represents a great threat to the integrity of Hawai'i's small island tropical ecosystem. Effects of invasive plant species on water supplies have received attention, because the macro-scale effects of invasive plant species on reduced available water resource supplies have been documented (Mair et al., 2007). These alterations in climate and land use are possibly resulting in a degradation of the supply of Hawaiian water resources.

One important component of a Hawaiian water resource is drinking water obtained from groundwater abstraction. For Hawai'i, groundwater accounts for 45% of the state's water needs and 99% of its drinking water (Gringerich and Oki, 2000). Water resource supplies subject to groundwater abstraction, downward trend in rainfall, and change in vegetation, are believed to cause limited water supplies and decreasing groundwater storages. This will cause serious challenges for satisfying demands for drinking water and are believed to have an impact on long term downward trend in base flow of Hawaiian streams in several islands resulting in dry streams (Oki, 2004). Dry streamflow is believed to reflect decreasing groundwater storages and is necessary to study.

Much research is required to determine physical impacts causing dry streamflow to keep the Hawaiian drinking water market sustainable. The high degree of spatial and temporal variability of climate and land characteristics in Hawai'i makes it more difficult to study this problem so that an integrated watershed approach is essential to successfully manage the solution of decreasing streamflow. Therefore, solid scientific tools and

environmentally sustainable technologies are necessary for predicting and determining the impacts on streamflow in Hawaiian watersheds.

Figure 1.1 Impression of Mākaha stream during dry and wet days

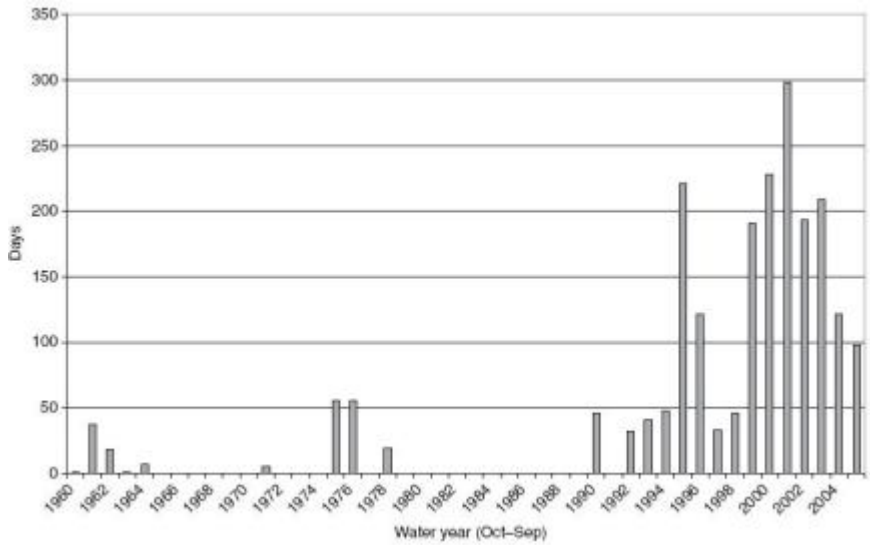

Figure 1.2 Total number of annual dry stream days (i.e., mean daily flow equal to zero) for the period 1960-2005 (Mair et al., 2007)

1.2 Case study: Mākaha Valley, O'ahu

Concerning declining trends in streamflow as a result of groundwater abstraction, changes in rainfall, and vegetation, Mākaha Valley is a representative example (Figure 1.1). Since the early 1800's, the Mākaha Valley has experienced significant changes which include the cultivation of sugarcane, installation of groundwater pumps, shafts, tunnels, and the construction of two 18-hole golf courses. The likely effect of groundwater pumping on streamflow began in 1945 by the construction of a 1,280-m long tunnel, known as the Glover Tunnel, in the mid-valley for sugarcane irrigation purposes. Since 1948, water from the tunnel was used for domestic and irrigation needs. Effects of groundwater pumping are believed to have a decreasing effect on streamflow the past 46 years of record with an

increase in the number of dry stream days per year, i.e., no flowing water in the stream at the stream gage (Figure 1.2). Changes in rainfall and the proliferation of invasive species were also anecdotal detected is this area (Mair et al., 2007). In addition to groundwater pumping, also the effects of rainfall and changing vegetation on streamflow should be determined.

Therefore, the Mohala group was initially formed in 1999, which was partially concerned with the restoration of the streamflow in the Mākaha Valley. The Mohala group also formed a partnership with the Honolulu Board of Water Supply (HBWS), the local water supplier, to study the effects of groundwater pumping by HBWS production wells and the spread of invasive species on streamflow. Due to lack of expertise, a project was set up in 2004 to assist Mohala and the HBWS in order to study the effects of groundwater pumping, rainfall, and vegetation changes on streamflow in Mākaha Valley (Fares et al., 2004). This project has four objectives: (1) produce detailed vegetation maps of the valley using remote sensing/GIS, depicting the spatial extent of invasive and native vegetation communities in Mākaha Valley, (2) determine the spatial-temporal variation of the different components of the hydrological cycle and their relations with streamflow in Mākaha Valley, (3) calibrate and validate a watershed model, and (4) use the model to evaluate the effect(s) of groundwater pumping, rainfall, and changing vegetation.

To these purposes, a few case studies have already been conducted to contribute to the main project. Harman (2004) determined by remote sensing the degree of infestation of invasive species in Mākaha Valley to support native species conservation and sustainable land management. It required assessment of the spatial distribution of invasive species by generating a vegetation map which assessed the degree of native species taken over by invasive plant species. Mair et al. (2007) studied the effects of rainfall and groundwater pumping on streamflow of Mākaha Valley, O'ahu. They reported statistical decline of streamflow between two periods of pre-pumping and pumping. Trends of rainfall decline and its effect on Mākaha stream's base flow reduction are not clear yet.

Further study is needed to assess the effect of groundwater pumping, changes in rainfall, and vegetation changes on streamflow by further characterizing the hydrologic cycle with respect to rainfall, infiltration, and groundwater recharge.

1.3 Objectives

The objective of this study is in line with the objective of the main project:

Investigating the impact of groundwater pumping, changes in rainfall, and vegetation changes on streamflow in Mākaha Valley.

This objective addresses some components of the second and third objectives of the main project and is divided in two parts:

1. Assessing an integral watershed model in describing streamflow of the watershed and determine the effects attributes of changes on streamflow;
2. Investigating the spatial distribution of the infiltration rates across the study area;

The integral watershed model should be able to model several components of the hydrologic cycle in the Mākaha Valley. For this study the Distributed Hydrological Soil Vegetation Model (DHSVM) was chosen (Wigmosta et al., 1994). The model will be used to determine

the effect(s) of changing groundwater pumping, changes in rainfall, and vegetation changes on streamflow on a highly detailed level and infinite range. This is required because of the highly spatial and temporal variability of climate and hydrological processes in the study area. Gaining knowledge regarding these two components, a partial solution to the restoration of the Mākaha streamflow is provided.

Infiltration is a key process of a water budget within a watershed and can be determined in various ways by field measurements. This may yield a better understanding of spatial variation of soil - water interaction across the watershed and is often an important input parameter for hydrological modeling.

1.4 Outline of the report

This study is divided in two. In chapter two the infiltration study is described by which the spatial distribution of infiltration for Mākaha Valley was determined for modeling input. Chapter three comprises the assessment of the integral watershed model (DHSVM) in describing streamflow of the watershed. The final chapter 4 summarizes all conclusions drawn in the previous chapters and will discuss the contribution of this study to the objective.

Chapter 2

Spatial variability of infiltration in Mākaha Valley

2.1 Introduction

2.1.1 Infiltration process and factors

Infiltration is one of the most important processes which control the amount of water over large areas in the hydrological cycle (Casanova, 2000). Infiltration is generally defined as the process by which the soil surface water drains into the soil profile (Figure 2.1). It is of major importance, because it often controls water budgets for irrigation systems in the agriculture, and runoff to a stream. This imposes that infiltration determines how much water drains into the unsaturated zone and/or will likely run off to a stream flow and this is important for determining the water balance over large areas. Within the hydrological cycle infiltration and evapotranspiration are the most important processes which control the water balance over large areas (Casanova, 2000). In addition, infiltration is the most sensitive variable in many models for predicting streamflow when excess rainfall is occurring (Singh and Woolhiser, 1976).

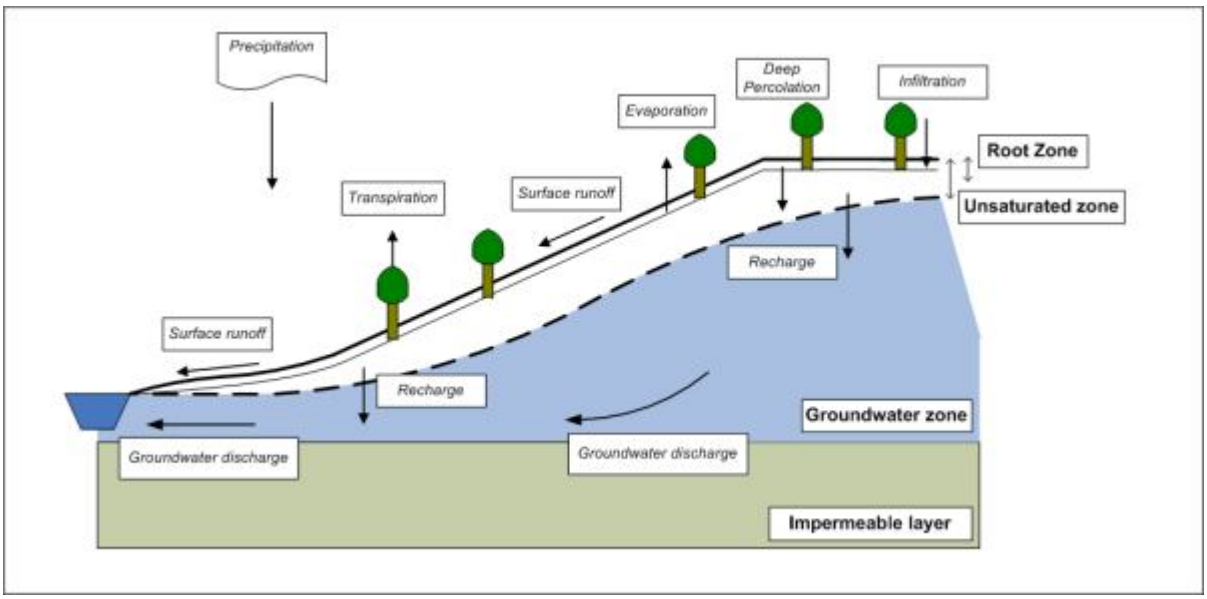

Figure 2.1 General conceptual water balance in a mountainous area

Many factors are influencing the infiltration rate. Infiltration is directly dependent on soil properties, and indirectly by evapotranspiration through its effect on the initial soil

water status and vice versa (Sharma et al., 1980). Likewise microclimatic properties, biological activities, and topographical aspects as slope, aspect, elevation, and land use / vegetation are important determinant factors for infiltration, because of their influence on soil properties (Mahler et al., 1979; Sullivan et al., 1996; Sauer and Logsdon, 1999). These aspects are also causing large variability of infiltration within short distances which means that it is difficult to quantify spatial variations of infiltration (Achouri and Gifford, 1984; Machiwal et al., 2005). For example by the presence of fine-textured soils, which are often found in the lower parts of slopes, areas have little water intake rates and higher runoff potential. Luk et al. (1993) showed that infiltration was significantly reduced on gentle slopes due to preferential development of surface crusting and sealing. Normally assumed for gentle slopes, is that infiltration and slope are inversely related under non-crusted conditions (Li et al., 1995). Hanna et al. (1982) found that the available water content was usually larger in soils on the north-facing slope than in soils on the south-facing slope in south-east Nebraska. This explains the difference in infiltration rates because of different soil water content and different evapotranspiration rates on north-facing slopes and south-facing slopes.

2.1.2 Quantifying infiltration

As previously outlined, many factors are influencing infiltration and cause large spatial variability of infiltration. Various methods in order to quantify spatial variations of infiltration are available for different scales depending on the objective. Scales vary from small agricultural plots to large watersheds. Three methods to determine spatial variability of infiltration over large areas were considered. These were scaling of soil–water properties based on the concept of similar media, expressing spatial variability by general statistics, and by geospatial techniques.

Scaling to the concept of similar media

Describing infiltration over large areas by scaling requires an infiltration model and allocation of same properties to similar media, i.e., scaling according to the concept of similar media (Sharma et al., 1980; Green et al., 1982; Sullivan et al., 1996; Machiwal et al., 2005). The advantage of the scaling theory lies in its potential to express spatial variability in terms of a single physically-based parameter. For example, by using Philips infiltration model where two constant parameters *S* (sorptivity) and *K* (hydraulic conductivity) at several locations are determined (Sharma et al., 1980). Subsequently, *S* and *K* are scaled by two dimensionless scaling parameters a_S and a_K and an optimal infiltration curve is obtained. A limitation regarding this method is that uncultivated and natural soils in a rugged watershed usually do not satisfy the strict similar-media requirements, and that theory may have to be applied in an approximate form (Sharma et al., 1980). Concluding, this method is less suited for an uncultivated watershed with highly variable aspects as vegetation, soil type, and topographical aspects.

Expressing spatial variability by general statistics

Because of possible large variability of infiltration, general statistical techniques are sometimes considered. In general, conventional statistics already provide an indication of spatial variability of infiltration but in a lumped way. Over larger areas this can be improved

by calculating differences of infiltration rates between topographical aspects. Sauer and Logsdon (2002) determined saturated hydraulic conductivities to characterize hydraulic and physical properties of stony soils among three soil types in a small watershed. This also involved determination of soil physical properties as porosity, and dry bulk density by taking soil samples. They used analysis of variances (ANOVA) to provide spatial information regarding soil hydraulic properties. Using this method made clear that there was a clear distinctive difference between the soil types in hydraulic conductivities and infiltration rates over several locations over the watershed. It provides a straightforward way to express differences in infiltration data at several locations.

Geospatial techniques

In this category infiltration rates are spatially distributed by using geospatial interpolation (Vieira et al., 1981; Ersahin, 2003; Haws et al., 2004). Using geospatial interpolation mostly implies the application of ordinary kriging and cokriging. Ordinary kriging uses spatial information on infiltration itself, while cokriging uses an additional correlated auxiliary variable to make estimations of an unobserved location. Before geospatial interpolation, information regarding spatial correlation data is required by calculating semivariances from infiltration data. When there is high spatial correlation and low variability in infiltration data, interpolation results are most optimal.

Vieira et al. (1981) characterized spatial variability of infiltration rates by semivariograms with 1280 measurements and concluded that observations of 50 m and less were spatially dependent and that 1280 measurements could be replaced by 128 measurements. Based on solely semivariogram analyzes, spatial dependency of infiltration rates on a large scale was determined at 200 m (Haws et al., 2004) to less than 10 m (Loague and Gander, 1990). Ersahin (2003) studied the application of ordinary kriging and cokriging to spatially interpolate infiltration rates. In this study, the auxiliary variables also comprised soil samples of porosity and dry bulk density. Interpolation by cokriging and ordinary kriging showed reasonable results, however, test results were only obtained from relative homogeneous soils. Cokriging only provided better results when the auxiliary variable was oversampled so that it can provide sufficient supportive data.

In previous studies, geospatial techniques have shown many benefits and offer relatively simple techniques. Calculating semivariograms are convenient methods to describe spatial correlation of infiltration data. Obtaining soil data as dry bulk density and porosity are possibly correlated with infiltration so that it provides additional information for soil hydraulic properties and usage for cokriging. However, geospatial interpolation of infiltration requires large amount of measurements and are because of the large spatial variability sometimes not applicable.

2.1.3 Field measurements

As previous techniques illustrated, it is often necessary to obtain infiltration data from field measurements. Field instruments for this usually determine infiltration by using steady state infiltration rates and/or (saturated) hydraulic conductivities. Saturated hydraulic conductivities (K_{sat}) are often measured as an indicator for infiltration and required by models as input parameter on which infiltration rates are based on (Singh and Woolhiser, 1976; Sullivan et al., 1996; Sauer and Logsdon, 2002).

2.1.4 Hawaiian case studies

Specific systematic studies for Hawaiian watersheds are limited regarding this topic in combination with field measurements. Green et al. (1982) conducted field measurements in order to characterize infiltration rates for typical Hawaiian soils. Statistical analysis suggested here that soil maps of Central O'ahu would not be particular useful in delineating soil areas of relative homogeneity with respect to hydrological properties, because of large variability in infiltration. This emphasizes the need for a new method to characterize soil hydraulic properties of importance such as K_{sat}. Now, delineated soil areas and estimates of K_{sat} are available for Mākaha Valley (USDA-NRCS, 2005) (Appendix A). However these are very rough estimates and are likely not representing the spatial distribution accurately (Mair 2007, personal communication). Given the difficulty in accurately estimating spatial distribution in K_{sat} and the importance of this parameter for model studies and infiltration in general, the spatial distribution of K_{sat} in Mākaha Valley will be further studied.

2.1.5 Objectives

The objective of this chapter is to determine the spatial variability of saturated hydraulic conductivity by: (1) conducting field tests in Mākaha watershed, (2) determining the saturated hydraulic conductivity, dry bulk density, and porosity from field data, (3) evaluating the field data by using conventional statistics, and geostatistics, and finally, (4) constructing the most representative spatial distribution of K_{sat} in Mākaha Valley.

2.2 Study area

This study is concerned with a watershed on the Hawaiian Island, O'ahu. In general, Hawaiian Islands are characterized by a large number of small and steep watersheds with highly permeable volcanic rocks and soils. Rainfall is strongly spatial and temporally variable resulting from a combination of both the location within the island (leeward vs. windward) and altitude. It can be higher than 5,000 mm in wet locations and lower than 250 mm per year in arid places. Each island has several small streams running directly from the mountains to the coastlines. Each of these streams is affected by the land use through which it passes.

This study area concerns Mākaha Valley which is located on the leeward coast (west) of the island of O'ahu, Hawai'i. Mākaha Valley encompasses a total area of 24.6 km^2. The HBWS owns the conversation land and manages six groundwater wells in the valley. The upper valley has been subject to human impact since the early Hawaiians established in the 1400's. Topography of the Valley is rugged and varies from sea level to the top of Mt. Ka'ala at 1,226 m (USDI-USGS, 1998a, 1998b, 1999). The lower to mid-valley areas are home to most of Mākaha's 8,000 residents (Key to the City, 2004). Two 18-hole golf courses are located in the mid-valley area. The upper valley is undeveloped and forms the Mākaha Valley subwatershed and comprises 5.5 km^2 (Figure 2.2 and 2.3). The subwatershed delineation is based on the location of the valley's lowest United States Geological Survey (USGS) stream gage and encompasses the initial area of interest. From the six groundwater wells, three are located in the subwatershed. Land use / land cover varies across the valley from high / low intensity development in the lower valley to a dry evergreen forest in the upper valley

(Figure 2.4). As a result of land use changes, only little native forest remains in Mākaha. Now, the vegetation tends to become a heterogeneous mosaic composed of various types of invasive secondary forest as Schinus Terebinthifolius, Psidium Cattleianum, and Coffea Arabica (Harman, 2004).

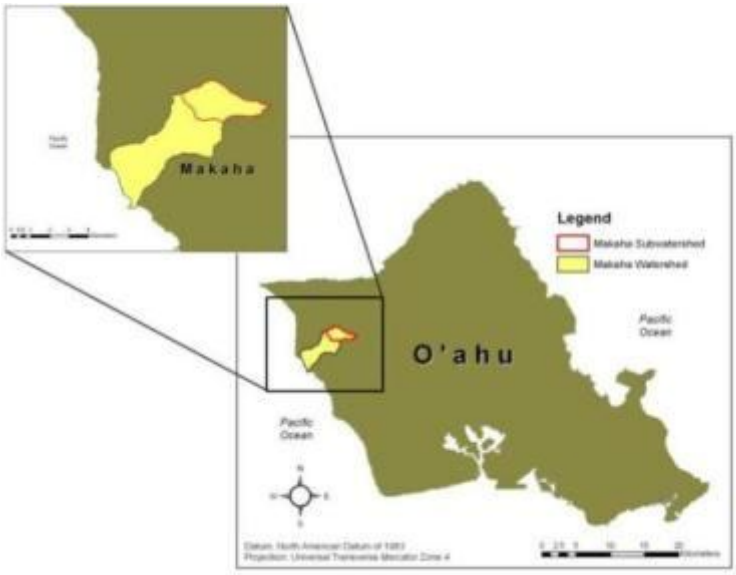

Figure 2.2 Location of Mākaha Valley watershed on the **Hawaiian island O'ahu**

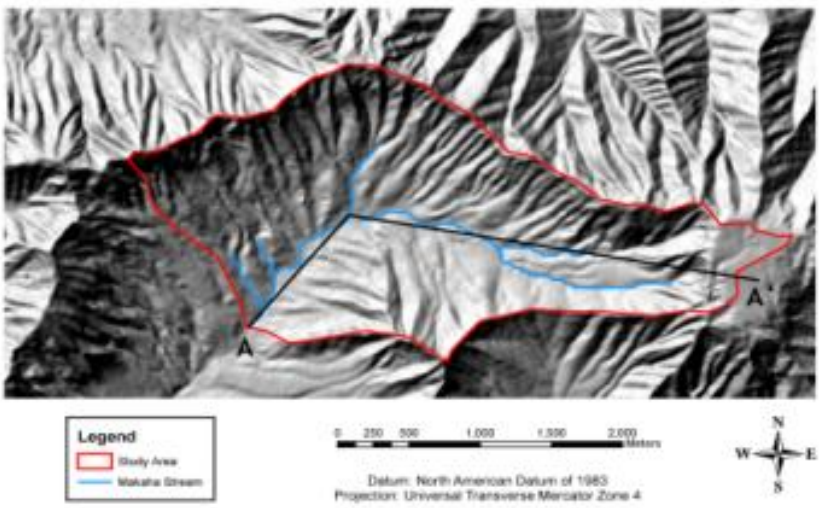

Figure 2.3 Study area perimeter of the subwatershed of Mākaha Valley

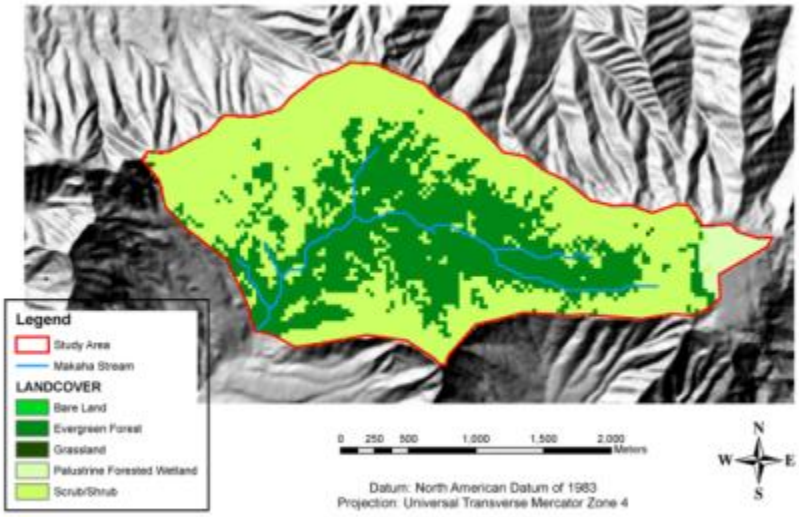

Figure 2.4 Landcover map for the subwatershed of Mākaha Valley (NOAA, 2001).

Rainfall is largely dictated by topography. About 40% of the valley receives more than 1,000 mm of rain a year (Mink, 1978). The greatest amount occurs near Mt. Ka‘ala (over 2,000 mm annually) and the least near the coast (Giambelluca et al., 1986). A small but unknown amount of recharge is contributed by fog drip intercepted by vegetation on the upper slopes of Mt. Ka‘ala. Streamflow at the outlet of the subwatershed area (elevation 296 m) is highly variable with a mean daily flow of 0.048 $m^3 s^{-1}$ and a maximum daily peak flow of 8 $m^3 s^{-1}$ (USDI-USGS 2005, unpublished report).

Figure 2.5 Impression of the deeply eroded valley in the upper part of Mākaha Valley.

Topographically, the study area consists of a deeply eroded Valley along the northwestern remnants of the Wai’anae volcano (Figure 2.5). The average slope of the subwatershed is 66%. Talus and basalt cover most of the areas along the steep valley walls and non-calcareous sediments overlie the valley floor (Mink, 1978). Soils in the study area comprises very stony clay loam (mollisol), silty loam (inceptisol), and silty clay (oxisol and ultisol) over the valley floor and southeastern ridge, while rock land and rock outcrop comprise the steep areas along the northern ridge and a portion of the southern ridge (Foote

et al., 1972). Mucky peat (histosol) comprises the soils around the wetland area at the top of Mt. Ka'ala (Figure 2.6). Infiltration rates, according to the U.S. Department of Agriculture Natural Resources Conservation Service (NRCS) hydrologic soil group, vary across the study area from higher conductivities in the lower valley and rock along the valley ridges to lower conductivities in the upper Valley (USDA-NRCS, 2007) (Figure 2.6 and 2.7). Estimations of K_{sat} are reported within ranges of 0 cm h^{-1} (Rock land) up to 45 cm h^{-1}(Mucky Peat) (Appendix A).

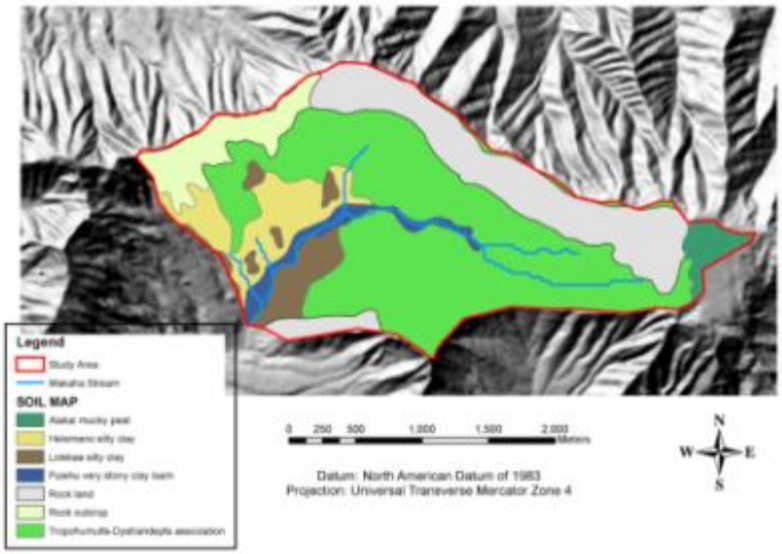

Figure 2.6 Soil map for the subwatershed of Mākaha Valley (USDA-NRCS, 2007).

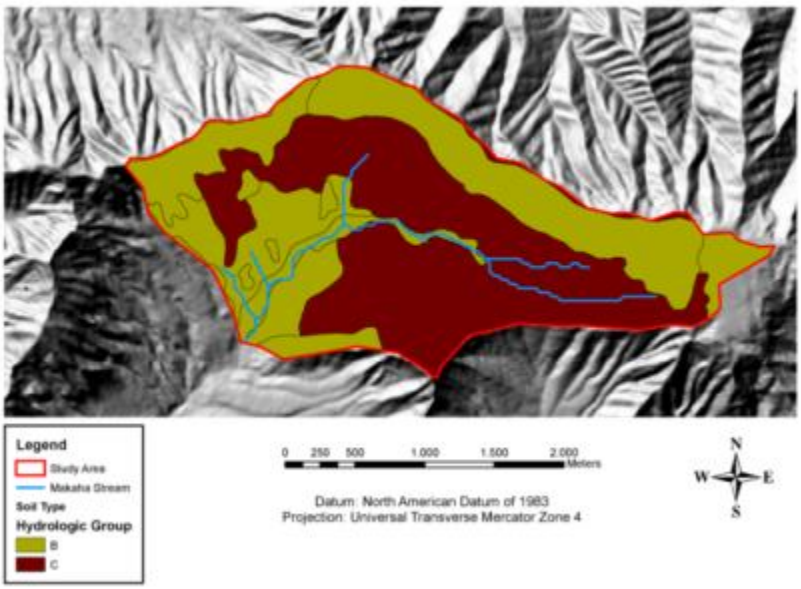

Figure 2.7 Map of conductivities expressed in hydrologic groups B and C (USDA-NRCS, 2007)

The subwatershed lies in the marginal dike sector of the rift zone with no evidence of dike complex or caldera rocks (Mink, 1978). Dikes are thin, near-vertical sheets of massive, intrusive rock that typically contain only fracture porosity and conductivity (Hunt, 1996). Deep groundwater between dikes possibly never reaches Mākaha streamflow because of unknown groundwater flows (Mair, 2007, personal communication). The composition of geology in the study area is alluvium and extends over the central portions of the Valley and is estimated to be over 10 meters thick at the center (Mink, 1978) (Figure 2.8 and 2.9). Basalt underlies the alluvium and is the source of the important high-level, marginal dike-based aquifers (Figure 2.9). Water development by HBWS in the study area has tapped into the high level, marginal dike-based aquifers. As is common in many Hawaiian streams, the upper reaches of Mākaha stream intersect the water table of the marginal dike-based aquifers allowing the stream to gain water and remain perennial in portions of the upper Valley (Mink, 1978).

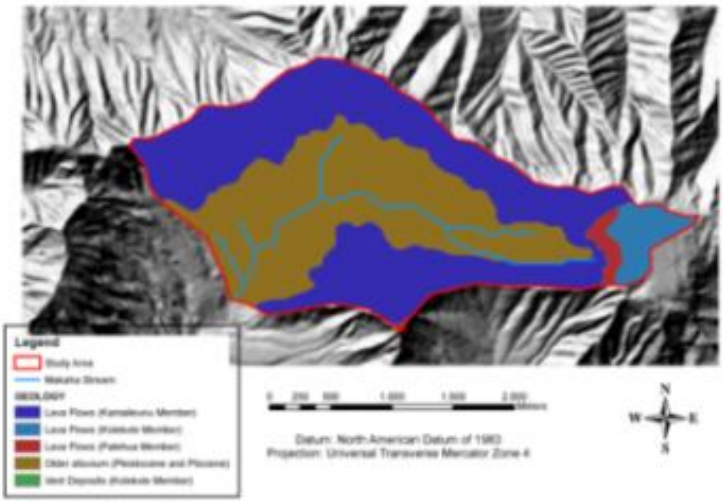

Figure 2.8 Existing geological framework map for the subwatershed of Mākaha Valley (USDI-USGS, 2007).

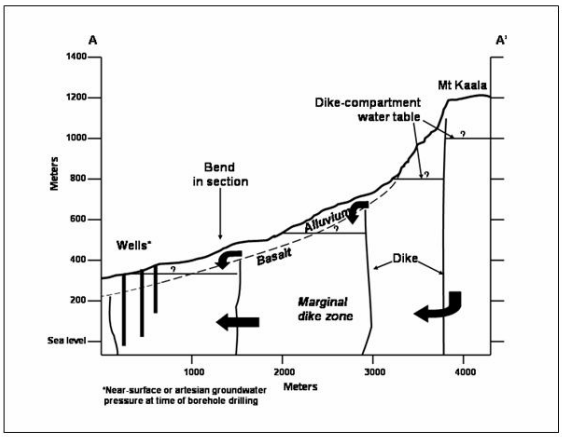

Figure 2.9 Conceptualized geologic cross section (A-A' from Figure 2.3) across the subwatershed area showing groundwater wells, marginal dike zones, and groundwater flow (Mair et al., 2007).

2.3 Material & Methods

2.3.1 Experimental site

Mair (2008) defined 18 candidate sites for hydrologic monitoring and investigation prior to this project by using a GIS-based analysis coupled with the review of high resolution satellite data. Selections were based on elevation, slope, landcover / vegetation, and soil type and have an overall representation for the study area. These sites were partially used for this field study and used for another case study (Mair, 2008). In addition, more locations were also chosen based on the same determinant topographical factors by retrieving information from GIS-analysis. This information was associated with a practical criterion, such as accessibility, considering the rugged character of the study area. Subsequently, coordinates of possible locations were obtained independently at locations with different degrees of slope and elevation, and various types of vegetation and soil. Locations of field measurements were recorded using a Garmin V GPS receiver (Garmin International Inc, USA) and yielded accuracies between 5 m and 7 m. To pursuit a sufficient number of measurements to represent the character of the study area, 54 locations were used for field measurements and taking soil samples. This amount of measurements was restricted by time and accessibility of the study area. Field measurements were conducted between the 21st of November 2007 and the 29th of January 2008.

2.3.2 Field measurements of K_{sat}

Several instruments are available and widely used to conduct infiltration tests and calculate infiltration parameters such as saturated hydraulic conductivity (K_{sat}). An available double ring infiltrometers (DR) and a tension infiltrometer (TI) are useful instruments to determine K_{sat} (Sharma et al., 1980; Green et al., 1982; Sullivan et al., 1996; Sauer and Logsdon, 2002; Ersahin, 2003; Haws et al., 2004; Machiwal et al., 2006).

Angulo-Jaramillo et al., (2000) reviewed both TI and DR extensively. They concluded that both instruments have advantages of estimating relative fast and accurate in-situ soil hydraulic properties. Ersahin (2003) successfully applied DR for comparing ordinary kriging and cokriging to interpolate infiltration rates. Green et al. (1982) applied DR for Hawaiian soils, and, Haws et al. (2004) who used the DR in order to measure infiltration rates for spatial dependency on an agricultural landscape. Sullivan et al., (1996) and Sauer and Logsdon, (2002) successfully applied TI to express spatial variability of infiltration rates. Sullivan et al. (1996) provided a spatial delineated map of infiltration in a small watershed by using scaling according to the similar media concept.

Some limitations of these techniques are also noticeable. For example, the DR requires large amounts of water which is not easy for difficult accessible areas and rough terrains. Also a constant depth of water should be maintained in both rings and the volume of water infiltrated with time must be recorded during the test. For sites like Mākaha Valley, the DR is time consuming and laborious. Another drawback of the DR is the overestimation of K_{sat} due to the possible presence of highly biological activity or macrospores (cracks and wormholes). These macropores may be filled during the measurement and causes preferential flow affecting K_{sat}, which might not be representative for the soil structure (Yolcubal et al., 2002).

There are also several limitations noticeable for TI. White et al. (1992) noted that simplifying assumptions of the analysis, used to calculate soil hydraulic properties from water flow measurements, can cause errors. Infiltration rates from a TI are basically point estimates so that they represent a relative small area. Li et al. (1995) concluded that, because of the small infiltration area, lateral leakage and the absence of raindrop impact to induce soil surface sealing, the estimated infiltration rates from infiltrometers are considered to be larger than actual rain infiltration rates. Logsdon (1997) summarized criticisms of some of the assumptions used for making quick infiltration tests under negative heads and also questioned the use of quasi-steady-state infiltration rates reached in short times. On the other hand, when long-time measurements are needed to reach steady state, they are often not achievable, because the soil structure may alter due to the weight of the TI which results in changes in infiltration rate. However, TI's do have the advantage of less water consumption and better portability in difficult accessible areas like Mākaha subwatershed.

The conclusion can be drawn that both TI's and DR's are very useful to determine K_{sat}. However, for this study time and accessibility are determining factors, which means that using the DR is abandoned due to the large equipment to be carried to relative difficult accessible field locations in Mākaha Valley.

Tension infiltrometer

In this study, an available 8 cm TI (Soil Measurement Systems, Tucson, Arizona, USA) was used to conduct field tests. A TI, also called a disc infiltration permeameter, measures the steady state infiltration rates. It consists of two water towers connected with a perforated circular base plate covered with a porous nylon mesh, a bubble tower, and a water tower (Figure 2.10). The bubble tower is used to create the tension under which water is held in a column. The amount of water that infiltrates, over a specified interval of time, is measured from the water tower with the help of an attached ruler. The infiltration rates are measured by putting the soil under a negative tension, forcing the soil to suck the water from the water chamber. The area of infiltration needs to be cleared and smoothed. The base plate is placed on a thin layer of fine sand equal to the radius of the TI's plate to prevent lateral flow through the sand layer. Sand is used to establish a good contact between the infiltration surface and the TI's base plate. The water and bubble tower are filled with water. Timing begins when the bubbling begins in the bubble tower. Measurements are taken at fixed time intervals until steady state readings are obtained.

Two tension method

In order to calculate K_{sat} (cm h^{-1}), the two tension method is followed (Ankeny et al., 1991), which uses the Wooding (1968) equation. Other methods used for TI include the measurement of both initial and final soil water content, the infiltration rate at the early infiltration stage, and the steady infiltration rates measured by two instruments at two locations (Angulo-Jaramillo et al., 2000). Calculating initial water content was difficult to determine because this TI seemed not very accurate during this stage which is likely caused by the thin layer of sand under the TI. Since there was only one TI available, the two tension method was chosen. This method offers a simple and reliable method to determine $K_{sat,}$ because only two steady state rates are required.

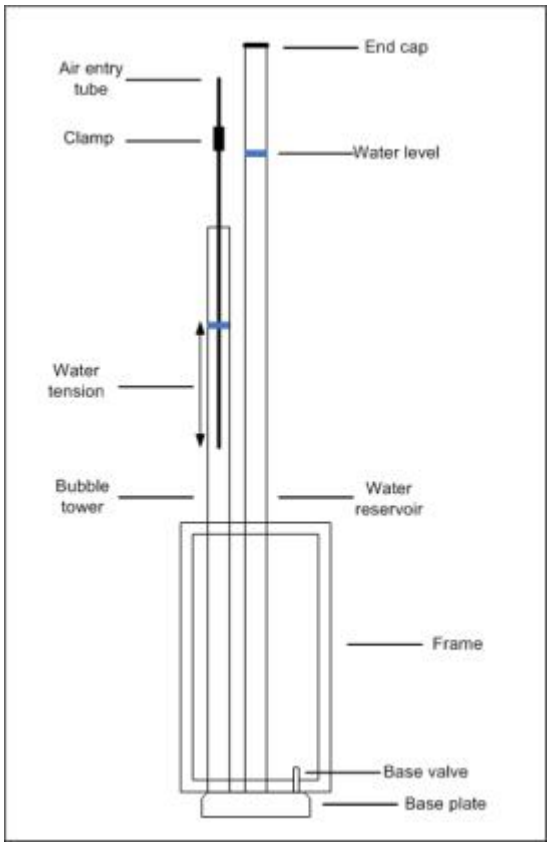

Figure 2.10 Schematic diagram of the TI (Soil Measurement Systems, Tucson, Arizona, USA).

Wooding's solution for steady-state, three-dimensional flow into the soil from a circular source is the basis for unsaturated hydraulic conductivity calculations from infiltrometer measurements (Wooding, 1968). This equation was has been evolved for many methods to obtain various hydraulic parameters from steady-state TI measurements (Angulo-Jaramillo et al., 2000). For the two tensions method and determining K_{sat}, it comprises the application of extrapolation through a pair of supply tensions (Ankeny et al., 1991). These calculations assume that the given supply tensions are constant and is not depending on soil conditions. However, in some circumstances, where flow rates are very high (e.g., cracked soils, and soils with macropores), measurements should be used carefully for determining near-saturated hydraulic parameters in macroporous soils where flow rate could be high which is the case in Mākaha Valley (Walker et al., 2006).

Wooding (1968) proposed, for approximation of steady-state unconfined saturated infiltration rates into soil from a circular source of radius *r* (cm) the following equation:

$$Q = \pi r^2 K\left(1 + \frac{4}{\pi r \alpha}\right) \tag{2.1}$$

Where Q (cm^3 h^{-1}) is the water flux, K (cm h^{-1}) is the hydraulic conductivity, and α (cm^{-1}) is the inverse macroscopic capillary length scale. Hydraulic conductivity is calculated given by Gardner (1958):

$$K = K_s \exp(\alpha\psi) \tag{2.2}$$

Where ψ(cm) is the negative tension provided during infiltration tests. By filling in equation 2.2 in 2.1 and measuring steady-state infiltration rates $Q(\psi_1)$ and $Q(\psi_2)$ at two water potentials, two unknown (K_{sat} and α) can be solved:

$$Q(\psi_1) = \pi r^2 K_{sat} \exp(\alpha\psi_1)\left(1 + \frac{4}{\pi r \alpha}\right) \tag{2.3}$$

$$Q(\psi_2) = \pi r^2 K_{sat} \exp(\alpha\psi_2)\left(1 + \frac{4}{\pi r \alpha}\right) \tag{2.4}$$

The K_{sat} can now be calculated (equation 2.6) from any pair of steady-state measurements (equation 2.3 or 2.4) by solving α from equation 2.5:

$$\alpha = \frac{\ln(Q(\psi_2)/Q(\psi_1))}{\psi_2 - \psi_1} \tag{2.5}$$

$$K_{sat} = \frac{Q(\psi_1)}{\pi r^2 \exp(\alpha\psi_1)\left(1 + \frac{4}{\pi r \alpha}\right)} = \frac{Q(\psi_2)}{\pi r^2 \exp(\alpha\psi_2)\left(1 + \frac{4}{\pi r \alpha}\right)} \tag{2.6}$$

Measurements were taken at negative tensions of -8 cm (high tension) and -2 cm (low tension). From observation, these tension levels showed significant differences between steady state rates. It was relatively easy to establish good contact for both tensions between the device and the soil. In this case steady state rates for high tensions were reached after 20 minutes and those during lower tensions took approximately half of the time.

2.3.3 Field measurements of soil hydraulic properties

The presence of rock fragments and organic matter in soil layers can have an effect on measured hydraulic properties (Sauer and Logsdon, 2002). Therefore knowledge regarding soil physical properties can provide useful knowledge of soil hydraulic properties. Variables as porosity θ_t (-) and dry bulk density ρ_b (g cm^{-3}) can show significant correlation with K_{sat} (Ersahin, 2003) and are in general less spatially variable than K_{sat}. If this is the case then it provides a proper auxiliary variable for cokriging interpolation. Therefore, undisturbed soil cores (internal diameter = 4.8 cm and height = 7.5 cm) were taken from the top soil layer using a sludge hammer soil sampler within a range of 50 cm at each TI measurement location. The soil cores were trimmed, sealed, and taken to the laboratory. In the laboratory, the soil cores were covered with nylon mesh and placed in water to saturate for 24 hours. After the saturated samples were weighted and oven dried for 24 hours at 105 ^{o}C, the samples were weighted again. Assumed is that 1 g of water is 1 cm^3.

Selected soil physical properties were determined for all measurement locations. The properties θ_t and ρ_b are determined as follows (Grossman and Reinsch, 2002; Flint and Flint 2002):

$$\theta_t = \frac{W_s - W_d}{V} \tag{2.7}$$

$$\rho_b = \frac{W_d}{V} \tag{2.8}$$

Where W_s (g) is the weight of saturated soil sample, W_d (g) is the weight if the over dried sample and V (cm^3) is the volume of soil sample.

2.3.4 Conventional statistics

Descriptive statistics are used for providing an indication of variability and distribution of K_{sat}, ρ_b, and θ_t. Descriptive statistics include minimum, maximum, skewness, kurtosis, mean, and coefficient of variation. Another statistical technique to spatially characterize soil hydraulic properties in a watershed, is analyzing sample variances of conducted measurements (Sauer and Logsdon, 2002). For several characteristics in Mākaha Valley, it is useful to determine whether there are significant differences between groups of sample means of K_{sat}, ρ_b, and θ_t. One-way Analyses of Variances (ANOVA) were therefore used to test the equality of means of two or more groups. ANOVA requires the assumptions that K_{sat}, ρ_b,, and θ_t are independent samples, taken from normally distributed populations with approximately equal variances. A normal probability plot and the Shapiro-Wilk normality test are calculated to test whether K_{sat} is normally distributed. If not, a second normality test is conducted by applying a lognormal transformation. In general, K_{sat} often shows a lognormal distribution (Angulo-Jaramillo et al., 2000). After, measured variables are grouped and evaluated independently based on chosen determinant factors. In this case, groups are chosen based on clearly distinctive dominant topographical factors influencing K_{sat} in Mākaha Valley.

First, from observation three topographical features obtained field data can be clearly distinguished: area located nearby the stream, v-shaped ridges, and gulches in between (Figure 2.5). Second, vegetation can be also a determinant factor of water flow in soil. Notes of vegetation were also taken during field measurements. Third, ANOVA is also calculated by dividing the watershed in other groups of dominant topographical factors as elevation, slope, aspect, and the division in estimated conductivities of hydrologic soil groups (USGS-NRCS, 2007). These divisions are calculated by GIS-analysis. Elevation is divided in approximately three equal groups of ≤ 400 m, 400-525 m, and ≥ 525 m. Three approximately equal groups of slope <25%, 25- 40%, and $\geq 40\%$ are taken. Aspect is divided in two groups < 180° and ≥ 180°. Finally, two equal groups of hydrologic groups (conductivities) from soil unit delineations are considered: hydrologic soil group B and C (Figure 2.7).

All statistical tests were completed at the p = 0.05 level of confidence. When the calculated p < 0.05 with a mean μ_i, the null hypothesis is rejected ($H_0 : \mu_A = \mu_B = \mu_C$ etc.) at the 0.05 level. A division of a topographical group can be considered to have significantly different means. For a $p \geq 0.05$, the division of a topographical group has no significantly different means for Mākaha Valley. ANOVA only shows whether topographical groups have significantly different means between chosen distinctions. When ANOVA calculate significant different means within a topographical group, the homogeneity of variance test

(Levene's test) is used for testing the equality of group variances. This test is not dependent on the assumption of normality, but a required assumption for ANOVA.

When lognormal transformations are used for ANOVA, untransformed means are presented in figures and plots that represent spatial distribution. An indispensable supplement to ANOVA is pair wise comparisons. It implies that means of groups of a division of a topographical group are compared and determined whether there are significantly different means between these pairs. Fisher's least significant difference test (LSD) will be conducted when ANOVA shows significant different means, otherwise this procedure is not used (Torrie, 1980). This assumes that the null hypothesis is given as H_0: $\mu_A = \mu_B$, H_0: $\mu_B = \mu_C$, and rejection is when H_1: $\mu_A \neq \mu_B$, H_1 : $\mu_B \neq \mu_C$. In this case, H_0 is rejected when the absolute difference between a pair of two means is larger than a certain calculated LSD_{AB} value.

In addition, Pearson's linear correlation coefficients were calculated among K_{sat} ρ_b, and θ_t. Also possible determinant factors, obtained from GIS-analysis, as elevation, slope, and aspect are correlated with measured values. A highly positive linear relationship shows values close to 1 and values close to -1 show a negative linear relationship. Values around 0 do not have a linear relationship. When variables are highly correlated, results are used for geostatistics to support cokriging interpolation.

2.3.5 Geostatistics

First, solely semivariogram analysis is applied and along with spatial dependency geospatial interpolation is considered. For expressing spatial variability between the measured variables at various measurement locations by using geospatial techniques, semivariograms have been constructed. Normal distributed and/or lognormal transformed semivariograms were calculated for K_{sat}, ρ_b, and θ_t to express the degree of spatial variability between neighboring observations, and subsequently, appropriate spherical model functions were fitted to the semivariograms. Other model types of semivariograms are also available but to show spatial correlation, this type is sufficient enough and widely used. The normal distributed semivariogram is calculated as follows (Goovaerts, 1997):

$$\gamma(h) = \frac{1}{2N(h)} \left\{ \sum_{i=1}^{N(h)} \left[Z(x_i + h) - Z(x_i) \right]^2 \right\} \tag{2.9}$$

Where $\gamma(h)$ (cm h^{-1})^2 is the is the semivariance for lag distance h (m), $N(h)$ is the number of pairs separated by lag distance (separation distance between sample positions), $Z(x_i)$ is a measured variable (i.e. K_{sat}, θ_t, and ρ_b) at location i, $Z(x_i+h)$ is a measured variable at spatial location $i+h$. The spherical modeled semivariogram is given by:

$$\gamma(h) = \begin{cases} C_0 + C_1 \left[1.5\frac{h}{a} = 0.5\left(\frac{h}{a}\right)^3 \right], h \leq a \\ C_0 + C_1, h > a \end{cases} \tag{2.10}$$

Where a (m) is the range, C_0 is the nugget, C_0+C_1 is the sill (horizontal asymptote), and h (m) is the lag distance.

In theory $\gamma(0)$ must be equal to zero, however this is not realistic. The origin often have non zero values and this is called the nugget. A variable can be subject to sampling

errors or is so erratic over a short distance that the semivariogram goes from zero to the level of the nugget effect in a distance less than the sampling interval, i.e., no spatial dependency (Davis, 2002). If results of the semivariograms are suggesting sufficient spatial dependency and/or highly correlated variables with K_{sat} are found, interpolation of K_{sat} will be performed by using ordinary kriging and/or cokriging.

2.3.6 Spatial distribution of K_{sat}

Based on all previous statistical calculations and derived conclusions, a best possible spatial distribution of K_{sat} is determined. This comprises the obtained results from conventional statistics and/or geospatial interpolation with sufficient spatial correlation.

2.3.7 Software

All statistical tests and analyses were performed using Statistix software package (Analytical Software 2003, Tallahassee, FL), and Microsoft Excel software (Microsoft Corporation, 2007). Spatial analyzes were performed using Arcmap 9.2 software (ESRI Inc., 2004).

2.4 Results & Discussion

2.4.1 Experimental site

Taking measurements around the wetland area (mucky peat) at the top of Mt. Ka'ala was not allowed due to restriction of this area by the army. Nevertheless it will be useful to plan future samples at that location, because of a different soil type and expected higher K_{sat} values. It also appeared that it was almost not possible to conduct field measurements outside the alluvium part of the subwatershed. The majority of the 54 infiltration tests and soil sampled were conducted on the alluvium geological framework of Mākaha Valley (Figure 2.11). Outside the alluvium of the subwatershed tends to become very steep and very difficult to access. In case of interpolation, the alluvium section will be used as a representative main study area within Mākaha Valley subwatershed.

2.4.2 Field measurements of K_{sat}

A common uncertainty with TI, is contact of the instrument with the soil which can cause errors in K_{sat} calculations. From field experience and observation, lower tension measurements (-2 cm) appeared to be more sensitive for bad contact than higher tension (-8 cm). For this version of the TI, it was not difficult to make good contact during high tension measurements. The presences of small pores are only filled during these circumstances and are less sensitive for overestimation of K_{sat}. However, in case of impeding areas as roots or macropores, steady state rates become very low and K_{sa4t} is extrapolated at a too large value. Also macropores such as wormholes and rooted areas below the sample location can also cause extremely high values during low tension measurements with steady state rates. In these cases and when the TI is not well leveled, the assumed supplied tension becomes also very sensitive and may have varied during field measurements.

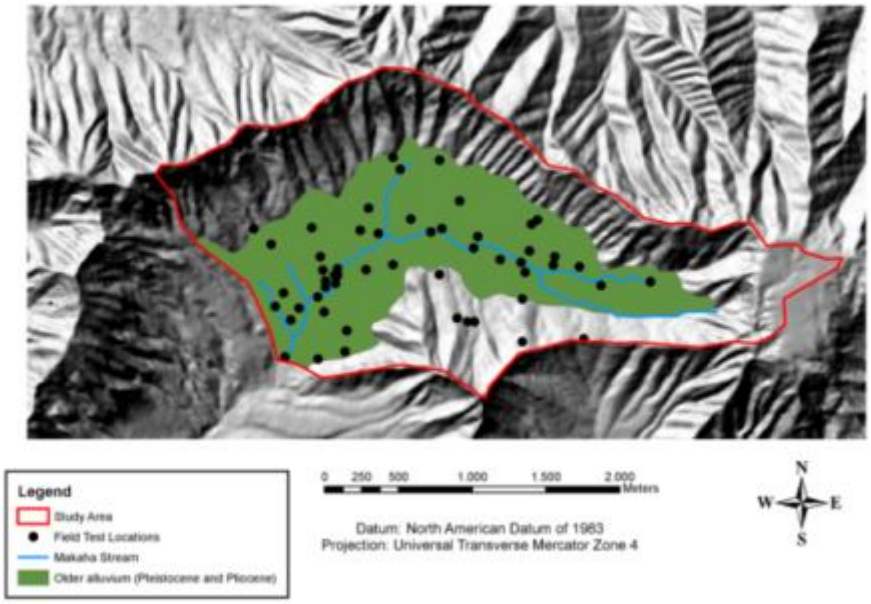

Figure 2.11 Study area and measurement locations in mainly the alluvium part of the subwatershed of Mākaha Valley.

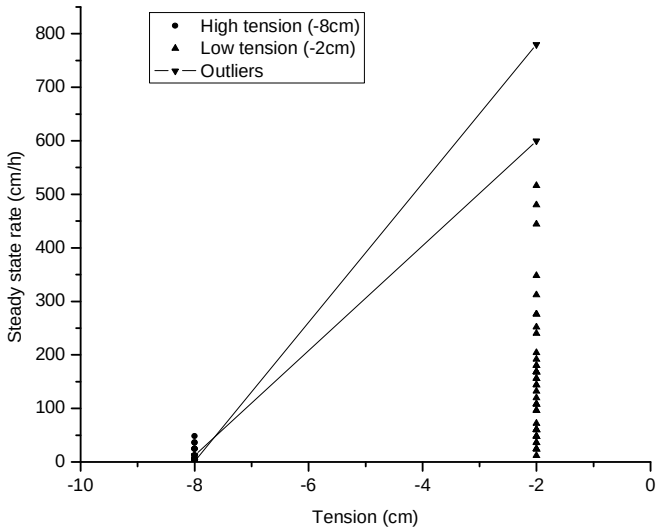

Figure 2.12 Steady state infiltration rates under two tensions and two observed outliers

Two values of measured low tension steady state measurements seemed much higher than other measurements (Figure 2.12). From field observation and experiences, this is imputed to bad contact. With respect to spatially characterizing K_{sat}, these two measurements will be excluded from the data set. This implies for ANOVA and determining spatial variability of K_{sat}. These two error measurements were still used for descriptive

statistics and correlation. Finally, all values of field test data at each location are given in Appendix B.

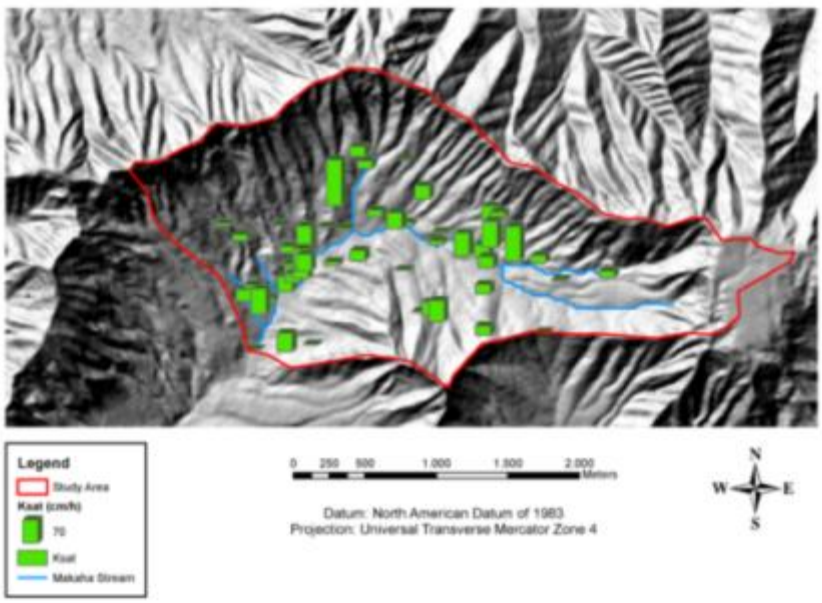

Figure 2.13 Values of K_{sat} for each measurement location in Mākaha Valley.

2.4.3 Field measurements of soil physical properties

In addition to K_{sat} calculations, soil core samples were taken at each test location. Observing the soil core samples provides information about the top soil structure where the TI measurements where taken. From observations, Mākaha Valley contains stony soils nearby the stream, and more organic matter where vegetation is densely present. This was clearly visible when soil core samples were dried. Observation of sample cores of which the volume highly shrinks, is an example of presence of organic matter in the soil sample. On the other hand, stony soil samples are likely to shrink less during the drying process and were also observed. Extreme values in θ_t and ρ_b are expected and results are affecting soil hydraulic properties, in this case K_{sat}. Large contents of organic matter will cause high θ_t and large contents of stones will give high ρ_b and low θ_t. Conventional statistics should provide more information regarding this relation.

Table 2.1 Descriptive statistics for K_{sat}, ρ_b, and θ_t.

	K_{sat} (cm h^{-1})	ρ_b (g cm^{-3})	θ_t (-)
Mean	43	0.82	0.70
Standard Deviation	69	0.15	0.06
Kurtosis	22	-0.34	2.41
Skewness	4.1	-0.04	-0.88
Minimum	0.39	0.48	0.47
Maximum	442	1.15	0.80
Coefficient of Variance (%)	162	18	9

2.4.4 Conventional statistics

An indication of the spatial distribution of K_{sat} can be given by plotting the values of K_{sat} distributed over the watershed (Figure 2.13). Values of K_{sat} seem randomly distributed over the watershed and no conclusions can be drawn concerning spatial distribution. Descriptive statistics (Table 2.1) show large variations of K_{sat} looking at the minimum and maximum values. Maximum values of K_{sat} are much higher than estimated conductivities (USGS-NRCS, 2007), however, not different than measured K_{sat} in other stony soils (Sauer and Logsdon, 2002). Stony soils and dense vegetation are likely to have macropores and cracks. On the other hand ρ_b and θ_t are not so various but likewise smoother distributed than K_{sat} as several studies already demonstrated and have smaller ranges (Sauer and Logsdon, 2002; Ersahin, 2003). In these studies, ρ_b and θ_t were normally distributed which is contrary to usually a lognormal distribution for K_{sat} (Angulo-Jaramillo et al., 2000). Further noticeable is that ρ_b shows a very low minimum and θ_t s very high maximum. This may be associated with an observed ashy type of soil in the upper stream part of the subwatershed which causes high θ_t and low ρ_b.

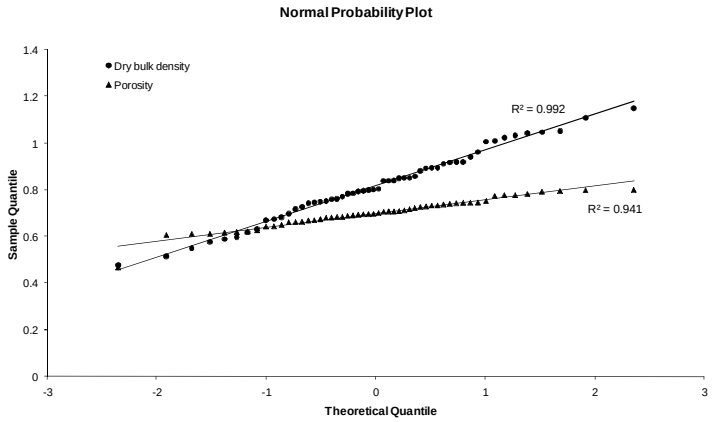

Figure 2.14 Normal probability plot of ρ_b, and θ_t with calculated linear regression coefficient.

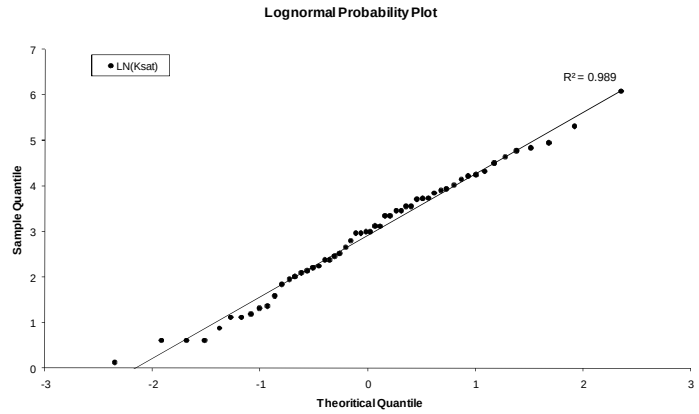

Figure 2.15 Lognormal transformed probability plot of K_{sat} with calculated linear regression coefficient (R^2).

Both θ_t and ρ_b have skewness close to zero which indicates a symmetric distribution which is not the case for K_{sat}. Positive skewness of K_{sat} indicates a right skewness, which means that the right tail is longer and the mass of the tail is concentrated on the left of the K_{sat} distribution. A large positive value of the kurtosis implies that K_{sat} has a sharper peak and flatter tails. Both indicators confirm the probability of a log normal distribution for K_{sat}, which corresponds to other studies concerning the distribution of K_{sat} (Sauer and Logsdon, 2002; Ersahin, 2003; Haws et al., 2004). This is illustrated by a lognormal probability plot (Figure 2.14) and confirmed by a Shapiro-Wilk normality test. A linear curve has been fitted in the scatter plot with a linear regression coefficient for K_{sat} which indicates a normal distribution of lognormal transformed K_{sat}. A calculated p-value ($p > 0.05$) confirmed the lognormal distribution by Shapiro-Wilk ($p=0.11$, $W=0.958$).

Table 2.2 ANOVA applied on K_{sat} for several divisions of topographical elements.

Topographical element	*P-value ($LN(K_{sat})$)*	*P-value (ρ_b)*	*P-value (θ_t)*
1. Elevation	0.417	**0.015**[1]	0.418
2. Slope	0.360	0.439	0.793
3. Aspect	0.655	0.695	0.890
4. Stream/ridge/gulch	**0.040**[1]	0.139	**0.047**[1]
5. Hydrologic soil group	0.425	**0.007**[1]	0.424

[1] Significance $p = 0.05$ level of confidence when $p < 0.05$

ANOVA was calculated for five groups. In first instance also the dominant vegetation species at each location was attempted to determine. However, it was often too difficult to determine dominant vegetation species, because of its heterogeneity so that providing an appropriate division of vegetation species for ANOVA was not applicable. Now, five topographical groups are analyzed and a first impression of the spatial distribution of K_{sat}, ρ_b, and θ_t is given by dividing measurements in topographical groups, and subsequently, calculating ANOVA (Table 2.2). When results of ANOVA show $p < 0.05$, a topographical group can be considered to have significantly different means at a $p=0.05$ level of confidence.

In contrast to estimates of conductivities of NRCS (USGS-NRCS, 2007), conductivities are not found to be significantly different in the lower part and upper of the subwatershed (hydrologic soil group B and C). One group was found to have significantly different means for K_{sat} at $p = 0.05$ level of confidence, which is the division stream, ridges, and in gulches ($p = 0.04$, Table 2.2). In this case the highest value of K_{sat} was found for gulches and lowest nearby the stream. Accordingly, this result is showing that infiltration can be significantly reduced on gentle slopes due to crusting and weathered parts of the subwatershed (Luk et al. (1993). No other topographical elements were found to have significant different means for K_{sat}. On the other hand, ρ_b shows significant different means for elevation and highly significance ($p < 0.01$, Table 2.2) for hydrologic soil group (conductivity B and C). This is explained by a negative correlation between ρ_b and elevation, where ρ_b declines as elevation increases due to an observed ashy type of soil. It also explains the highly significant different means between hydrologic soil group B and C. Hydrologic soil group C is located at the upper part of the valley while group B is present more downstream. This can also clarify the estimates of conductivities (USGS-NRCS, 2007), although K_{sat} results did not demonstrated

this. Assuming that TI measurement errors are not significant, the rugged and various character of the study area are causing highly variable values of K_{sat}. θ_t also shows a significant difference between areas nearby the stream, on the top of the ridge, and in the gulches. Also this result is likely to be imputed to the different composition of the soil samples taken in these areas, where sample nearby the stream are stony and samples on higher elevation more ashy. For all significant different means of ANOVA, the necessary assumption of equal variances within these topographical groups needed to be confirmed by Levene's Test. This is assumed when a calculated p-value is larger than 0.05. For all significant results from ANOVA, K_{sat} (p=0.48), ρ_b (p=0.39 and p=0.24), and θ_t (p=0.09) have assumed equal variances.

Table 2.3 Fisher's LSD pair wise mean comparison of significant different groups when p<0.05 with ANOVA. The hydrologic soil groups division for ρ_b was not necessary, because of only two groups in this classification (A and B).

	Group	*Mean (μ)*	*Mean comparisons*
K_{sat} (cm h^{-1})	Gulch (μ_A)	27	μ_A
	Ridge (μ_B)	22	$\mu_A = \mu_B$, $\mu_B = \mu_C$
	Stream (μ_C)	10	$\mu_A \neq \mu_C$
ρ_b (g m^{-3})	≤400 m (μ_A)	0.87	μ_A
	400-525 m (μ_B)	0.85	$\mu_A = \mu_B$, $\mu_B \neq \mu_C$
	>525 m (μ_C)	0.74	$\mu_A \neq \mu_C$
θ_t (-)	Gulch (μ_A)	0.73	μ_A
	Ridge (μ_B)	0.70	$\mu_A = \mu_B$, $\mu_B = \mu_C$
	Stream (μ_C)	0.68	$\mu_A \neq \mu_C$

In case of rejection of null hypothesis of ANOVA, (i.e., significantly different means) and equal variance, Fisher's LSD was determined and compared for each pair significant differences of divided topographical groups. A significantly different mean was found for Fisher's LSD between stream and gulch (Table 2.3) ($\mu_A \neq \mu_C$). This was also the case for different means of θ_t in the gulch and nearby the stream ($\mu_A \neq \mu_C$). ρ_b shows a significantly different mean for measurements taken at elevations ≤400m and >525 m ($\mu_A \neq \mu_C$), 400 - 425m ($\mu_A \neq \mu_C$), and a different mean for gulch and stream ($\mu_A \neq \mu_C$). Also considering the intermediate correlation between ρ_b and elevation (R^2= -0.48), ρ_b can be likely considered to have a relation with elevation in Mākaha Valley (Table 2.3).

Table 2.4 Pearson's correlation coefficient (R^2) of measured variables and topographical aspects in Mākaha Valley.

Pearson Correlation (R^2)	*LN(K_{sat})*	ρ_b	θ_t
LN(K_{sat})	-	-	-
ρ_b	0.02	-	-
θ_t	-0.00	-0.30	-
Aspect	0.14	-0.17	-0.01
Slope	-0.11	-0.28	-0.11
Elevation	-0.20	-0.48	-0.01

Calculated Pearson's linear correlation coefficients between measured variables were poor contrary to result of Ersahin (2003) (Table 2.4). Only low negative linear correlation between ρ_b and θ_t is calculated (R^2 = -0.30). Normally this value should be larger negatively correlated. When the dry particle density (ρ_d) is calculated, it is noticeable that these values are ranging too large for a ρ_d (1.26 g cm^{-3} - 3.68 g cm^{-3}). Likely there were errors made in calculating either ρ_b or θ_t. This probably involved the procedure of determining θ_t. It was calculated by using both wet weight and dry weight of the soil core sample. Based on observations, soil core samples during saturation may have caused errors because of the presence of large stones and wood in many samples. This possibly affects the saturation process of the soil core samples by air bubbles or impeding the water flow through the core sample. Subsequently this can cause large errors in θ_t.

Also variables obtained from GIS-analysis are not correlated with measured variables except for a low negative correlation between elevation and K_{sat} (R^2 =-0.20). There should be noted that coordinates obtained from field measurements are involved with errors from the GPS receiver and that GIS attributes are aggregated to 10 m x 10 m. Finally, geospatial interpolation by using cokriging is not applied due to lack of correlation of an auxiliary variable.

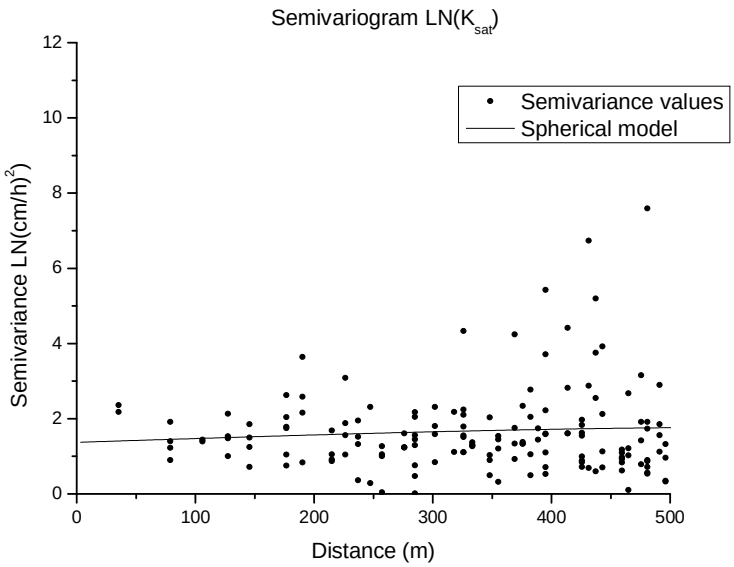

Figure 2.16 Semivariogram of lognormal transformed K_{sat} with fitted spherical model.

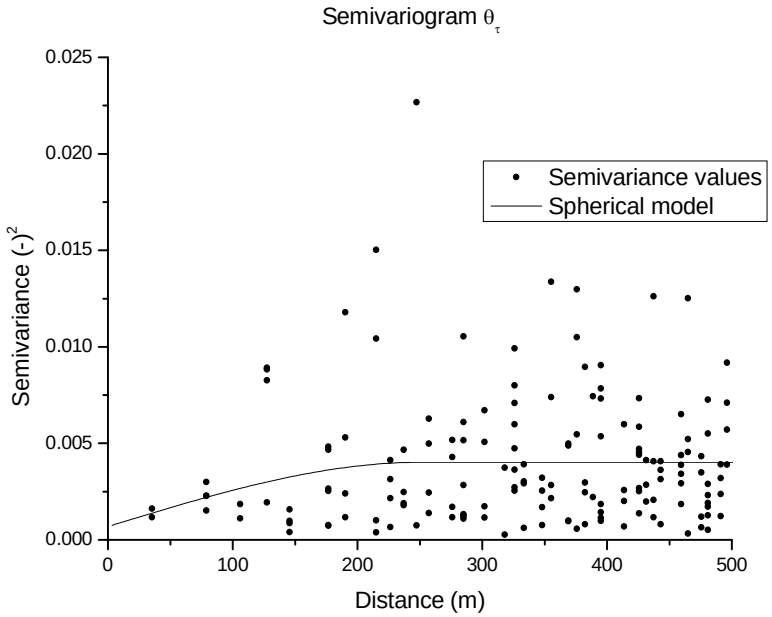

Figure 2.17 Semivariogram of normally distributed θ_t with a fitted spherical model.

2.4.5 Geostatistics

In contrast to agriculture landscapes (Haws et al., 2004), spatial dependencies of measured values of K_{sat} are generally small (Achouri, 1984). In order to illustrate this, semivariograms were calculated, and in addition, model parameters of the spherical modeled semivariograms of the three measured variables were fitted.

Table 2.5 Semivariogram models of Mākaha Valley, where C_0 = nugget, a = range, and $C_0 + C_1$ = sill.

Model parameters	C_0	*a*	$C_0 + C_1$
$LN(K_{sat})$	1.37	593	1.77
ρ_b	0.017	593	0.03
θ_t	0.001	252	0.004

As expected, a semivariogram with a pure nugget effect (approximately a horizontal line) is calculated (Figure 2.16), which indicates no spatial dependency between the measurements of K_{sat}. Since the sample lag size has been calculated over 50 m, it implies that K_{sat} is so erratic over Mākaha Valley that it is largely variable within a few meters, which account for Hawaiian soils in general (Green et al., 1982). On the other hand, θ_t shows a little spatial correlation within 250 m by showing a relative small nugget compared to the sill (Figure 2.17). In general, this can be contributed to a less variable character of soil physical properties across a watershed. However, this is contradictive to the lack of spatial correlation of ρ_b (Table 2.5). This may be caused by various compositions of soil core samples taken within a short distance. Differences in these soil samples involved the contents of stones and organic matter in a soil sample which likely caused erratic values.

2.5 Spatial distribution of K_{sat}

To obtain an appropriate distributed representation of K_{sat}, previous results from conventional statistics are taken into account, and subsequently, used for a best possible indication of spatially distributed K_{sat}. Since semivariograms did not show spatial correlation of K_{sat}, and geospatial interpolation depends on semivariance, interpolation by using ordinary kriging or cokriging was not relevant. Geospatial interpolation will not perform better than a simple interpolation method as inverse distance weighting or nearest neighbor with such poor spatial correlation. Results from conventional statistics for K_{sat} were retrieved by ANOVA and Fisher's LSD. This showed that dividing the subwatershed in three groups of measurement locations (stream area, ridges, and gulches) illustrated different mean values for K_{sat} (i.e., significantly different means for stream areas and gulches). The purpose is now to indentify these typical locations and plot them in a map over the subwatershed.

Results concerning the values of K_{sat} were dependent on notes taken during measurements. Notes were taken to determine whether a measurement location was a stream area, ridge, or gulch. This information was not sufficient to spatially retrieve these specific locations distributed over a watershed scale. It may be better to use GIS information to retrieve and spatially distribute these locations over a watershed. Therefore, specific characteristics of these locations were required. In this case a GIS-analysis extraction method was applied where maximum infiltration areas have been identified in order to retrieve aquifer vulnerability to contamination (Brito et al., 2005). This method applied a simple weighted algorithm where infiltration potentials at each location can be calculated by using weighted topographical aspects.

Derived from this method, stream areas, ridges, and gulches can be determined in an approximately similar way. Available topographical GIS-data were used so that a representative input can be generated to extract possible stream areas, ridges, and gulches within Mākaha Valley subwatershed. Based on field observation and experience, two input variable derived from GIS-analysis, were used and are most likely to indentify these topographical elements. First, slopes, and second, flow accumulations were derived from the DEM (Appendix C). Flow accumulation is determined by accumulating the weight for all cells that flow into each downslope cell. This variable indicates potential drainage paths with is almost zero for ridges and intermediate values for gulches. Stream areas in Mākaha Valley are concerned with relatively gentle slopes and very high flow accumulation. Ridges can be identified by steep slopes and almost no flow accumulation. Gulches between the ridges are concerned with intermediate steep slopes and intermediate flow accumulation. Based on these criteria, the determination of a topographical element (*TE*) at location x_0 is written down as a weighted algorithm:

$$TE(x_0) = \sum_{i=1}^{N} W_i C_i(x_0) \tag{2.11}$$

Where W_i is the weight of the topographical parameter *i* (flow accumulation and slope), and $C_i(x_0)$ is the class code of the topographical parameter *i* at location x_0. The weights and class codes are illustrated in Table 2.6. Slopes were divided in four categories due to presence of highly various slopes. Steep slopes above 100% were therefore automatically considered as a ridge and were given a high class code. Flow accumulation was divided in three categories

so that it clearly represented potential stream areas, ridges and gulches with low class codes for ridges and high class codes for stream areas. The sum of weights is one and initially weights of the topographical parameters were assumed to be equal. However, by varying the weights iteratively, a heavier weight given to flow accumulation (0.6) seemed to better. Flow accumulation seemed to be a better indicator to distinguish ridges and gulches than slope. Slopes can still be fairly gentle on top of a ridge. Based on the outcomes of *TE*, classifications of the three topographical elements were ranged in Table 2.7. Ranges of classification codes were straightforward to determine in three topographical aspects, because equation 2.11 only provides a few outcomes.

Table 2.6 Division and classification of the topographical elements slope and flow accumulation with given weights

Topographical parameter(i)	*Weight*	*Classification*	*Class code*
Slope	0.4	0-20%	1
		20-50%	2
		50-100%	3
		>100%	4
Flow accumulation	0.6	>10000	1
		3-10000	2
		0-3	3

Table 2.7 Ranges of TE(x_0) for distinguishing stream areas, ridges, and gulches at a location x_0

Topographical aspect	*Outcomes of TE(x_0)*
Stream area	≤1.60
Gulch	>1.60, ≤2.20
Ridge	>2.20

Results of the classification can now be illustrated in three topographical aspects within the alluvium geological framework (Figure 2.18). It gives an impression of a location within the study area which is possibly a stream area, ridge, or a gulch. Also the mean values and ranges of K_{sat} are given.

2.5.1 Discussion

The objective is obtaining a spatial distribution for K_{sat} using as possible model input data. Due to lack of clear spatial results, an attempt has been made to translate results from ANOVA and Fisher's LSD into an integral spatial distribution for K_{sat}. For this part of the subwatershed this method gives an impression where significantly different means for K_{sat} in stream area and gulches were found. It can possibly be used as a distributed model input map of soil by using the different means of K_{sat} over the subwatershed. However, this map still only covers partially the subwatershed and it only provides values for K_{sat} (Singh and Woolhiser, 1978), and not yet for ρ_b, θ_t, and other soil parameters. Using it as a distributed soil map for a detailed hydrological model should be considered carefully.

It should also be noted that the real measurement locations are very difficult to verify with the calculated stream areas, ridges, and gulches (Figure 2.18). The coordinates of measurement locations rely on the accuracy of the GPS receiver. In addition, grid maps are

aggregated representations (10x10m) of topographical parameters (flow accumulation and slope) so that it often not indicates the right topographical aspect as it was noted during measurements. Very small ridges or narrow gulches can not be identified by this resolution of grid maps. It should also not be considered as a real world interpolation of K_{sat}. Results were obtained from conventional statistics and a simple method to extract these topographical aspects by arbitrary weights. It comprises only an approximately schematic representation of these different locations where significant different mean values for K_{sat} were measured. Nevertheless, this method can be very useful to study further in more detail and it provides a relative easy way to obtain future spatially distributed model input data for also different kinds of variables. When more field data is available regarding K_{sat} and its relation with topographical aspects, this method can be expanded in more detail. This should include for example verification of high values of K_{sat} by using a different field instruments as a DR. Another possibility is investigating the possible correlation of K_{sat} with vegetation. In combination with a detailed vegetation map this provides an extra topographical parameter (besides flow accumulation and slope) and more spatial knowledge of K_{sat} can be obtained.

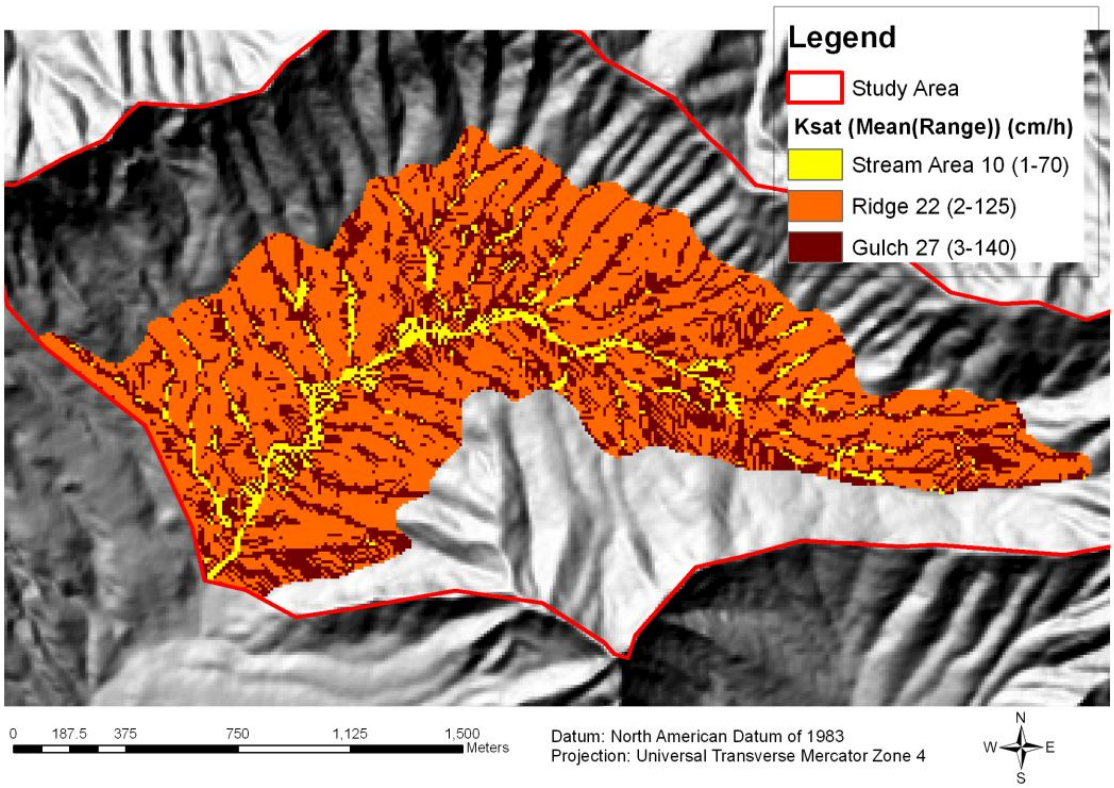

Figure 2.18 Classification of spatial distribution of K_{sat} by using significant different means (Fisher's LSD) between measurement at stream areas and in gulches. Locations were identified by GIS from flow accumulation and slope.

Chapter 3

Modeling streamflow using the Distributed Hydrological Soil Vegetation Model (DHSVM)

3.1 Introduction

Outlined in chapter one, Mākaha Valley streamflow is significantly decreasing (Mair et al., 2007). Whether this is possibly affected by groundwater pumping, change in rainfall, and vegetation changes can be determined hydrological modeling. In order to establish this goal, a suitable model needs to be tested. This chapter focuses on this aspect of the main project (Fares et al., 2004) so that the objectives become: (1) setting up a watershed model for Mākaha Valley subwatershed, (2) calibrating and validating the watershed model on streamflow, and (3) testing sensitivity of streamflow to groundwater pumping, changing rainfall, and vegetation changes.

3.2 Model choice

Many possibilities with respect to modeling streamflow in a watershed are available. Main modeling is empirical, conceptual, and physically based (Rientjes, 2005). Which model choice is made is mostly based on this classification and depending on the objective (Table 3.1). In case of Mākaha Valley, an integral hydrological watershed model was most desired, because spatial distributed hydrological processes on a highly detailed level are required to be studied (Fares et al., 2004). This is required because of large spatial variability of hydrological processes as rainfall, soil moisture and distribution of vegetation in Mākaha Valley. A physically based distributed hydrological model was therefore recommended to test for Mākaha Valley. A conceptual model also satisfies many case studies but processes in the model are more considered as a black box. However gray and white boxes are also available in this category, but detailed and distributed simulations of hydrological processes is more difficult. Empirical models provide output based on a function of model input by for example using regression equations. Processes in these models are also considered as a black box.

Table 3.1 Characterization of hydrological models (Rientjes, 2005)

Model approach	Spatial discretisation			System dimension		
	Distributed	Semi-distributed	Lumped	1-D	2-D	3-D
Empirical	-	-	x	x	-	-
Conceptual	x	x	x	x	x	-
Physically based	x	x	-	x	x	x

Many physically based distributed hydrological models are available. TOPMODEL, WATFLOOD, and MIKE-SHE etc., are examples of widely applied models. These models are able to simulate streamflow and have shown large reliability. However, spatial discretisations (grid cell size) and river basin sizes are usually much larger than Mākaha Valley. Only WATFLOOD has been used for small watersheds (15 km^2), whereas use grid sizes were still relatively large (1 km x 1 km). Providing a detailed distributed view of hydrological processes in a small watershed as Mākaha Valley is therefore more difficult.

For this study, the Distributed Hydrological Vegetation Model was suggested based on previous studies using this model. The advantage of this model is that is has been applied to model streamflow for very small watersheds in tropical environments (0.94 km^2) (Cuo et al., 2006; Thanapakpawin et al., 2007) and mountainous watersheds (Vanshaar et al. 2002b; Kelleher, 2006) which are relatively similar conditions to Mākaha Valley.

3.3 Model description

The Distributed Hydrological Soil Vegetation Model (DHSVM) was originally developed by Wigmosta et al. (1994, 2002) and simulates a dynamic (one day to one hour time-step) representation of the spatial distribution of soil moisture, snow cover, evapotranspiration, and runoff production. The version applied in this study has one modification that has been made in addition to the official version 2.0 of DHSVM (Lettenmaier, 2008). This modification has been applied by researchers working as a part of the Puget Sound (WA, USA) Regional Synthesis Model (PRISM) and the Climate Impact Group (CIG) at the University of Washington (PRISM and CIG, 2008). A brief description of this model is summarized for the official version 2.0 (Wigmosta et al., 2002) including the modified version (PRISM and CIG, 2008).

The eight modules in DHSVM are evapotranspiration, snowpack accumulation and melt, canopy snow interception and release, unsaturated moisture movement, saturated subsurface flow, surface overland flow, channel flow, and the deep groundwater component. Originally, the modified groundwater component has been developed so that underestimated low summer flows may be better simulated within the Hood Canal region (WA, USA) (PRISM and CIG, 2008). In this study, the deep groundwater component is used to deal with the more complex geological framework for Mākaha Valley since the study area is subject to groundwater pumping and possible loss of water due to flow in the dike complex (Mair, 2007, personal communication) (Figure 2.9). This module is used to test whether it has additional value for Mākaha Valley to deal with permanent loss of water.

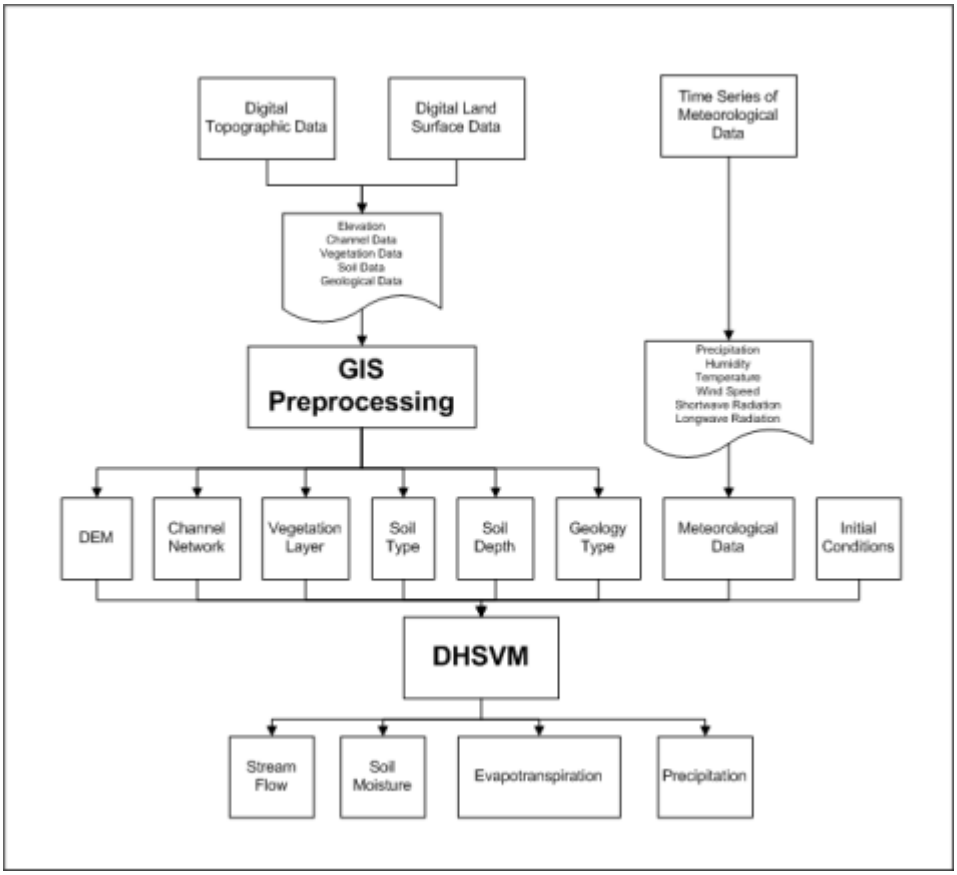

Figure 3.1 DHSVM modeling inputs and possible outputs

The major inputs of DHSVM are digital elevation, vegetation, soil, geology, and meteorological data (Figure 3.1). DHSVM is a physically based distributed model that provides an integrated representation of watershed processes at a spatial scale described by digital elevation model (DEM) data. Modeling the landscape is obtained by using computational grid cells which are centered on DEM nodes. Vegetation characteristics, soil properties, and geological properties are assigned to each model grid cell. These properties may vary spatially throughout the basin. In each grid cell the modeled land surface can be considered as a combination of vegetation, soil, and geology. The model provides results with respect to energy and water balance equations for every grid cell in the watershed at each time step. Individual grid cells are linked through surface, subsurface flow, and groundwater flow routing. Surface, subsurface, and groundwater flow are routed downslope toward a stream channel where it may be intercepted (Wigmosta et al., 2002). The drainage network is calculated as a series of connected reaches with each reach passing through one or more DEM grid cells. Additional canopy snow interception and release is modeled using a one-layer mass- and energy balance model, but this part of the model is not relevant for Hawai'i. For facilitating the model setup and the analysis of model output, a Geographical Information System (GIS) is used (ArcGIS 9.2 and ARC/INFO). The GIS can delineate watershed boundaries, and likewise, assign spatially distributed model input parameters to DEM grid cells using overlays of soils, vegetation, and stream channels from the raw input data.

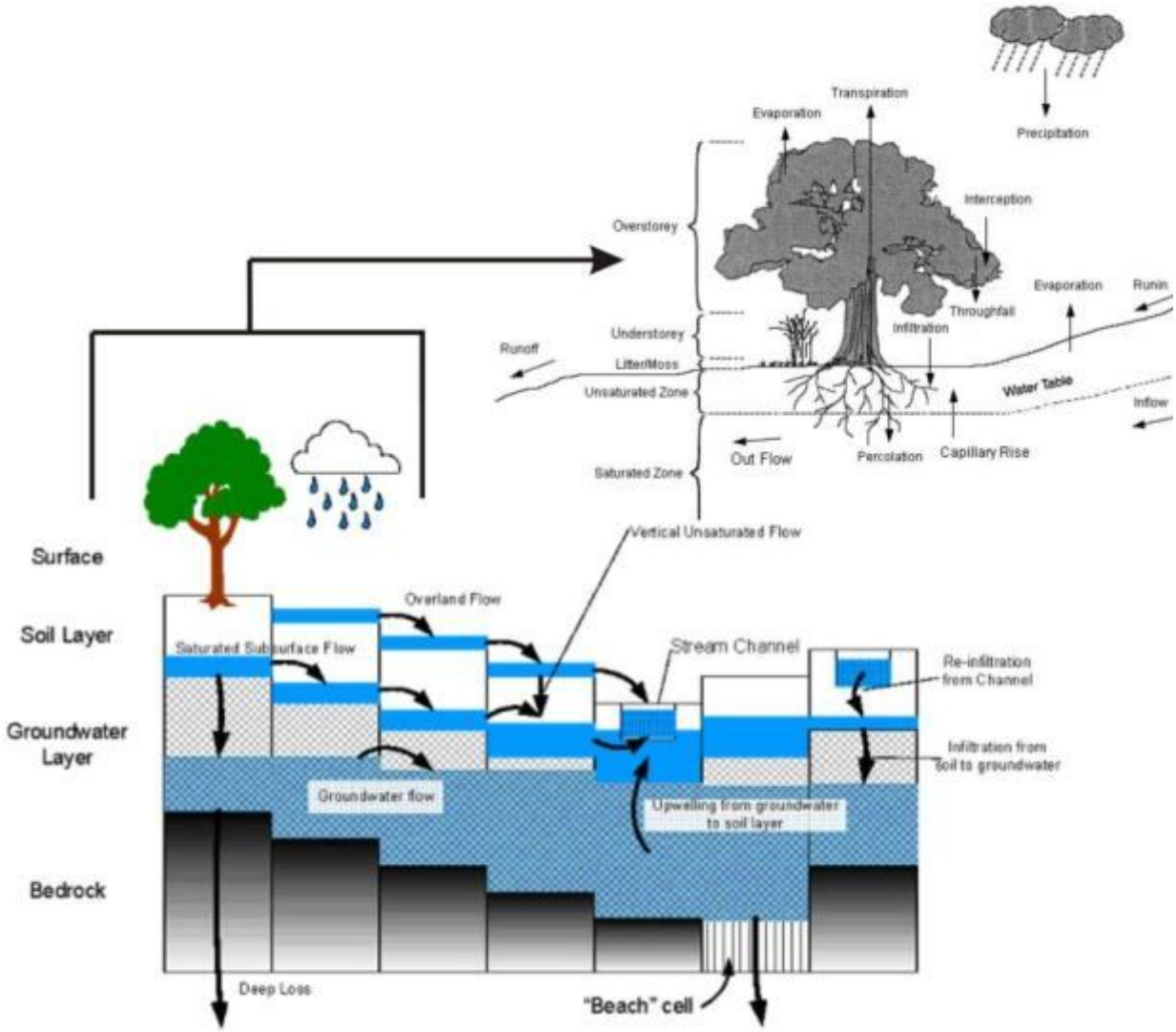

Figure 3.2 Schematic representation of potential pathways in modified DHSVM with an additional deep groundwater component. In this case an example of bedrock as geological framework is shown (Chen et al., 2005; PRISM and CIG, 2008).

3.4 Model applications

Due to its high resolution, DHSVM is often applied to determine the effects of land use changes on hydrological processes as soil moisture, evapotranspiration, and streamflow. No studies were conducted which determined the effects of groundwater extraction, and precipitation trends on streamflow. All studies described below, involved the official version except for the final paragraph.

Recently, Thanapakpawin et al. (2007) studied the effects of landcover changes on streamflow in a catchment with humid and tropical conditions. This study was performed in the Mae Chaem watershed in Chiang Mai, Thailand. Basin hydrologic responses were

simulated using DHSVM and involves analyzing impacts of changes from forest to crop and opposite. The Mae Cheam watershed appeared to be relatively little sensitive to changes in runoff (+/- 5% total runoff) with migration from trees to crops due to decreasing evapotranspiration.

Vanshaar et al. (2002b) studied four catchments in the Columbia River Basin (USA), ranging from 26 km^2 to 1033 km^2, to demonstrate the sensitivity of streamflow with respect to land cover changes in comparison with a regional scaled model (VIC) (Liang et al., 1994). Comparisons with the macroscale variable infiltration capacity (VIC) model, which parameterizes topographic effects, show that runoff predicted by DHSVM is more sensitive to land-cover changes than runoff predicted by VIC. This is explained by model differences in soil parameters and evapotranspiration calculations, and by the more explicit representation of saturation excess in DHSVM and its higher sensitivity to LAI changes in the calculation of evapotranspiration. The accuracy of DHSVM here involved showing the advantage of using physically based distributed model in comparison with a regional scaled model.

In a different watershed with a tropical climate, DHSVM was applied in the mountainous 0.94 km^2 Pang Khum Experimental Watershed (PKEW), northern Thailand (Cuo et al., 2006). The study object was calibrating and testing variables as soil moisture and streamflow measurements. After, the model was run again without the road and keeping parameter settings and meteorological data the same. Model results with and without roads are used to study road effects on evapotranspiration, soil moisture, depth to water table, and stream discharge. Soil moisture at the four measurement sites was well simulated in all three root-zone soil layers. DHSVM simulated soil moisture at four measurement sites and three depths very well. On the other hand, streamflow was adequately estimated in only 2 of the 3 years tested. Model results show that the road causes relatively small changes to averaged monthly total evapotranspiration and streamflow in PKEW.

Using the deep groundwater modification, Waichler et al. (2004) conducted a recharge study. The purpose of this study was to improve estimates of natural recharge from the Cold Creek watershed (WA, USA) to the unconfined aquifer along the edge of a larger domain. Therefore, two modes of recharge were evaluated in the watershed: streamflow run-on and subsurface flow above a basalt bedrock surface. Relevant here was that streamflow processes were improved substantially for application in this arid setting by using a groundwater component. On the other hand, lack of data limited initial calibration and verification due to expansion of the modified model.

3.5 Study Area

The study area is the same study area as described in section 2.2.

3.6 Data

First, meteorological data are required as model forcing input data. In addition, the used version of DHSVM including the deep groundwater component requires eight GIS input data sets: digital elevation model (DEM), watershed boundary, flow network, terrain shadowing and percent open sky, vegetation, soil texture, soil thickness, and geology. Finally, observed stream gage data are required to compare simulated and observed

streamflow. Basin layers in DHSVM were represented in GIS grids over 5.47 km^2 of 30-meter grid cells for the entire Mākaha Valley subwatershed. More detailed procedures of manipulation and processing input map are described in Appendix D.

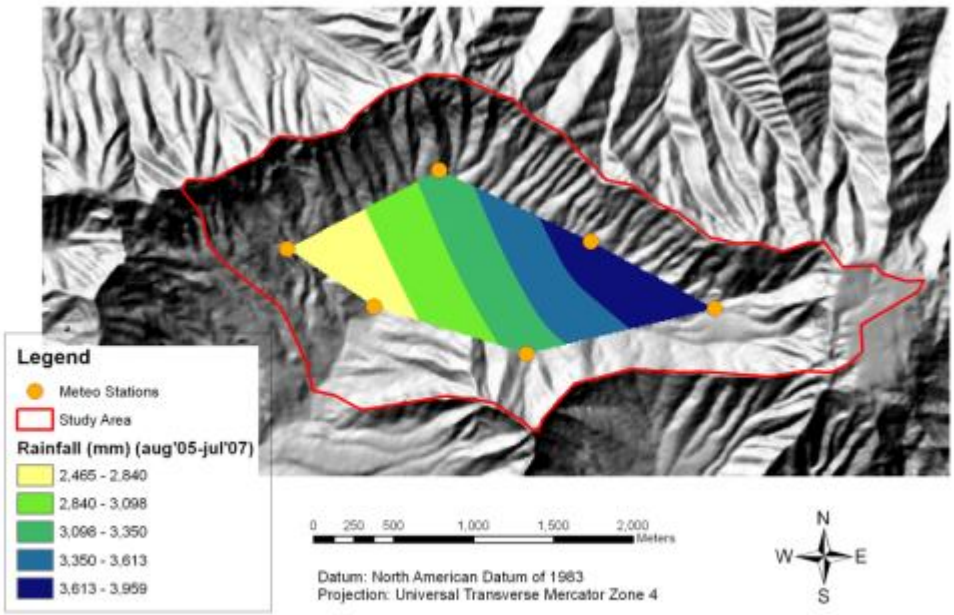

Figure 3.3 Map of meteorological stations and total rainfall (August 2005 – July 2007) used for DHSVM (Meteorological data collected by Mair (2008))

1. Meteorological Data

DHSVM requires also meteorological forcing data as input. Mair (2008) collected at six locations meteorological data from August 2005 to July 2007 across the subwatershed of Mākaha Valley (Figure 3.3). These hourly meteorological data include precipitation, wind speed, humidity, air temperature, and incoming shortwave solar radiation. Required incoming longwave radiation data were estimated from measured values of shortwave radiation, air temperature, and relative humidity by using Stefan Boltzmann's law and takes into account the change in emissivity with cloud cover (Prata, 1996: Allen et al., 2005). Meteorological data can be interpolated within DHSVM by three standard methods: inverse distance, nearest neighbor, and various cressman. In this study inverse distance interpolation was chosen. Interpolation of rainfall is not an issue in this study and a standard method was chosen.

2. Streamflow Gage

The focus in this study lies on the outlet of the basin. Time series of recorded streamflow data are required to calibrate streamflow in DHSVM. Therefore, hourly USGS 16211600 stream gage data were obtained for the period September 2005 to September 2007 without any data gaps.

3. Digital Elevation Model (DEM)

The DEM is the basis for DHSVM and its distributed parameters because it provides the topographic controls required for DHSVM's calculations. The DEM for Mākaha Valley was compiled from eight USGS 7.5-minute, 10-meter DEM files. The DEM (Appendix C) was clipped, filled, and aggregated to a floating 30 x 30 meter grid by ArcGIS 9.2 software.

4. Watershed Boundary Mask

Using a USGS stream gage as streamflow outlet, the subwatershed mask for Mākaha Valley can be delineated and provides the domain for all DHSVM calculations. Using the ArcGIS 9.2 watershed delineation option, the entire subwatershed watershed grid contained 18110 (30m x 30m) grid cells, and comprises an area of 5.47 km^2 (Figure 3.3). DHSVM only simulates hydrologic processes on cells within the mask from the delineation.

5. Flow Network

A flow network can be generated by running a series of Arc Macro Language processes (AML) that represent the flow network as a series of distinct reaches, modeled as cascading linear reservoirs. The network is based on the grids created from the ARC/INFO commands and is used to calculate the travel time to the basin outlet. Each channel reach has assigned attributes such as channel width, depth, maximum infiltration, and roughness. Channel dimensions were estimated by observations. Since DHSVM is not a hydraulic model and channels should only be able to discharge streamflow, exact channel dimensions are not of major importance. Output from the AML files includes the stream network grid for routing water, a map file that contains stream hydraulic properties for each segment, and a network file that contains the routing scheme from one reach to the next.

5. Terrain Shadowing and Percent open sky

DHSVM contains the option to apply topographic controls on incoming direct and diffuse shortwave radiation regarding evapotranspiration calculations. These are terrain shadowing maps and describe the combination of slope, aspect and terrain shadows at the midpoint for each time step in a typical day for each month of the year. Percent open sky maps provide information about the amount of sky visible from each model pixel. These two layers are computed using an AML algorithm based on the geographic position of the watershed and the elevation map.

6. Vegetation

Vegetation data were downloaded from The National Oceanic and Atmospheric Administration (NOAA, 2001). This data set is the result of a comprehensive inventory of Landsat Thematic Mapper satellite imagery. Hawaiian State data were provided as a 30-meter grid, and subsequently, clipped to the watershed boundary mask. Vegetation classes in the data set are reclassified to the DHSVM classification scheme. DHSVM uses dominant vegetation type of each grid cell and all grid cells with identical vegetation classifications are then assigned to one set of vegetation dependent parameters through a lookup table in the input file (Appendix D).

7. Soil Textures

Initially, the soil texture data were obtained and used from the SSURGO soil data set and represents the dominant soil texture classes in polygons (USDA-NRCS 2007). This state soil map is converted to a grid with a resolution of 30 m by using the general USDA soil classification system. DHSVM uses only the dominant soil texture of each grid cell. All grid cells with identical soil classifications are then assigned to one set of soil dependant hydraulic parameters through a lookup table contained in the input file. However, given the objective of this study, a map with distributed permeabilities (K_{sat}) was generated in previous chapter. Only this map partially covered the values of K_{sat} over the subwatershed. Depending on sensitivity of streamflow to K_{sat}, this generated map is used for calibration. Otherwise the SSURGO soil data map is still used for calibration.

8. Soil Depth

Although soil depth data does not exist for Mākaha Valley, the soil texture grid still requires a soil depth grid to transport subsurface flow. Therefore, a soil depth grid was generated by using an Arc Macro Language process generally used for DHSVM studies (Lettenmaier, 2008; PRISM and CIG, 2008). The values for soil depth are calculated using an algorithm that estimates soil depth based on slope, upstream contributing area and elevation. The script calculated deep soil depths on shallow slopes and in areas of high flow accumulation. Conversely, shallower soil depths were found on steeper slopes. The soil depth from ranged from 0.85 meters to 1.5 meters (map in Appendix E). This range can be multiplied in the configuration file of the modified DHSVM for calibration purposes.

9. Geology Textures

The modified version of DHSVM requires a geological framework is required below the soil depth. O'ahu geology textures were clipped from a U.S. Geological Survey polygon map (USDI-USGS, 2007). This clipped polygon map is converted to a grid with a resolution of 30 m. Similar to vegetation and soil textures, DHSVM uses only the dominant geological texture of each grid cell. All grid cells with identical geological classifications are then assigned to one set of geological dependant parameters through a lookup table contained in the input file.

3.7 Methods

3.7.1 Calibration

Before beginning calibration, the initial water conditions of the watershed should be set. The initial state of DHSVM is a dry watershed. To establish representative initial water conditions, a simulation was performed prior to calibration so that the output from this simulation can be used as initial conditions of the watershed. DHSVM requires initial conditions concerning the state of water in soil, water interception by vegetation, groundwater level, and water level in stream channels. The period used for setting the initial conditions is 14 months from August 2005 to October 2006. This provided a relative dry watershed since there is almost no rainfall during the summer months.

Model calibration is done by optimizing streamflow to observed streamflow. There are many methods applicable to calibrate streamflow. Calibrating streamflow in DHSVM is

not a straightforward process, because of the large number of available parameters and wide range of possible values. There are parameters being assigned to a specific soil type, vegetation type, and geology type. Besides, there are also parameters which are constant over the study area as constant ground roughness and rain threshold. Constant parameters are usually not applied for calibration, because they have an overall representation not sensitive to significant change in hydrological processes (Lettenmaier, 2008). A total overview of parameters is given in Appendix F.

Considering this complexity, choices must be made regarding calibration parameters. Therefore, calibration for DHSVM is generally performed manually and by iteration. This has the disadvantage that results are more difficult to reproduce, due to the dependency on the knowledge of the modeler. Moreover, the large numbers of parameters are also making it more difficult for the modeler to find an optimal model performance, because of possible interdependency between parameters. Also the long simulation runs are making it a time consuming activity. By using the modified version of DHSVM with the deep groundwater component, calibration becomes even more complex. The deep groundwater component also contains parameters which are likely to be potential calibration parameters. Yet, good results have been obtained by applying manual calibration of DHSVM. Univariate calibration have been successfully applied multiple times, in spite of the complexity of optimal parameter settings (Vanshaar et al., 2002b; Chen et al., 2005; Cuo et al., 2006; Kelleher, 2006; Thanapakpawin et al. 2007).

To create insight in parameter sensitivity, a sensitivity analysis is conducted to study sensitivity of streamflow to changes in parameters prior to calibration. Results of the sensitivity analysis are interpreted by sensitivity to model assessment criteria. Subsequently, two separate calibration methods are done to optimize model performance of simulated streamflow. First, a univariate calibration is performed, and second, a bivariate calibration. All calibration simulations were done with the same initial condition files to provide similar conditions for each simulation. Calibration simulations were done for the period from November 5th 2005 to June 1st 2006. For this period a complete record of hourly streamflow was available.

Sensitivity analysis

In the sensitivity analysis the sensitivity of streamflow to changes in parameters is determined. With a default parameter setting, values of these parameters are varied one at a time. In the official version of DHSVM, soil parameters are commonly used as calibration parameters (Lettenmaier, 2008; Cuo et al., 2006; Kelleher, 2006; Thanapakpawin et al., 2007). Mentioned key soil parameters are soil depth, soil lateral hydraulic conductivity, exponential decrease in depth, vertical hydraulic conductivity, and maximum infiltration rate. These parameters are all assigned to a specific soil type except for soil depth. The generated soil depth grid for the study area can be adjusted by a multiplier. Soil lateral hydraulic conductivity represents the lateral movement of water through a saturated pixel and is the single most important calibration parameter (Wigmosta et al., 2002). This parameter is influenced by the exponential decrease in depth of lateral flow. The maximum infiltration rate determines the maximum rate of infiltrated water into the soil. Finally, vertical hydraulic conductivity (K_{sat}) influences the vertical water flow from the unsaturated

zone to the saturated zone. This parameter can be adjusted for different root layers, but is assumed to have one value due to lack of data regarding root zones. As previously outlined, the standard SSURGO soil map is used because it covers already the whole study area. In case of sensitivity of streamflow to change in K_{sat}, the spatial distributed map from chapter two is used and analyzed.

Mentioned key geological calibration parameters in the modified version of DHSVM were not found in literature. These parameters are also probably influencing streamflow. Similar to soil parameters, they have separate conductivity parameters (vertical and horizontal) which affect the amount of subsurface flow to streamflow (PRISM and CIG, 2008). Considering the deep groundwater layer, three geological parameters were also selected to test model sensitivity on streamflow: geological vertical conductivity, geological lateral conductivity, and geological base layer conductivity. The base layer conductivity indicates the rate of deep loss of ground water and this flow of water will never return (Figure 3.2). This parameter can possibly be used as a representative groundwater extractor, i.e., groundwater pumping and loss through dike complex. All parameter used for the sensitivity analysis are outlined in Table 3.2.

Table 3.2 Default values of soil and geology parameters for sensitivity analysis derived from literature

Soil Parameters	*Silty Clay Loam*	*Clay Loam*	*Silty Clay*	*Muck*
Lateral Hydraulic Conductivity (m/s)	0.01	0.01	0.01	0.01
Exponential Decrease (-)	3.0	3.0	3.0	3.0
Maximum Infiltration Rate (m/s)	3.E-05	1.E-05	1.E-05	1.E-05
K_{sat} (m/s)	0.01	0.01	0.01	0.05

Geological Parameters	*Alluvium*	*Basalt*	*Breccia and Tuff*
Lateral Conductivity (m/s)	1.E-06	1.E-06	1.E-06
Vertical Conductivity (m/s)	5.E-06	1.E-06	1.E-07
Base Layer Conductivity (m/s)	1.E-09	1.E-10	1.E-12

Constant Basin Parameter	*Study Area*
Soil Depth (m)	0.85-1.5

Univariate Calibration

This method is mostly applied to calibrate DHSVM (Vanshaar et al., 2002b; Chen et al., 2005; Cuo et al., 2006; Kelleher, 2006; Thanapakpawin et al. 2007). Univariate calibration involves varying the value of one parameter while the other parameters remain constant. This method is an iterative procedure and it focuses first on parameters which are relevant to calibrate the total water balance. The total simulated streamflow should be similar to observed streamflow. Subsequently, another set of parameters are varied to calibrate the shape of the hydrograph in order to fine tune the model performance.

Multivariate / bivariate calibration

Bivariate calibration is chosen to provide more insight in interdependency between parameters. From default settings, this involves varying two (bivariate) parameters keeping the other parameters at their default level. In this study one pair of interdependent parameters is studied to find eventually an optimal model performance. This type of

calibration method has not explicitly been conducted explicitly in DHSVM studies and can be relevant to provide better optimal model performance between parameters.

3.7.2 Validation

Calibration is the process of fine tuning a model and validation is a confirmation whether optimized calibration settings are also sufficiently simulating observed streamflow during other periods. In this study it concerns the two calibration settings. Subsequently, the model is considered validated if the results from the validation period are approximately similar to the calibration period. The period of validation is from November 1st 2006 to June 1st 2007.

3.7.3 Model assessment & assumptions

In order to determine model performance during calibration and validation, and to avoid subjectivity, assessment criteria are used. In this study a multi-objective function Y is used which takes into account Nash and Sutcliffe coefficient (1970) (NS) and the Relative volume Error (RE) (Akhtar et al., 2008):

$$Y = \frac{NS}{1+|RE|} \tag{3.1}$$

$$NS = 1 - \frac{\sum_{i=1}^{i=N}\left[Q_s(i) - Q_0(i)\right]^2}{\sum_{i=1}^{i=N}\left[Q_o(i) - \overline{Q}_0\right]^2} \tag{3.2}$$

$$RE = 100\frac{\sum_{i=1}^{i=N}\left[Q_s(i) - Q_0(i)\right]}{\sum_{i=1}^{i=N} Q_o(i)} \tag{3.3}$$

Where i is the time step, N is the total number of time steps, Q_s is simulated discharge ($m^3 s^{-1}$), Q_o is the observed discharge. For good model performance NS should be close to unity and RE to zero. Subsequently, Y should also be close to one. Streamflow was usually assessed in previous DHSVM studies by using NS. Resulting in -0.76 to 0.5, (Cuo et al., 2006) and -2.22 - 0.79 (Thanakpakwawin et al., 2007), various results of model performance can be expected.

3.7.4 Scenario analysis

The possible impacts of groundwater pumping, rainfall, and vegetation changes on streamflow is studied by using available information regarding these factors and translating them into best possible model scenarios. Periods used for these scenarios are depending on calibration and validation performance. When validation shows good model performance, the validation period is used. Otherwise, the best performing calibration simulation is used due to lack of more periods of meteorological data. Using DHSVM for this purpose should provide more insight in suitability of this model to model the effect(s) of changing vegetation patterns, climate, and groundwater pumping on streamflow in Mākaha Valley.

Groundwater pumping

Mair et al. (2007) studied effects of groundwater pumping on streamflow. The number of dry stream days between the pre-pumping (1960-1990) and pumping period (1991-2005) increased from 8 to 125 days a year. The mean and median annual streamflow declined 42% and 56% respectively. Information of monthly groundwater pumping data is available for year 2005 and 2006 (Appendix G) and descriptive statistics in Table 3.3 for a larger period (Mair et al., 2007). Annual mean pumping is 116m with a minimum and maximum of 22 and 302 mm respectively over the whole subwatershed. In this case two scenarios are implemented. Scenarios are provided with similar conditions to model streamflow subject to groundwater pumping, the base layer conductivity is iteratively adjusted so that it approximately approached minimum, mean, and maximum groundwater extraction amounts.

Table 3.3 Descriptive statistics for streamflow and groundwater pumping (Mair et al., (2007))

Period	*Parameter*	*Stream Gage*	*Ground-Water Pumping**
1960–1990	Mean	324	–
	Standard deviation	146	–
	Standard error	26	–
	Median	312	–
	Minimum	127	–
	Maximum	620	–
	N	31	–
	Missing	0	–
1991-2005	Mean	189	116
	Standard deviation	183	78
	Standard	47	20
	Median	137	103
	Minimum	12	19
	Maximum	747	309
	N	15	15
	Missing	0	0

Units in mm⁄ yr.
* Collective pumping rate for three wells in subwatershed

Rainfall

Data of rainfall are available from 1960 -2005. Decrease in rainfall has been studied by comparing two periods of pre-pumping (1960-1990) and pumping (1991-2005) (Mair et al., 2007). Between these two periods mean annual rainfall significantly declined by 14% at the outlet of the subwatershed. On the other hand, the upstream part on Mt. Ka'ala did not show decline in rainfall between pre-pumping and pumping period (Mair et al., 2007). There may be a decrease in rainfall, but no trend has yet been discovered. A realistic scenario regarding decrease in rainfall can therefore not be implemented. Yet, to determine sensitivity of streamflow subject to change in rainfall a scenario is implemented by decreasing annual hourly rainfall with 15% (≈ 14% decrease in rainfall). To determine how streamflow is affected by increase in rainfall, hourly rainfall is also increased with 15%. It can be useful to gain knowledge on how streamflow responds to both changes in rainfall.

Vegetation

The increase of invasive species is likely to alter the ecosystem of a watershed in Hawai'i. Exact numbers of vegetation changes have also not been studied yet for Mākaha Valley. Trends of invasive species are observed and a vegetation map has been generated which partially assessed the degree of invaded native species by alien plant species (Harman, 2006). Also the effects of vegetation changes can not yet be directly translated into model scenarios. Yet, in order to provide an idea of the effect of vegetation changes on change in streamflow two scenarios are implemented.

First, default vegetation classes are changed into all bare ground. Bare landcover has neither an overstory nor an understory and is basically a soil surface and can be relevant to study. It is likely to increase streamflow by lack of intercepted water by vegetation. It also has an affect on evapotranspiration because there is only evaporation from soil. Second scenario is changing default vegetation classes into all evergreen forest. Trees have a dominant effect on evapotranspiration, due to evaporation from rainfall interception by vegetation and transpiration by absorbing water from roots.

3.7.5 Model assumptions

Modeling streamflow is inherent to assumptions regarding DHSVM and data: (1) recorded streamflow data and meteorological data are assumed to capture climatic conditions within the Mākaha Valley subwatershed, and (2), input file parameters are a sufficient representation of Mākaha Valley subwatershed, except for calibration parameters.

3.8 Results

3.8.1 Data

Processing input data resulted in an elevation, watershed mask, soil depth, geology, soil type, vegetation, and a derived stream network map. All maps are converted into floating binary files required by DHSVM. This input comprises topographical representation of Mākaha Valley subwatershed. In addition, six meteorological data files have been processed containing hourly temperature, humidity, precipitation, incoming shortwave, longwave radiation, and wind speed data. All input data is assumed to spatially represent model forcing data for Mākaha Valley subwatershed.

3.8.2 Calibration

Sensitivity analyses

The multi-objective function Y values were calculated for default values. All mentioned soil and geological parameters were simulated ranging at least within 50% and 150% of the default values and values of Y were also calculated (Figure 3.4 and 3.5). In contrast to other DHSVM model studies, more parameters can be calibrated for streamflow than usually was done for calibration (Cuo et al., 2006; Kelleher, 2006; Thanapakpawin et al., 2007). Parameters showed high sensitivity to change in streamflow and therefore model performance. Concerning soil parameters, the vertical hydraulic conductivity showed very low sensitivity to change in streamflow, whereas it can be an important parameter during rainfall excess events (Singh and Woolhiser, 1978). Although default values of this parameter (0.01 m s^{1} = 3600 cm h^{-1}) are already too high for Mākaha Valley, decreasing this

parameter is not affecting streamflow. The vertical hydraulic conductivity only accounts for vertically movement of water flow in a pixel and is of less importance than the lateral conductivity which accounts for the whole horizontal soil profile ending up in streamflow. This implies that spatial distributed map of K_{sat} is not having a significant effect on streamflow, confirming that it has not yet relevancy for this model study.

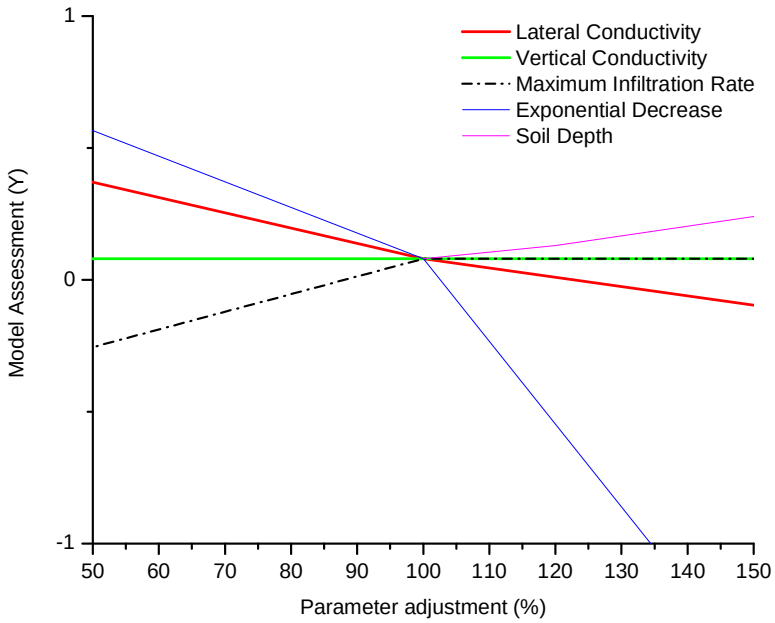

Figure 3.4 Sensitivity analysis for soil parameters

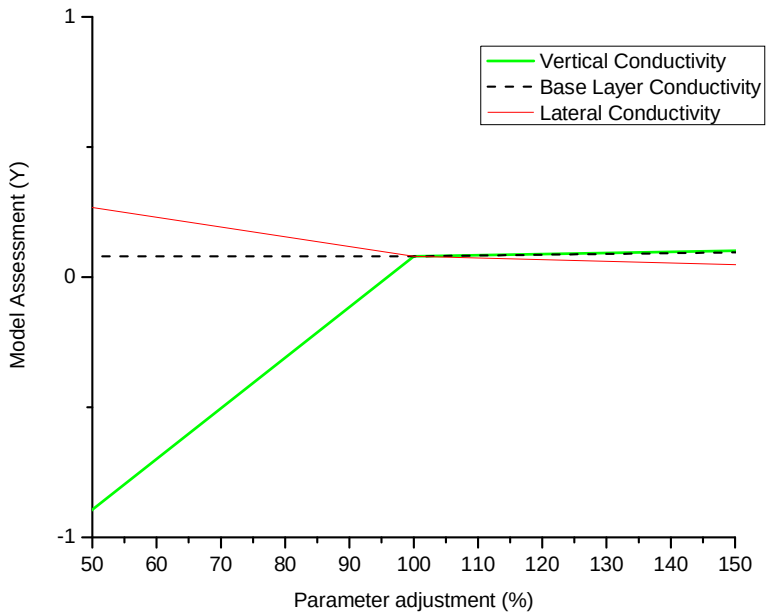

Figure 3.5 Sensitivity analysis for geological parameters

As suggested, soil lateral conductivity is also a calibration parameter as this is the most used calibration parameters and sometimes also the only one (Lettenmaier, 2008; Kelleher, 2006; Thanapakpawin et al., 2007). This also accounts for exponential decrease in depth which is also very sensitive. Both parameters delay subsurface flow to streamflow and are likely interdependent. These parameters can be considered as lumped parameters and therefore account for the whole watershed. The maximum infiltration rate also showed low sensitivity. However, it influences peak flows by increasing overland flow when rates are set at lower values. Increasing soil depth gave streamflow much higher baseflow. Soil depth has only been increased by multiplying the initial soil depth with 1.2, 1.5, and 2.0 (Y=0.13, 0.24, 0.11). Decreasing soil depth was not possible because of the root depths of vegetation which need to smaller than the soil depth. Otherwise it conflicts with the root depth settings from vegetation parameters. Soil depth is inherent to the subsurface water capacity and reaction time of eventually discharge. Initially a thinner soil depth was taken which makes it more sensitive to large rain events, and subsequently, higher peak flows occur. However, the shape of the hydrograph runs less smooth back to baseflow so that it will represent the shape of observed discharge not as good when having a ticker soil depth.

Geological parameters were also tested and responded approximately equivalent to changes in soil parameters on Y. Geological lateral conductivity and vertical conductivity are sensitive and have more or less the same function as both soil conductivities. Base layer conductivity is influencing the total volume by loss through deep drainage. At first sight this parameter showed very low sensitivity to change streamflow, but that is due to a very low default value (Table 3.2). Increasing this parameter with several orders of magnitude did is improve model performance significantly.

Based on model assessment performance and sensitivity to change in streamflow, several parameters are used for calibration of streamflow. Using geological lateral and vertical hydraulic conductivities as calibration parameters are excluded. These parameters function similar to soil conductivity parameters and possibly provides multiple optimal parameter settings, i.e., equifinality. This makes calibration much more complex and disorderly. Only the base layer conductivity parameter is included as a calibration parameter from the geological parameters. This choice is made because the base layer conductivity can provide more insight regarding loss of water in the subwatershed. Since the soil parameters soil depth, lateral hydraulic conductivity, maximum infiltration rate, and its exponential decrease in depth have shown changes in streamflow and also Y, these parameters are also included for calibration.

Univariate calibration

The order of used parameters of this calibration is shown in Table 3.4. Concerning a univariate calibration, a stepwise optimization was performed as is usually applied. In this case it started with simulation of the total water balance. The total water balance is iteratively adjusted since the default simulation is overestimating the total volume of calibration largely and in particular baseflow (RE= 0.939). Available parameters for this purpose are soil depth and also base layer conductivity due to loss of water. Both parameters affect the total capacity of holding water in the soil and are adjusted until good model performance is obtained. First soil depth was multiplied with 1.5. Adjusting soil

depth is rather an arbitrary assumption than a parameter for finding an optimal model performance. Soil depth was multiplied by 1.5 and gave better model performance Y than multiplying soil depth with 1.2 and 2.0. Subsequently, base layer conductivity was iteratively adjusted (5e-7m s^{-1}) until best model performance Y is obtained.

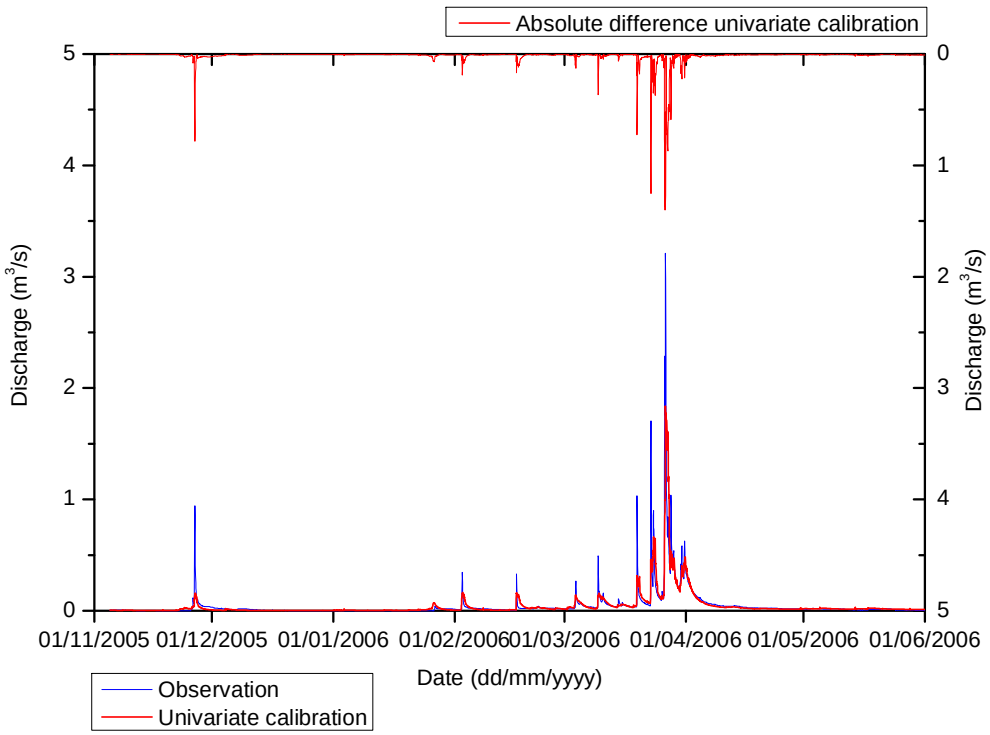

Figure 3.6 Univariate calibration with soil depth=x 1.5 , base layer conductivity=5e-7 m s^1, lateral conductivity=0.01m/s, exponential decrease=3.0, and max infiltration rate=4e-5 m s^1 (Y=0.732, NS=0.733, RE=-0.0003)

Then, calibration parameters as lateral hydraulic conductivities, its exponential decrease in depth, and maximum infiltration rate were adjusted to obtain better model performance. However, model performance did not improve by varying lateral hydraulic conductivity and exponential decrease. Finally, by varying maximum infiltration rate model performance gave reasonable results (Y=0.73, NS=0.733, RE=-0.0003), because of a slightly increase of peak flow (Figure 3.6).

Table 3.4 Calibration parameters used for both calibration methods.

Univariate calibration Parameters	*Bivariate calibration parameters*
1. Soil depth (multiplier)	- Soil lateral hydraulic conductivity (m/s)
2. Base Layer Conductivity (m/s)	- Exponential Decrease (-)
3. Lateral Conductivity (m/s)	
4. Exponential Decrease (-)	
5. Maximum Infiltration Rate (m/s)	

Bivariate calibration

This calibration takes into account the interdependency between the lateral conductivity and exponential decrease. Both parameters affect the subsurface flow directly and influence both volume and shape of the hydrograph. Bivariating these two parameters yield possibly an optimal combination. Forty-seven simulations were performed where lateral conductivity has been varied between 2.5e-4 m s^{-1} and 1e-2 m s^{-1} and exponential decrease in depth between 3.0 and 8.0. A good optimal value (Y=0.781, NS = 0.78, RE = 0.003) was found between those ranges (Figure 3.7 and Table 3.5).

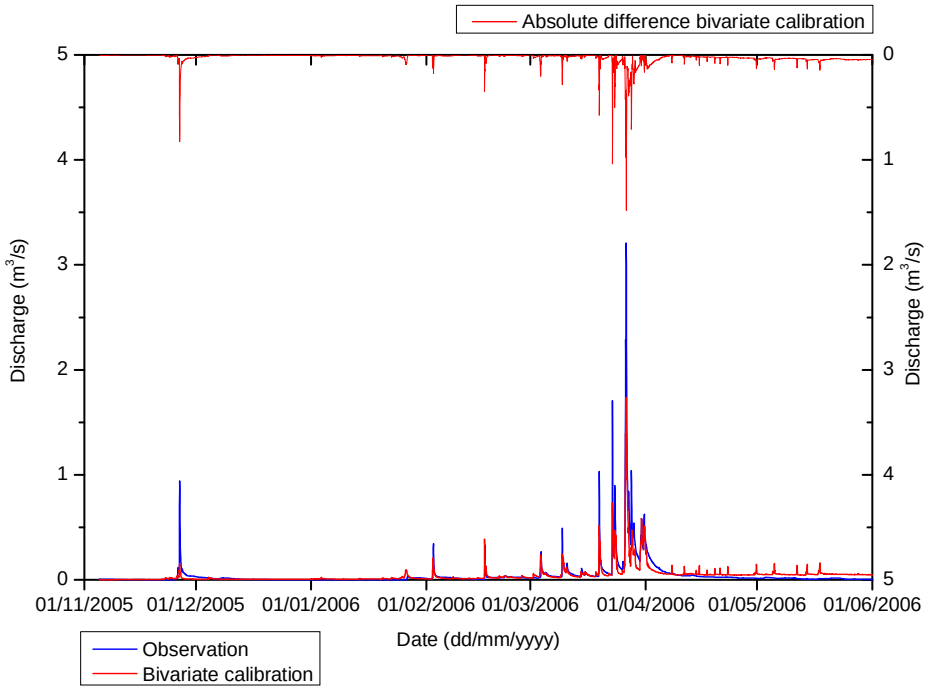

Figure 3.7 Bivariate calibration with lateral conductivity=0.0085m/s, exponential decrease=7.5 (Y=0.78, NS=0.78, RE=0.003)

Table 3.5 Result of bivariate calibration by varying soil lateral conductivity and exponential decrease in depth. Optimal value of Y is determined at 0.0085 and 7.5 (Y=0.781)

Y	Lateral conductivity (m/s)	0.0045	0.0055	0.0065	0.0085	0.01
Exponential decrease (-)						
5		0.687	0.69	0.69	0.677	0.666
5.5		0.711	0.714	0.721	0.716	0.698
6		0.728	0.732	0.781	0.741	0.731
6.5		0.742	0.745	0.747	0.759	0.745
7		0.746	0.757	0.759	0.772	0.763
7.5		0.73	0.753	0.771	**0.781**	0.776
8		0.716	0.739	0.755	0.768	0.778

3.8.3 Validation

Two validation simulations were performed with univariate and bivariate calibration settings. Results are shown in Figure 3.8 and Table 3.6. Model performance is relatively poor (Y= 0.24 and 0.28 respectively). In particular, peak flows showed very poor simulations for both validation simulations. The total volume of simulations overestimated the observed discharge also largely (RE=0.50 and RE=0.70).

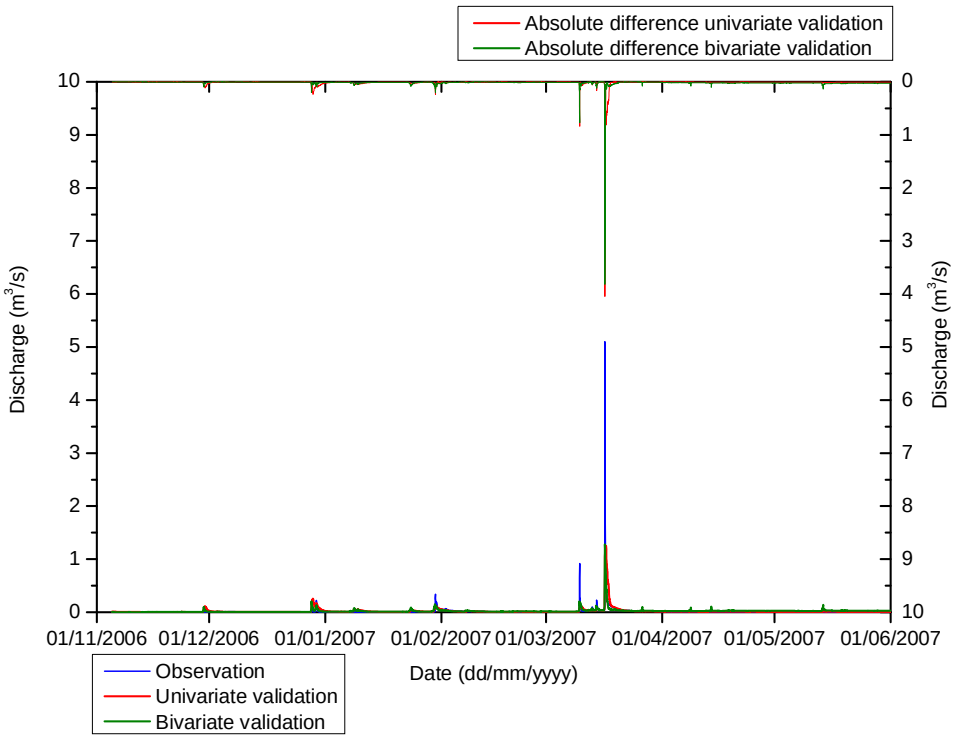

Figure 3.8 Two validation simulations (Univariate validation: Y=0.24, NS=0.36, RE=0.50; Bivariate validation: Y=0.28, NS=0.48, RE=0.70)

Table 3.6 Mass balance from calculated from DHSVM calibration (11-2005 – 05-2006) and validation simulations (11-2006 - 05-2007)

	Univariate calibration	*Univariate validation*	*Bivariate calibration*	*Bivariate validation*
Initial Storage (mm)	**1368**	**1368**	**1368**	**1368**
Final Storage (mm)	**2063**	**1771**	**2097**	**1798**
Input (mm)	**1260**	**968**	**1260**	**968**
Precipitation (mm)	1260	968	1260	968
Output (mm)	**565**	**565**	**531**	**538**
Runoff (mm)	144	69	142	72
Evapotranspiration (mm)	388	466	389	466
Loss to deep groundwater zone (mm)	33	30	0.34	0.32

3.8.4 Scenario analysis

Groundwater pumping

Base layer conductivity was iteratively adjusted to $1e^{-7}$ m s^{-1} and $4e^{-7}$ m s^{-1} (compared to 1e-12 m s^{-1} for calibration) so that deep losses from groundwater were 73 mm and 275 mm (Figure 3.9, Table 3.7). These values represent approximately the amounts of yearly mean and maximum values for groundwater pumping over the past years. Results of streamflow change by adjusting the base layer conductivity ($1e^{-7}$ m s^{-1}), illustrates that streamflow is relatively not so sensitive to average groundwater pumping for both baseflow and peakflow. For maximum pumping, streamflow was significantly changed (Figure 3.9, Table 3.7) and largest peakflow decreased with 0.8 m^3 s^{-1}. Baseflow decreased to zero streamflow from April 2006 whereas bivariate calibration still showed baseflow during this period. Both peak and baseflow decreased because three times more water (than average pumping) becomes available in the geological framework than pumping. This implies that there is also three times more water contributed from the upper soil layer to the geological framework. Consequently, less water is present in the upper soil layer so that water storages from soil are significantly less contributing to streamflow. Total runoff also decreased more than two times (Table 3.7).

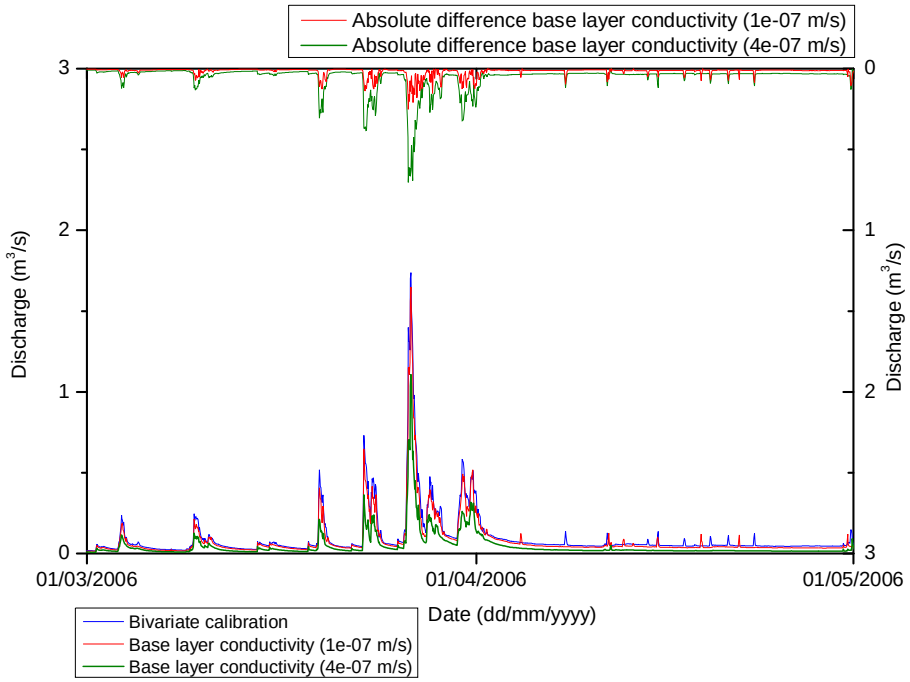

Figure 3.9 Streamflow changes by adjusting the base layer conductivity, and absolute differences for bivariate calibration data

Table 3.7 Water balances of implemented scenario simulations

	Index	***Groundwater pumping***		***Rainfall***		***Vegetation***	
	Bivariate calibration	*Base layer conductivity (1e-07 m/s)*	*Base layer conductivity (4e-07 m/s)*	*+15%*	*-15%*	*Bare*	*Evergreen forest*
Initial Storage (mm)	**1368**	**1368**	**1368**	**1368**	**1368**	**1368**	**1368**
Final Storage (mm)	**2097**	**2049**	**1900**	**2216**	**1965**	**2070**	**2010**
Input (mm)	**1260**	**1260**	**1260**	**1450**	**1070**	**1260**	**1260**
Precipitation (mm)	1260	1260	1260	1450	1070	1260	1260
Output (mm)	**531**	**579**	**728**	**602**	**473**	**558**	**618**
Runoff (mm)	142	117	64	201	97	139	120
Evapotranspiration (mm)	389	389	389	401	376	419	498
Loss to deep groundwater zone (mm)	0.34	73	275	0.35	0.32	0.34	0.34

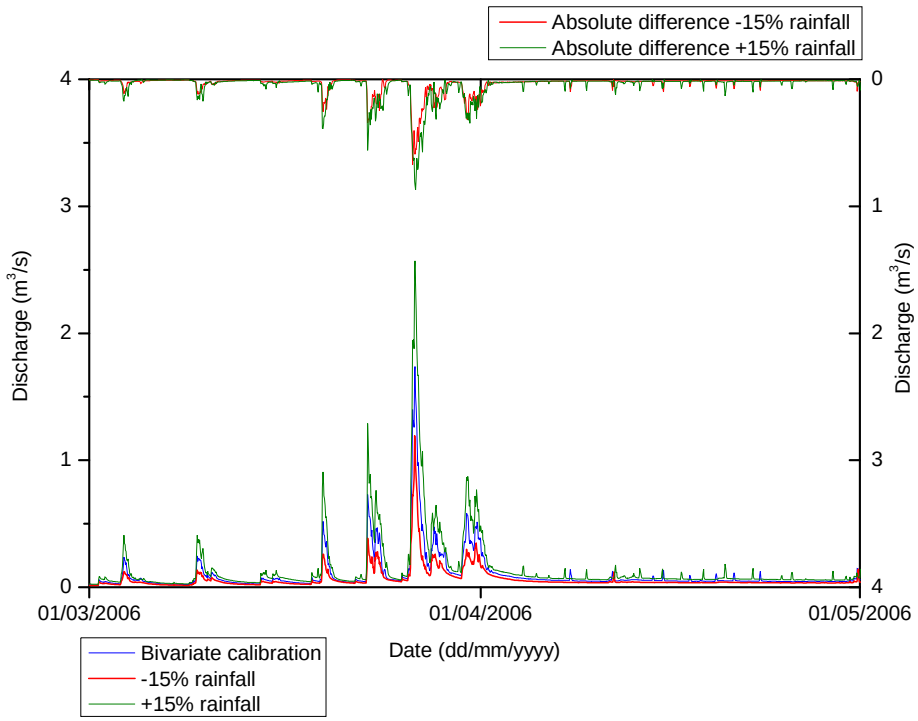

Figure 3.10 Streamflow changes by increasing and decreasing annual hourly rainfall with 15%, and absolute differences for bivariate calibration data

Rainfall

No trends in rainfall have been studied yet, but a decrease and increase of hourly rainfall data with 15% showed that there is only a large sensitivity noticeable in peakflows (Figure 3.10). Baseflow is almost not affected by this change of weather condition. For this calibration deep loss is unaffected, meaning that rainfall is hardly increasing groundwater storages. Total runoff in both scenarios also increased and decreased significantly compared to bivariate calibration (Table 3.7).

Vegetation

By changing the vegetation into complete bare landcover or evergreen forest, almost no sensitivity was noticeable for streamflow (Figure 3.11). Total runoff was not significantly different, even though no rainfall was intercepted by vegetation (8% for calibration and 17% for evergreen forest). However, other components of the water balance are affected as there has been calculated a significant increase in evapotranspiration (Table 3.7). This is common for a study area totally covered by evergreen forest. Remarkable is that the bare landcover scenario also increased evapotranspiration compared to bivariate calibration and only gave slightly less total runoff. Usually less water is removed and there is no interception by vegetation, which can provide higher peakflows. However, DHSVM calculates the evaporation from saturated soils at the potential evaporation rate. The evaporation rate increases as the soil water content is near saturation (Wigmosta et al., 2002). Since the upper soil depths are also relatively shallow (maximum 1.5m) and near saturated pixels were likely occurring, it possibly caused the increase in evapotranspiration. For large areas containing shrubs (only an understory) less water was evaporated than a bare landcover simulation.

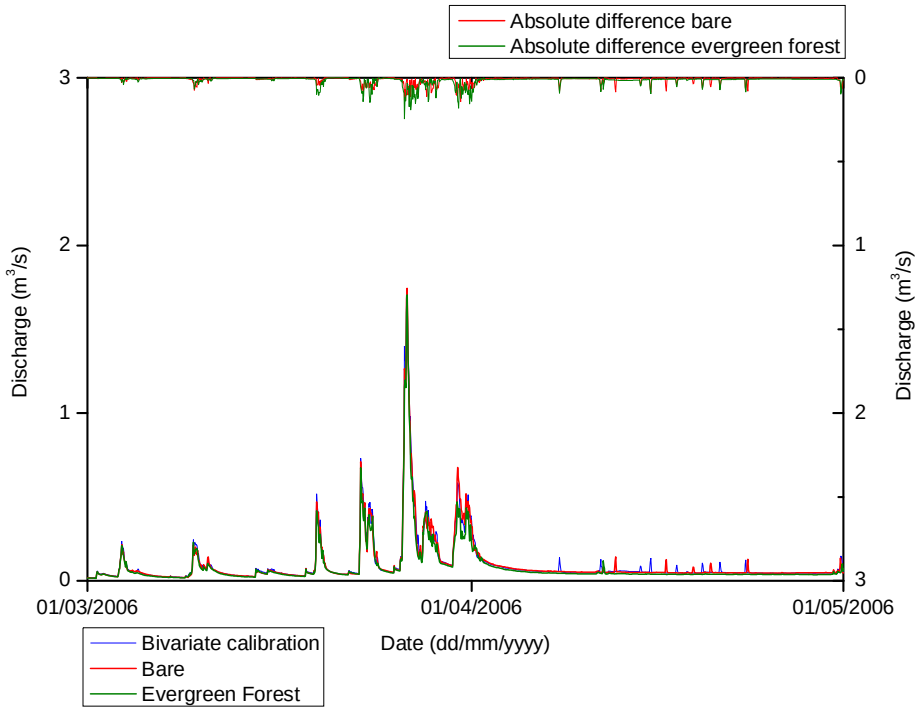

Figure 3.11 Streamflow changes by changing all original vegetation classes into bare and evergreen forest, and absolute differences for bivariate calibration data

3.9 Discussion

Calibration

Calibrating sensitive parameters not always improves model performance in combination with other parameters. One optimal value of a parameter can impede other optimal

parameter setting so that it can not increase model performance. This can be contributed to interdependency between parameters. Subsequently, several parameter settings possibly lead to an equally acceptable model performance of simulated streamflow and this is called equifinality (Beven and Freer, 2001). Several parameters of DSVM models are likely interdependent. They affect each other in which they affect streamflow. The two parameters exponential decrease in depth and the lateral hydraulic conductivity are examples of interdependent parameters. Both parameters influence the movement of subsurface flow and final calibration values of these parameters with bivariate calibration are both impeding subsurface flow. If only the lateral conductivity was varied and calibrated, the final calibration setting of this parameter is a low value. Changing the exponential decrease parameter has no significant influence on streamflow anymore. This also accounts for the opposite case. Supposedly, when conductivities in the geological framework are calibrated, it gives even more calibration possibilities and an optimal parameter setting is even more difficult to achieve in DHSVM. Therefore in this case, a reasonable model performance is not always reflecting the most optimal calibration setting.

Both calibrations showed reasonable model performance, however, differences between the two calibration methods are clearly visible with respect to both baseflow and peak flow. Bivariate calibration simulated peak events slightly better than the univariate calibration. Recession curves and baseflow were better simulated by univariate calibration. The use of the base layer conductivity with univariate calibration caused a significant decease in baseflow (almost no baseflow). Since observed streamflow is not perennial (mean of 125 dry stream days), univariate calibration is closer to dry streamflow conditions, however model performance was less good. Conversely, bivariate calibration settings did not reduce base flow as univariate calibration settings did. Bivariate calibration still showed baseflow during April and May 2006 (Figure 3.7), whereas no streamflow was observed during the same period. This can be imputed to geological and soil parameter settings. There was almost no deep loss to groundwater so there is also less exchange between the geological framework and the upper soil layer. Because of the relative shallow soil depth, more water is available in subsurface flow so that it continuously can contribute to baseflow.

Although univariate calibration simulated good baseflow, the value of base layer conductivity extracted more groundwater than actual groundwater pumping did (33 mm against 6.58 mm equivalent depths over the subwatershed). Contrary, bivariate calibration had almost no deep groundwater loss (0.34 mm). Concerning pumping data, it should be noticed that mean annual groundwater pumping (116 mm equivalent over the subwatershed) can be much larger. It is also possible that water can disappear through dike complexes in the geological framework and never flows into streamflow (Mair, 2007, personal communication). This implies that there is a large uncertainty in groundwater flow in the geological framework. However, since base layer conductivity significantly influenced baseflow, and groundwater pumping is usually larger, it is likely that groundwater extraction is considerably influencing baseflow.

In spite of reasonable model performance with calibration, both calibrations are still subject to significant errors and uncertainties. In accordance with Waichler et al., (2004), who also concluded for this modified version of DHSVM, that these uncertainties exist due to lack of data limited initial calibration and verification due to expansion of the modified

model. For these calibration errors can be assigned due to lack of groundwater storage data. In this case an improvement is providing water table depth data. Other possible improvements are using different observed variables as soil moisture and evapotranspiration (Cuo et al., 2006). Other improvements of calibration in DHSVM should focus on better parameter optimization of the usual calibration parameters by studying more interdependent parameter combinations. Bivariate calibration obtained good model performance. By studying interdependency, also automatic calibration becomes an option so that the calibration process can be done faster and more accurately.

Validation

Again, peakflows were largely underestimated. Noticeable also is that the validation period had significant less rainfall and streamflow. The uncertainty in groundwater storages is complicating validation. Exchanging calibration and validation period may be useful to compare settings for further study and short time series of meteorological data. For further research it may be better to use approximately similar conditions for calibration and validation. This is because groundwater pumping rates are varying per year and this has a different impact on streamflow. In this case, also different conditions affected evapotranspiration rates. Total output during validation is not significant less than calibration, but evapotranspiration is clearly larger during validation (Table 3.6). A possible explanation is that evapotranspiration was more influenced by interception of rainfall by vegetation (Wigmosta et al., 2002). Since precipitation decreased, relative more rainfall is intercepted by vegetation and more evapotranspiration can occur. Prior estimates of rainfall lost to evapotranspiration over the entire Mākaha watershed are ranging from 34% (Mink, 1978) to 79% (Takasaki, 1971). Lao (2002, HBWS, unpublished report) estimated evapotranspiration to be 59% of the rainfall. Yet, conclusions can not be drawn since evapotranspiration during calibration and validation was calculated at 31% and 48% of total rainfall and also seemed to be fluctuating.

Scenario analysis

Simulations subject to groundwater pumping confirmed that this likely has an impact on streamflow since it affects groundwater storages and baseflow. Although exact quantification is still very uncertain, literature showed that the number of dry stream days increased (no runoff at stream gage) between periods of pre-pumping (Table 3.3) and pumping from 8 to 125 days (Mair et al., 2007). Groundwater flows should be studied extensively, because isolated water in dike zones are also possible causing different contributions to streamflow. They provide different groundwater storages and water table depths in contrast to a normal mountainous watershed with a hydraulic gradient assumption for groundwater as used in DHSVM. Groundwater pumps are located in the lower part of the subwatershed and this area is likely to have different groundwater storages and water table depths than the upstream part of the study area. The deep groundwater component in this study did not provide sufficient information of groundwater flow and losses. To deal with this complex dike system, more detailed geological data is required concerning dike zones water table levels. A detailed groundwater model that can deal with complex dike complexes can be used. Monthly pumping data were obtained, but providing

hourly pumping data would provide more information on temporal fluctuations in pumping and response in streamflow.

Changes in rainfall changed peakflows, but this was likely not affecting baseflow. This simulation had not deep loss and so that groundwater storages could contribute to baseflow. However, again there is also still a large uncertainty. It was not possible to implement a real representative scenario due to lack of clear rainfall trends. Although rainfall stations were available in relative high density, more research is desired to determine the exact distribution of rainfall and trend analysis of rainfall to determine the effect of rainfall on streamflow.

In accordance with Thanapakpawin et al., (2007) (section 3.3), small changes of streamflow were noticeable by changing vegetation. Although vegetation changes did not provide significant changes in streamflow, it likely alters ecosystems in other ways. Evaporation from interception by vegetation can also be an important component contributing to changes in the water balance. Mair (2007, personal communication) determined that total interception of rainfall by vegetation can be 30%, whereas a full evergreen forest only calculates 17% of rainfall. In addition, the bivariate calibration simulation calculated only 8% evaporation from intercepted rainfall by vegetation. Taking this into consideration, calibration should also focus on vegetation parameters affecting the amount of rainfall interception by vegetation. An example is the LAI multiplier which alters the Leaf Area Index (LAI). The Leaf Area Index is the ratio of total upper leaf surface of vegetation divided by the surface area of the land on which the vegetation grows.

Finally, DHSVM showed to be an extensive hydrological model which captures streamflow and taking into account many hydrological processes. Since this model is considered as a physically based model, many data and parameters are required to successfully simulate streamflow. Yet, it seemed that the groundwater component is still not sufficient because of lack of sufficient groundwater data. Nevertheless, it is a suitable hydrological model when sufficient data are available and an integrated watershed approach is still desired.

Chapter 4

Conclusions & Recommendations

4.1 Conclusions

The objective is to investigate the impact of groundwater pumping, changing rainfall, and vegetation changes on streamflow in Mākaha Valley. To establish this objective, the following two studies have been conducted in following order: 1) Investigating the spatial distribution of the infiltration rates across the study area, and 2) assessing the performance of an integral watershed model, DHSVM, in describing streamflow of the watershed.

4.1.1 Spatial variability of infiltration in Mākaha Valley

By using the tension infiltrometer (TI) and the two tension method, saturated hydraulic conductivity (K_{sat}) was determined. K_{sat} is an indication for the infiltration rate and is often an important parameter input parameter for hydrological models. 54 field measurements were taken based on prior chosen locations regarding slope, elevation, aspect, and vegetation. In addition, soil core samples were taken at each measurement location to determine porosity (θ_t) and dry bulk density (ρ_b) to use for additional geospatial interpolation. Taking measurements on the wetland area at the top of Mt. Ka'ala was not allowed due to restricted access. It was almost not possible to take measurements outside the alluvium area because of very steep slopes. Lower tension measurements (-2 cm) appeared to be more difficult for making a good contact than higher tension (-8 cm). Macropores such as wormholes or root holes under the sample locations possibly caused extremely high values of K_{sat} during low tension measurements. Two measurements were excluded based on field experiences.

Descriptive statistics showed large variability in values of K_{sat} (0.39 – 442 cm h^{-1}), a minimum value for ρ_b (0.48-1.15 g cm^{-3}), and a high maximum value for θ_t (0.48-0.80). A calculated p-value ($p > 0.05$) confirmed the lognormal distribution of K_{sat} by Shapiro-Wilk and was required for ANOVA. ANOVA was calculated for five topographical characteristics. Stream areas, ridges, and gulches were found to have significantly different means for K_{sat} at $p = 0.05$ level of confidence, which are different means of measurements taken nearby the stream, on top of the ridges, and in gulches ($p = 0.04$). No other topographical elements were found to have significantly different means for K_{sat}. ρ_b showed significantly different means for different elevations and highly significance for hydrologic soil groups (B and C). θ_t also showed a significant difference between areas nearby the stream, on ridges, and in gulches. A necessary assumption and confirmed for ANOVA with significant differences was that measured variables, divided in these topographical aspects, were found to have equal variances by using Levene's Test. Pair wise comparison of means (Fisher's LSD) showed that a significant different mean was found between stream and

gulch for K_{sat} and for θ_t. ρ_b showed a significantly different mean for measurements taken lower than 525 m and higher 525 m. Finally, no correlations were found between K_{sat} and other variables. This means that geospatial interpolation as cokriging is not relevant. Also confirmed by the semivariogram analysis was that K_{sat} did not show spatial correlation so that geospatial interpolation was excluded.

To obtain a representative spatial distribution of K_{sat}, information of K_{sat} was obtained from ANOVA and Fisher's LSD by dividing the subwatershed in three distinctive areas: stream area, ridges, and gulches. Results from notes taken during the measurements were not sufficient to spatially distribute K_{sat} over a watershed. Therefore, a GIS extraction method was used to indentify these three topographical elements in the study area. From observations, slope and flow accumulation were appropriate indicators to determine stream areas, ridges, and gulches for Mākaha Valley. This method only gives an approximately spatial representation of significantly different means in which K_{sat} was measured across the study area. The map can possibly be used as a spatial model input map by using the significantly different mean values of K_{sat} obtained from Fisher's LSD. The method relies on accuracy of the GPS receiver and aggregated GIS data and it only covers the alluvium part of the study area.

4.1.2 Modeling streamflow using the Distributed Hydrological Soil Vegetation Model (DHSVM)

This model requires meteorological data, a digital elevation model (DEM), a watershed boundary, a flow network, terrain shadowing, percent open sky, vegetation data, soil (depth)data, and geological data. Six meteorological data files were processed containing hourly temperature, humidity, precipitation, incoming shortwave, longwave radiation, and wind speed data. Model sensitivity analysis showed sensitivity of streamflow to soil and geological parameters. Only streamflow was not sensitive to K_{sat} contrary to other model studies. Calibration parameters were base layer conductivity, soil depth, lateral hydraulic conductivity, and its exponential decrease in depth.

Univariate calibration was conducted by adjusting soil depth, base layer conductivity, and maximum infiltration rate separately. After optimizing base layer conductivity and soil depth, model performance did not improve by varying lateral hydraulic conductivity and exponential decrease even though streamflow initially appeared to be sensitive to these parameters. This may be caused by equifinality which means that different combinations of parameters result in similar outcomes. Univariate calibration provided reasonable model performance (Y=0.73, NS=0.733, RE=-0.0003). Bivariate calibration was performed by finding the optimal combination of lateral hydraulic conductivity and its exponential decrease in depth. This gave a reasonably good model performance. (Y=0.781, NS = 0.78, RE = 0.003). Univariate calibration result was more representative for Mākaha streamflow because baseflow was not perennial. Bivariate calibration resulted in low values of lateral hydraulic conductivity and a high exponential decrease in depth. These parameters affect subsurface flow and this was impeded by this parameter combination. Despite this low subsurface flow, bivariate calibration continuously contributed to baseflow. Both calibrations were underestimating peakflows considerably. From both calibrations can be concluded that there is no unambiguous to provide

reasonable model performance so that there is no clear method to calibrate DHSVM. Subsequently, both calibrations settings were used for validation and resulted in poor model performance (Univariate validation: Y=0.24, NS=0.36, RE=0.50; Bivariate validation: Y=0.28, NS=0.48, RE=0.70). Peakflows from both settings were largely underestimated. Conditions of the validation period were significantly different than the calibration period because of lower rainfall and streamflow.

Based on better model performance, the bivariate calibration parameter settings and period were used for a scenario analysis. Scenario analysis showed sensitivity of base flow to varying base layer conductivity as a mimic for groundwater extraction. Base layer conductivity was set at $1e^{-7}$ m s^{-1} and $4e^{-7}$ m s^{-1} so that deep losses from groundwater were 73 mm and 275 mm respectively. During high pumping (base layer conductivity = $4e^{-7}$ m s^{1}), peakflow also became more sensitive. The sensitivity of streamflow to groundwater abstraction confirmed that groundwater pumping likely has an impact on streamflow since it affects baseflow. However, there is a large uncertainty in groundwater storages in the study area. Decreasing and increasing hourly rainfall data with 15% showed that there is a large sensitivity noticeable in change of peakflows. By changing the vegetation from normal into complete bare and into evergreen forest, almost no change in streamflow was found. Although vegetation changes did not show significant changes in streamflow, it increased losses by evapotranspiration.

It can be concluded that both groundwater pumping and decreasing rainfall contribute to a decreasing streamflow. A decreasing effect on streamflow was shown by groundwater pumping which affected groundwater storages and baseflow. The effect of rainfall on streamflow was only noticeable in peakflow. Changes in vegetation or land cover have little effect on streamflow. Assessing DHSVM learned it is a suitable hydrological model when sufficient data are available and a detailed integrated watershed approach is still desired.

4.2 Recommendations

Concerning the fact that majority of measurements were taken on the alluvium area in Mākaha Valley, it is also useful to conduct measurements on the wetland area at the top of Mt. Ka‘ala. The area has a different soil type, gentle slope, perennial streamflow, and is assumed to have larger conductivities. Also the possible correlation between vegetation and infiltration should be determined in more detail to improve knowledge on the spatial distribution of infiltration rates. To verify the large variability of K_{sat}, other available field instruments as a double ring infiltrometer can possibly be used for this purpose as well. Taking measurement at different depths would also provide more information on conductivities across the study area. These field data regarding K_{sat} and its relation with topographical aspects as vegetation will contribute to more knowledge about the spatial distribution of K_{sat} and more reliable model input. Finally, it may also be useful to continue first which determinant factors are significantly affecting streamflow for hydrological modeling purposes.

Using DHSVM showed that it is a suitable model by using it as an integral watershed model and that it simulates several distributed hydrological processes. Although DHSVM provided reasonable results after calibration, many aspects can be improved regarding

calibration. Model performance can be improved by further optimizing the calibration parameters. This involves studying the interdependency of parameters which are sensitive to have an impact on streamflow. Decreasing lack of data, which provided uncertainty in initial calibration and verification due to expansion of the modified model, should also contribute to a better model performance. This implies gathering data regarding water tables and the temporal impact of groundwater pumping by using hourly or daily pumping data are possible solutions. DHSVM can also possibly be calibrated on variables as water table depths and soil moisture. Considering the improvement of determining the impact of groundwater pumping and changing rainfall, these factors should be studied in a more detailed manner related to streamflow. Using a groundwater model, which can deal with this complex type of geology subject to groundwater abstraction, can provide more insight in the uncertainty of groundwater storages in the Mākaha Valley. Further studying rainfall trends to provide a more detailed scenario analysis gives more information about the effect of changing rainfall on streamflow. Although streamflow was not sensitive to vegetation changes, a proper evapotranspiration simulation by studying vegetation parameters is still necessary. Rainfall interception by vegetation is an example of an important process related to evapotranspiration and the total water balance.

References

Angulo-Jaramillo, R., Vandervaere, J.P. Roulier, S., Thony, J.L., Gaudet, J.P., Vauclin, M., 2000. Field measurement of soil surface hydraulic properties by disc and ring infiltrometers - A review and recent developments. Soil and Tillage Research, 55(1-2): 1-29.

Achouri, M., Gifford, G.F., 1984. Spatial and seasonal variability of field measured infiltration rates on a rangeland site in Utah, Journal of Range Management, 37: 451–455.

Allen, R.G., Walter, I.A., Elliott, R.L., Howell, T.A., Itenfisu, D., Jensen, M.E., and Snyder, R.L.,2005. The ASCE standardized reference evapotranspiation equation, 2005. Technical Committee report to the Environmental and Water Resources Institute of the American Society of Civil Engineers from the Task Committee on Standardization of Reference Evapotranspiration, ASCE, 173 pp.

Ankeny, M. D., Ahmed, M., Kaspar, T. C., and Horton, R. 1991. Simple field method for determining unsaturated hydraulic conductivity, Soil Science Society of America Journal, 55: 467-470.

Beven, K.J. and Freer, J., 2001. Equifinality, data assimilation, and uncertainty estimation in mechanistic modelling of complex environmental systems, Journal of Hydrology, 249: 11–29.

Bodhinayake, W., Si, B.C. and Noborio, K., 2005. Determination of hydraulic properties in sloping landscapes from tension and double-ring infiltrometers. Vadose Zone Journal, 3(3): 964-970.

Brito, M.G., Costa, C.N., Almeida, J.A., Vendas, D. and Verdial, P.H., 2006. Characterization of maximum infiltration areas using GIS tools. Engineering Geology, 85(1-2): 14-18.

Casanova, I.M.A.J., 2000. Influence of aspect and slope gradient on hydraulic conductivity measured by tension infiltrometer. Hydrological Processes, 14(1): 155-164.

Cerda, A., 1997. Seasonal changes of the infiltration rates in a Mediterranean scrubland on limestone. Journal of Hydrology, 198(1-4): 209-225.

Chen, J.M., Chen, X., Ju, W. and Geng, X., 2005. Distributed hydrological model for mapping evapotranspiration using remote sensing inputs. Journal of Hydrology, 305(1-4): 15-39.

Cuo, L., Giambelluca, T.W., Ziegler, A.D. and Nullet, M.A., 2006. Use of the distributed hydrology soil vegetation model to study road effects on hydrological processes in Pang Khum Experimental Watershed, northern Thailand. Forest Ecology and Management, 224(1-2): 81-94.

Davis, J.C., 2002. Statistics and data analysis in geology (Third edition). John Wiley and Sons, Kansas.

Ersahin, S., 2003. Comparing ordinary kriging and cokriging to estimate infiltration rate. Soil Science Society of America Journal, 67(6): 1848-1855.

Fares, A., Miura, T. and Deenick, J., 2004. Determining the impacts of water pumping and alien species invasion on stream flow for a sustainable water resource management in Mākaha Valley, Hawai'i USDA-TSTAR Funding.

Flint, A.L., Flint, L.E., 2002. Porosity. In Dick W.A. (Editor), Methods of soil analysis, Part 4. Physical Methods. Edn Soil Science Society of America, Madison, WI, USA, pp. 241-254.

Foote, D.E., Hill, E.L., Nakamura, S., Stephens, F., 1972. Soil survey of Islands of Kauai, O'ahu, Maui, Molokai, and Lanai, State of Hawai'i. US Department of Agriculture Soil Conservation Service in cooperation with the University of Hawai'i Agricultural Experiment Station, 1–232.

Gardner, W.R., 1958. Some steady-state solutions of the unsaturated moisture flow equation with application to evaporation from a water table. Soil Science, 85: 228-232.

Giambelluca, T.W., M.A. Nullet, and T.A. Schroeder, 1986. Rainfall atlas of Hawai'i. Department of Land and Natural Resources, Report R76. Honolulu, Hawai'i, 267 pp.

Gingerich, S.B. and Oki, D.S., 2000. Groundwater in Hawai'i, U.S. Geological Survey Fact Sheet 126-00, pp. 6.

Goovaerts, P., 1997. Geostatistics for natural resources evaluation. Oxford University Press, New York.

Green, R.E., Ahuja L.R., Chong, S.K., and Lau, L.S., 1982. Water conduction in Hawai'i oxic soils. Technol. Rep. 143. Water Resources Research Center. University of Hawai'i, Honolulu.

Grossman, R.B., Reinsch, T.G., 2002. Bulk density and linear extensibility. In Dick W.A. (Editor), Methods of soil analysis, Part4. Physical Methods. Edn Soil Science Society of America, Madison, WI, USA, pp. 201-228.

Hanna, Y. A., Harlan, P.W., and Lewis, D. T., 1982. Soil available water as influenced by landscape position and aspect, Agronomical Journal, 74: 999-1004.

Harman, M.R., 2004. Mapping invasive species in Mākaha Valley, O'ahu using fine Resolution satellite imagery, BSc-thesis, University of Hawai'i at Manoa.

Hunt, D.H, 1996. Geohydrology of the Island of O'ahu, Hawai'i. U.S. Geological Survey Professional Paper 1412-B.

Kelleher, K.D., 2006. Streamflow calibration of two sub-basins in the Lake Whatcom watershed, Washington. MSc-thesis, University of Washington.

Lettenmaier, D., 2008. Distributed Hydrology Soils and Vegetation Model, Documentation, http://www.hydro.washington.edu/Lettenmaier/Models/DHSVM/documentation.shtml.

Li, G., Luk, S. H., and Cai, Q. G. 1995. Topographic zonation of infiltration in the hilly loess region, North China, Hydrological Processes, 9: 227-235.

Liang, X., Lettenmaier, D.P., Wood, E.F. and Burges, S.J., 1994. A simple hydrologically based model of land-surface water and energy fluxes for general-circulation Models. Journal of Geophysical Research-Atmospheres, 99(D7): 14415-14428.

Loague, K. and G.A. Gander. 1990. R-5 revisited: 1. Spatial variability of infiltration on a small rangeland catchment. Water Resources Research 26: 957–971.

Logsdon, S. D. 1997. Transient variation in the infiltration rate during measurement with tension infiltrometers, Soil Science, 162: 233-241.

Logsdon, S.D. and Jaynes, D.B., 1993. Methodology for determining hydraulic conductivity with tension infiltrometers. Soil Science Society of America Journal, 57(6): 1426-1431.

Luk, S. H., Cai, Q. G., and Wang, G. P. 1993. Effects of surface crusting and slope gradient on soil and water losses in the hilly loess region, North China, Catena Suppl., 24: 29-45.

Machiwal, D., Jha, M.K., Mal, B.C., 2006. Modelling infiltration and quantifying spatial soil variability in a wasteland of Kharagpur, India, Biosystems Engineering, 95 (4): 569–582.

Mair, A., Fares, A. and El-Kadi, A., 2007. Effects of rainfall and ground-water pumping on streamflow in Mākaha, O'ahu, Hawai'i. Journal of the American Water Resources Association, 43(1): 148-159.

Mair, A. 2008. Hydrology of upper Mākaha valley: effects of rainfall variability on groundwater recharge and streamflow. PhD dissertation. University of Hawai'i at Manoa, Honolulu, Hawai'i.

Mink, J.F, 1978. Waianae Water Development Study. Honolulu Board of Water Supply, 109 pp, 6 appendices.

Nash, J.E., Sutcliffe J.V., 1970. River flow forecasting through conceptual models, Part I: a discussion of principles, Journal of Hydrology, 10: 282–290.

NOAA (National Oceanic and Atmosperic Association) Coastal Service Center. 2001. Coastal Change Analysis Program (C-CAP), NOAA Coastal Sevice Center, Downloaded from http://www.csc.noaa.gov/crs/lca.Hawai'i.html, Accessed December 20, 2007.

Prata, A.J., 1996. A new long-wave formula for estimating downward clear-sky radiation at the surface. Q.J.R. Meteorological Society, 122: 1127–1151.

PRISM and CIG, 2008, Puget Sound Regional Synthesis Model (PRISM) and the Climate Impacts Group (CIG), University of Washington, Documentation, http://www.tag.washington.edu/research/dv24/dv24.htm.

Rientjes, T.H.M., 2005. Modelling in hydrology. Lecture notes from: International institute for geo-information science and earth observation. Department of water resources ITC, Enschede.

Sauer, T.J. and Logsdon, S.D., 2002. Hydraulic and physical properties of stony soils in a small watershed. Soil Science Society of American Journal, 66(6): 1947-1956.

Sharma, M.L., G.A. Gander, and C.G. Hunt. 1980. Spatial variability of infiltration in a watershed. Journal of Hydrology, 45: 101–122.

Singh, V.P. and Woolhiser, D.A., 1976. Sensitivity of linear and nonlinear surface runoff models to input errors. Journal of Hydrology, 29, pp. 243–249.

Sullivan, M., Warwick, J.J. and Tyler, S.W., 1996. Quantifying and delineating spatial variations of surface infiltration in a small watershed Journal of Hydrology, 181(1-4): 149-168.

Takasaki, K.J, 1971. Ground Water in the Waianae district, O'ahu, Hawai'i. U.S. Geological Survey hydrologic investigations atlas A-358, Washington, District of Columbia, 2 maps.

Thanapakpawin, P., Richey, P. J., Thomas, D., Rodda, S., Campbell, B., Logsdon, M., 2007. Effects of land use change on the hydrologic regime of the Mae Chaem river basin, NW Thailand. Journal of Hydrology, 334(1-2): 215-230.

USDA-NRCS (U.S. Department of Agriculture – Natural Resources Conservation Service. 2007. SSURGO soil series map for O'ahu. Downloaded from http://datagateway.nrcs.usda.gov/. Accessed December 20, 2007.

USDI-NRCS (U.S. Department of Interior – U.S. Geological Survey). 2007. Geologic Map of the island of O' ahu. Downloaded from http://pubs.usgs.gov/of/2007/1089/. Accessed December 20, 2007.

Vanshaar, J., Haddeland, I. and Lettenmaier, D.P., 2002b. Effects of land-cover changes on the hydrological response of interior Columbia River basin forested catchments. Hydrological Processes, 16(13): 2499-2520.

Vieira, S.R., Nielsen, D.R. and Biggar, J.W., 1981. Spatial variability of field-measured infiltration rate. Soil Science Society of America Journal, 45: 1040--1048.

Waichler, S.R., Wigmosta, M.S., Coleman, A., 2004. Natural recharge to the unconfined aquifer system on the Hanford Site from the Greater Cold Creek Watershed: Progress Report. Pacific Northwest National Laboratory prepared for the U.S. Department of Energy.

Warrick, A.W., Mullen, G. J., Nielsen, D.R., (1977a). Prediction of the soil-water flux based upon field-measured soil-water properties. Soil Science Society of America Journal, 41: 4–19.

Warrick, A.W., Mullen, G. J., Nielsen, D.R., (1977b). Scaling field measured soil hydraulic Properties using similar-media concept. Water Resources Research, 13: 355–362.

White, I., Sully, M. J., and Perroux, K. M. 1992. Measurement of surface-soil hydraulic properties: disc permeameter, tension infiltrometer, and other techniques, In: Topp, G. C., Reynolds, W. D. and Green, R. E. (Editors), Advances in measurement of soil physical properties: bringing theory into practice. Soil Science Society of America, Madison, WI, USA, pp. 69-103.

Wigmosta, M.S., Lettenmaier, D.P. and Vail, L.W., 1994. A distributed hydrology-vegetation model for complex terrain. Water Resources Research, 30(6): 1665-1679.

Wigmosta, M.S., Nijssen, B., and Storck, P., 2002. The distributed hydrology soil vegetation model. In: Singh V.P., Frevert, D. (Editors), Mathematical models of small watershed hydrology and applications. Water Resources Publications, LLC, Highlands Ranch, pp. 7-42.

Wooding, R.A., 1968. Steady infiltration from a shallow circular pond. Water Resources Research, 4(6): 1259-1273.

Yolcubal, I. Brusseau, M.L., Artiola, J.F., Wierenga, P., and Wilson, L.G., 2004. Environmental physical properties and processes, In Artiola, J.F., Pepper, I.L., Brusseau M.L. (Editors), Environmental, monitoring and characterization, Academic Press, San Diego, 207-241.

Walker, C., Lin, H.S., and Fritton, D., 2006. Is the tension beneath a tension infiltrometer what we think it is? Vadose Zone Journal, 5:860-866.

Appendices

A. Soil Properties

Map Symbol	Soil Name	Hydrologic Group	Depth	Permeability (Ksat) (cm/h)	USDA Texture
HLMG	HELEMANO SILTY CLAY	B	0-25cm	2-6	Silty Clay
			25-100cm	0.6-2	Gravelly Silty Clay
			100-150cm	0.6-2	Very Gravelly Silty Clay
LoD	LOLEKAA SILTY CLAY	B	0-25cm	2-6	Silty Clay
			25-110cm	2-6	Silty Clay
			110-160cm	2-6	Silty Clay Loam
LoE	LOLEKAA SILTY CLAY	B	0-25cm	2-6	Silty Clay
			25-110cm	2-6	Silty Clay
			110-160cm	2-6	Silty Clay Loam
PvC	PULEHU VERY STONY CLAY LOAM	B	0-50cm	0.6-2	Very Stony Clay Loam
			50-150cm	0.6-2	Stratified Sand To Silty Clay Loam
rAAE	ALAKAI MUCKY PEAT	C	0-20cm	6-20	Mucky Peat
			20-80cm	6-20	Muck
			80-125cm	0-0.1	Clay
rRK	ROCK LAND	D	0-10cm	0.6-2	Silty Clay
			10-20cm	0.6-2	Silty Clay Loam
			20-50cm	0-0.6	Unweathered Bedrock
rRO	ROCK OUTCROP	D	0-150cm	-	Unweathered Bedrock
rRT	ROUGH MOUNTAINOUS LAND	D	0-12.5cm	2-6	Silty Clay Loam
			12.5-65cm	2-6	Very Cobble Clay Loam
			65-75cm	0.1-6	Weathered Bedrock
rTP	TROPOHUMULTS-DYSTRANDEPTS ASSOCATION	C	0-25cm	2-6	Silty Clay
			25-125cm	2-6	Silty Clay, Silty Clay Loam
			125-150cm	0.1-6	Weathered Bedrock

B. Field measurement results

Date	Station	UTM Zone 4		Elevation (m)	Slope (%)	Aspect (degrees)	Bulk density (g/cm3)	Porosity (-)	Tensions (cm)		Steady state Infiltration rate		Qhigh(cm3/hr)	Qlow(cm3/hr)	α (cm-1)	Ksat (cm/hr)	Remarks
		X	Y						High	Low	High Tension	Low Tension					
21/11/2007	TI2.2	584746	2378789	477	34	138	1.0102	0.7259	-8	-2	36	132	182.41	668.85	0.22	8.03	ridge, open, dry, silty clay
21/11/2007	TI2.1	584742	2378782	477	34	138	0.9625	0.6490	-8	-2	36	156	182.41	790.46	0.24	10.75	ridge, open, dry, silty clay
21/11/2007	TI1.3	585291	2378414	343	22	243	0.8950	0.6948	-6	-1	12	600	60.80	3040.24	0.78	90.16	close to stream, clay, stony, christmas berry
29/11/2007	RI1	586000	2378474	512	26	335	0.8396	0.6059	-8	-2	12	36	60.80	182.41	0.18	1.85	ridge,silty clay, mixed vegetated
29/11/2007	RI2	586122	2378177	611	54	18	0.7844	0.6430	-8	-2	6	36	30.40	182.41	0.30	3.08	clay, mixed vegetated
29/11/2007	RI3	586191	2378153	607	43	21	0.8955	0.6624	-8	-2	3	168	15.20	851.27	0.67	42.18	gulch, organic, mixed vegetated, loose soil
29/11/2007	TI4	586240	2378111	601	32	39	0.7440	0.6104	-8	-2	6	276	30.40	1398.51	0.64	63.86	stony, clay, mixed vegetated
30/11/2007	RI4	585587	2378752	399	16	184	1.0437	0.6212	-8	-2	3	48	15.20	243.22	0.46	6.94	mango/open, close to stream
30/11/2007	RI5	585212	2378502	364	51	74	1.0338	0.6102	-8	-2	48	144	243.22	729.66	0.18	7.40	open, close to stream, stony, clay
30/11/2007	TI3	585686	2379268	538	58	155	0.9210	0.6609	-8	-2	6	168	30.40	851.27	0.56	31.41	silty clay, strawberry guava/open
02/12/2007	TI5.2	586626	2378813	600	34	280	0.7948	0.6743	-8	-2	6	36	30.40	182.41	0.30	3.08	silty clay, ridge, rooted, strawberry guava
05/12/2007	RI8	586262	2378730	501	65	170	0.5909	0.7004	-8	-2	24	96	121.61	486.44	0.23	6.24	organic matter, clay, stony, coffee tree
05/12/2007	RI7	586235	2378652	475	17	283	1.1507	0.6420	-8	-2	24	144	121.61	729.66	0.30	12.31	stony, clay, close to stream, coffee tree
05/12/2007	RI9	585807	2378848	438	41	245	0.8393	0.7071	-8	-2	4	108	30.40	547.24	0.55	19.87	gulch, organic matter, clay, stony, mixed vegetated
05/12/2007	RI6	585945	2378762	430	27	311	0.9118	0.6906	-8	-2	4	204	20.27	1033.68	0.66	49.27	close to stream, clay, mixed vegetated
12/12/2007	TI5.1	586667	2378842	609	38	293	0.7522	0.7446	-8	-2	6	108	30.40	547.24	0.48	16.52	silty clay, ridge, rooted, strawberry guava
12/12/2007	RI10	586556	2378555	531	22	350	1.0239	0.6834	-8	-2	4	180	20.27	912.07	0.63	41.26	native vegetated, silty clay, close to stream
12/12/2007	RI11	586612	2378632	538	34	197	0.7722	0.6809	-8	-2	6	444	30.40	2249.78	0.72	124.88	rooted, strawberry guava
13/12/2007	RI15	585141	2378787	429	13	119	0.8418	0.6965	-8	-2	12	36	60.80	182.41	0.18	1.85	ridge, open dry, silty clay
13/12/2007	RI12	584956	2377914	298	48	298	0.8051	0.6612	-8	-2	3	24	15.20	121.61	0.35	2.43	close to stream(gage), mixed vegetated, clay
13/12/2007	RI13	584864	2378678	420	43	206	1.0474	0.6164	-8	-2	6	120	30.40	608.05	0.50	19.28	gulch, stony loosely clay, mixed vegetated
13/12/2007	RI14	585196	2378593	362	11	84	0.7634	0.7164	-8	-2	4	108	20.27	547.24	0.55	19.87	gulch, silty clay, mixed vegetated
14/12/2007	RI16	587099	2378398	658	48	321	0.5160	0.6180	-8	-2	6	48	30.40	243.22	0.35	4.86	ashy soil, coffee tree, rooted
14/12/2007	TI6	587434	2378421	725	76	333	0.4781	0.7998	-8	-2	6	120	30.40	608.05	0.50	19.28	ashy clay, mixed vegetated, high elevation
14/12/2007	RI17	586586	2378487	544	20	0	0.8581	0.7284	-8	-2	6	180	30.40	912.07	0.57	34.69	close to stream, coffee tree, stony, clay
14/12/2007	RI18	586416	2378572	526	21	357	0.6758	0.4657	-8	-2	3	240	15.20	1216.10	0.73	69.66	ridge, strawberry guava, organic matter, rooted
19/12/2007	RI19	585505	2378506	400	39	297	0.9417	0.6693	-8	-2	2	60	10.13	304.02	0.57	11.56	ridge, mixed vegetated, silty clay, rooted
19/12/2007	RI22	584889	2378256	345	31	209	0.6844	0.7735	-8	-2	6	180	30.40	912.07	0.57	34.69	gulch, mixed vegetated, loosely clay
19/12/2007	RI21	585177	2378321	352	9	315	0.7270	0.7365	-8	-2	12	276	60.80	1398.51	0.52	47.26	close to stream, mixed vegetation, stony, loosely clay
19/12/2007	RI20	585311	2378511	382	11	243	0.6987	0.7395	-8	-2	3	348	15.20	1763.34	0.79	117.05	Same as station TI1.3
20/12/2007	RI24	585362	2377951	418	32	306	0.7494	0.6688	-8	-2	1.71	12	8.66	60.80	0.32	1.13	ridge, stony, clay
20/12/2007	RI23	585178	2377901	374	42	293	1.0072	0.6836	-8	-2	6	252	30.40	1276.90	0.62	56.12	gulch, loose clay, stony, mixed vegetated
20/12/2007	RI25	585375	2378092	397	48	346	0.8518	0.6954	-8	-2	3	516	15.20	2614.61	0.86	202.26	gulch, stony, mixed vegetated, organic matter
20/12/2007	RI26	585219	2378220	349	25	303	0.8502	0.6925	-8	-2	1.71	780	8.66	3952.32	1.02	441.91	same as station TI1.3
21/12/2007	RI28	586003	2379248	543	69	158	0.6194	0.7442	-8	-2	1.71	24	8.66	121.61	0.44	3.26	gulch, rooted, organic matter, strawberry guava
21/12/2007	RI30	586020	2378784	441	21	230	0.8520	0.7524	-8	-2	2.4	60	12.16	304.02	0.54	10.67	same as station TI1.3
21/12/2007	RI27	585736	2379186	491	46	167	0.7604	0.7063	-8	-2	2	96	10.13	486.44	0.65	22.61	ridge, mixed vegetated, silty clay
21/12/2007	RI29	586140	2378971	487	41	166	0.7191	0.7329	-8	-2	24	312	121.61	1580.93	0.43	40.79	gulch, mixed vegetated
28/12/2007	RI33	585465	2378774	425	43	249	0.8932	0.7115	-8	-2	24	72	121.61	364.83	0.18	3.70	ridge, mixed vegetated, clay
28/12/2007	RI34	584947	2378349	378	16	176	0.7973	0.7424	-8	-2	1.5	48	7.60	243.22	0.58	9.51	christmas berry, densed, organic matter
28/12/2007	RI32	585688	2378539	449	30	261	1.1099	0.7085	-8	-2	1.33	108	6.74	547.24	0.73	31.53	ridge, mixed vegetated, clay
28/12/2007	RI31	585522	2378923	468	29	168	0.7861	0.6881	-8	-2	6	480	30.40	2432.20	0.73	139.31	rooted, strawberry guava, silty clay
11/01/2008	RI35	586785	2378594	602	9	236	0.5504	0.7921	-8	-2	4	60	20.27	304.02	0.45	8.42	ridge, mixed vegetated, rooted
11/01/2008	RI37	586952	2378525	604	23	257	0.6340	0.7986	-8	-2	12	168	60.80	851.27	0.44	22.78	gulch, mixed vegetated, clay
11/01/2008	RI36	586774	2378537	583	52	168	0.9198	0.7222	-8	-2	4	348	20.27	1763.34	0.74	104.45	gulch, stoney, mixed vegetated
25/01/2008	TI1.4	585291	2378471	347	11	234	1.0533	0.6802	-8	-2	1.2	24	6.08	121.61	0.50	3.86	same as station TI1.3
25/01/2008	RI39	585229	2378429	348	27	103	0.8824	0.7060	-8	-2	1.71	48	8.66	243.22	0.56	8.98	mango, close to stream
25/01/2008	RI40	585049	2378246	336	35	150	0.9186	0.7456	-8	-2	1.2	60	6.08	304.02	0.65	14.37	silty clay, christmas berry, stony
25/01/2008	TI1.5	585311	2378467	350	15	239	0.8002	0.7325	-8	-2	3	192	15.20	972.88	0.69	50.91	same as station TI1.3
25/01/2008	RI38	585229	2378387	345	23	135	0.8014	0.7772	-8	-2	0.92	168	4.66	851.27	0.87	67.39	stony, mixed vegetated, clay
25/01/2008	RI41	584993	2378165	331	17	153	0.7457	0.7822	-8	-2	2.4	240	12.16	1216.10	0.77	76.13	stony, mixed vegetated, silty clay
29/01/2008	RI44	586982	2378037	757	53	349	0.5978	0.7942	-8	-2	12	36	60.80	182.41	0.18	1.85	high elevation, ridge, open, ashey soil
29/01/2008	RI42	585564	2378307	604	26	343	0.6717	0.7770	-8	-2	6	156	30.40	790.46	0.54	28.22	strawberry guava, hillslope
29/01/2008	RI43	585564	2378017	736	93	306	0.5778	0.6255	-8	-2	6	156	30.40	790.46	0.54	28.22	mixed vegetated, rooted, ridge

C. Digital Elevation Model (DEM)

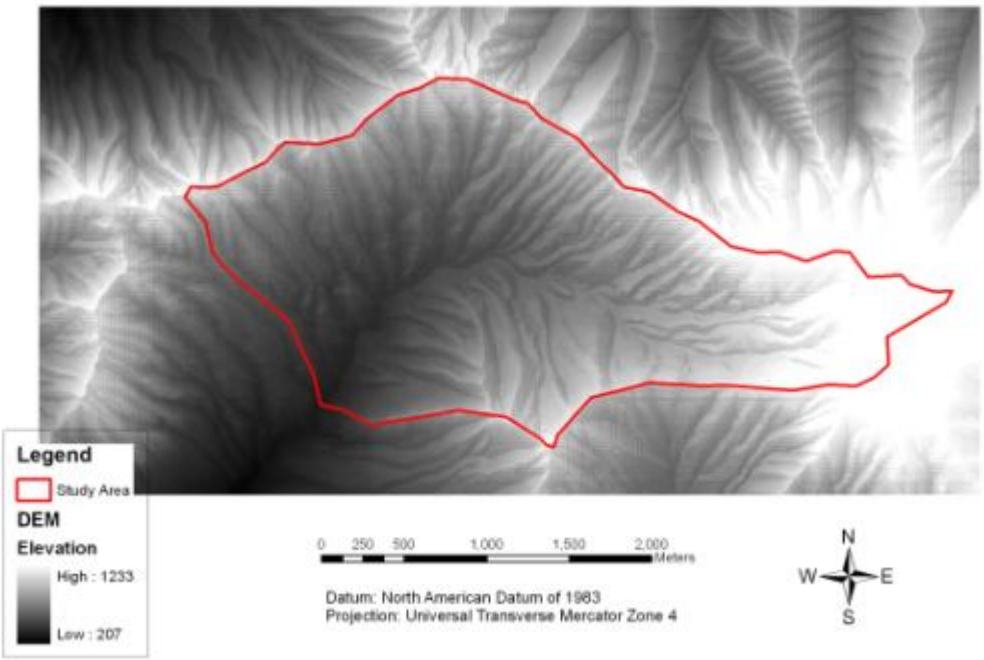

D. Mākaha Valley DHSVM basin setup

Kelleher (2006) provided the procedure for a basin setup by ArcGIS and cygwin for DHSVM. In this case, adaptations are made for Mākaha Valley subwatershed.

Create DEM grid

1. Create a workspace. I created a folder on the C drive called makaha and created a folder within Mākaha for dems. (C:\makaha\dem)
2. Resample DEMs to 30 m by 30 m pixel resolution.

a. Set analysis environment

Open ArcToolbox→Data Management tools→Raster→Resample→environment

Under General Settings tab:

Current Workspace: (C:\makaha\dem)

Scratch Workspace (C:\makaha\dem)

Output coordinate system: Same as layer "makahadem"

Output Extent: Same as layer "makahadem"

Under Raster Analysis settings tab:

Cell size: 30

Mask: None

→OK

b. Resample:

Input Raster: "makahadem"

Output Raster: "dem30"

Cell size: 30
Resampling Technique: Nearest
→OK

Create watershed mask

1. Create another folder within the makahafolder "watershed".
2. Fill sinks to even out the dem
Open hydrology / models toolbar→Fill Sinks
Input surface: dem30
Fill limit: <Fill_All>
Output raster: C:\makaha\watershed\filldem
→OK
3. Perform flow direction on the filled DEM. This grid is necessary for determining the watershed boundary.
Open hydrology / models toolbar→Flow direction
Input surface: filldem
Output raster: C:\makaha\watershed\flowdir
→OK
4. Perform flow accumulation. This grid is also necessary for determining the watershed boundary.
Open hydrology / models toolbar→Flow accumulation
Direction raster: flowdir
Output raster: C:\makaha\watershed\flowacc
→OK
5. Set interactive properties to create a watershed boundary
Open hydrology / models toolbar→Interactive properties
Flow direction: flowdir
Flow accumulation: flowacc
→OK
6. Create the watershed boundary
Click the watershed button from the hydrology / models toolbar.
This is an interactive tool which will determine the boundary of the watershed based on the destination cell. Coordinates of a USGS gage station in the watershed were used as the outlet of the subwatershed.
Output raster: C:\makaha\watershed\watershed
7. Create a watershed polygon
I created a watershed polygon that is used to clip the grids that are necessary input for DHSVM.
Open ArcToolbox→Conversion Tools→From Raster→Raster to Polygon
Input raster: C:\makaha\watershed\watershed
Output polygon features: C:\makaha\watershed\watershedpoly
→OK

Create landcover grid

The landcover file is already a 30 m by 30 m raster grid, so it was not required to be converted.

1. Clip landcover grid to watershed boundary.

Set analysis environment:

Click Spatial Analysts toolbar→ Options

Working directory: C:\makaha\landcover

Analysis mask: watershedpoly

Extent: watershedpoly

Cellsize: 30

Output raster: C:\makaha\landcover\temp_landcover30

2. Reclassify vegetation classifications to DHSVM classifications

Open ArcToolbox→Spatial Analyst→Reclass→Reclassify

Set general and raster analysis environments

Input Raster: temp_landcover30

Output Raster: landcover30

Reclass Field: Value

Then:

NOAA	NOAA	DHSVM	DHSVM
5	Grassland	10	Grassland
7	Evergreen Forest	2	Evergreen Broadleaf
9	Scrub/Shrub	8	Closed Shrub
10	Palustrine Forested Wetland	4	Deciduous Broadleaf
17	Bare land	12	Bare

Create soil texture grid

1. Convert soil polygon to raster.

Open ArcToolbox→Conversion Tools→To Raster→Feature to Raster

Set analysis environments by clicking on the Environments button

Under General Settings tab:

Current Workspace: (C:\makaha\soil)

Scratch Workspace (C:\makaha\soil)

Output coordinate system: Same as layer "dem30"

Output Extent: Same as layer "dem30"

Under Raster Analysis settings tab:

Cell size: 30

Mask: None

OK to close environments setting

Input features: soil

Field: MUID

Output raster: C:\makaha\soil\soil30

Output cell size: 30

→OK

2. Clip soil grid to watershed

Set analysis environment:

Click Spatial Analysts toolbar→ Options

Working directory: C:\makaha\soil
Analysis mask: watershedpoly
Extent: watershedpoly
Cellsize: 30
3. Reclassify soil grid in USDA textures as in the table above.

Create soil depth and streamnetwork grids

Soil depth and stream network grids were obtained by using Arc/Info and using the createstreamnetwork.aml file in the amlscripts folder downloaded from the DHSVM homepage (Lettenmaier, 2008).

1. Create a workspace
Create a new folder: C:\temp\soild
and C:\temp\soild\amlscripts
Copy the watershed grid (watershed), the clipped dem (dem30) and the amlscript files from the DHSVM folder into the "soild" folder.
Check to ensure that your system has Java Runtime Environment (JRE). To check for JRE, open Arc and type:
Arc: &sys java –version
You should get something like:
Java version "1.4.2_04……"
The watershed mask values must be defined within the subwatershed with "1" and outside the subwatershed "NODATA". Otherwise the AML will create a stream network for the entire raster. Also before running the AML, make sure to change the path to AddAat2.class from with the createstreamnetwork.aml. If this step is skipped, the AML will give errors, but will continue to run anyway. Check in the stream.network.dat file at the segment column is not giving values of zero.
2. Run the AML
Open ARC.
Type:
ARC: &workspace C:\temp\soild
ARC: &amlpath C:\temp\soild\amlscripts
ARC: &run createstreamnetwork dem30 watershed soild30 stream MASK 200000 0.8 1.5
The last three numbers are variables representing the minimum contributing area (m^2) before a channel begins the minimum soil depth, and maximum soil depth (in meters).

Create a series of shading/shadow maps

1. Create a workspace.
Create a new folder: C:\temp\shadow
Copy the clipped dem (sheddem) into this folder using ArcCatalog. The solar AML (process_solar1 is not available in the amlscripts folder in the DHSVM tutorial, but can be found on the website of PRISM and CIG (2008). This file should also be copied into the shadow folder. Process_solar.aml requires 3 "C" files to run. Compile these by using for example 'gcc' in cygwin. The compiled files are make_dhsvm_shade_maps.exe, skyview.exe, and average_shadow.exe. Copy these files into the 'shadow' folder.

2. Run the AML.
Type:
Arc: &workspace C:\temp\shadow
Arc: &amlpath C:\temp\shadow\amlscripts
Arc: &process_solar1 watershed dem30 1 -158
The basin name is "watershed" and the elevation grid is "dem30". The last two numbers represent the model time step and longitude in degrees, respectively. Rename each file (Shadow.01.hourly.bin in shadow.01.bin).
Export DEM, soil type, soil depth, vegetation, and watershed to ascii grid files
Example:
For the watershed grid, Type:
Arc: & workspace C:\TEMP\watershed (with "watershed" grid)
Arc: grid
GRID: watershed.asc = gridascii(con(isnull(watershed),14,watershed))
GRID: q
Ascii grid files to binary grid files
Convert the ascii grids (soilclass.asc, vegclass.asc, and mask.asc) to binary files using "myconvert.exe" in the input file. This was done by using cygwin (Linux-like environment for Windows).
The correct variable type for each grid is as follows:
watershed, landcover, soil type: unsigned character or uchar
Dem, soildepth: float
Example (for mask, landcover, soil type) and type in cygwin:
./myconvert.exe ascii uchar watershed.asc watershed.bin 99 190
Example (for dem, soildepth):
./myconvert.exe ascii float DEM30.asc DEM30.bin 99 190
Where:
./myconvert.exe [source_format] [target_format] [source_file] [target_file] [number_of_rows] [number_of_columns]
Set initials condition for dhvm
1. Create initial channel state files by cygwin:
./MakeChannelstate.exe stream.network.dat stream.map.dat channel.state.11.01.2005.01.00
2. Create model state files by cygwin:
I used initialstate.txt that is found in the dshvm tutorial and changed the path, date, and # of rows and columns. Then:
./MakeModelStateBin.exe InitialState.txt
This creates the initial Interception, Snow, and Soil state files for the date that is specified in the initialstate.txt file. The date indicates the beginning of the model simulation.

E. Soil Depth Map obtained for DHSVM

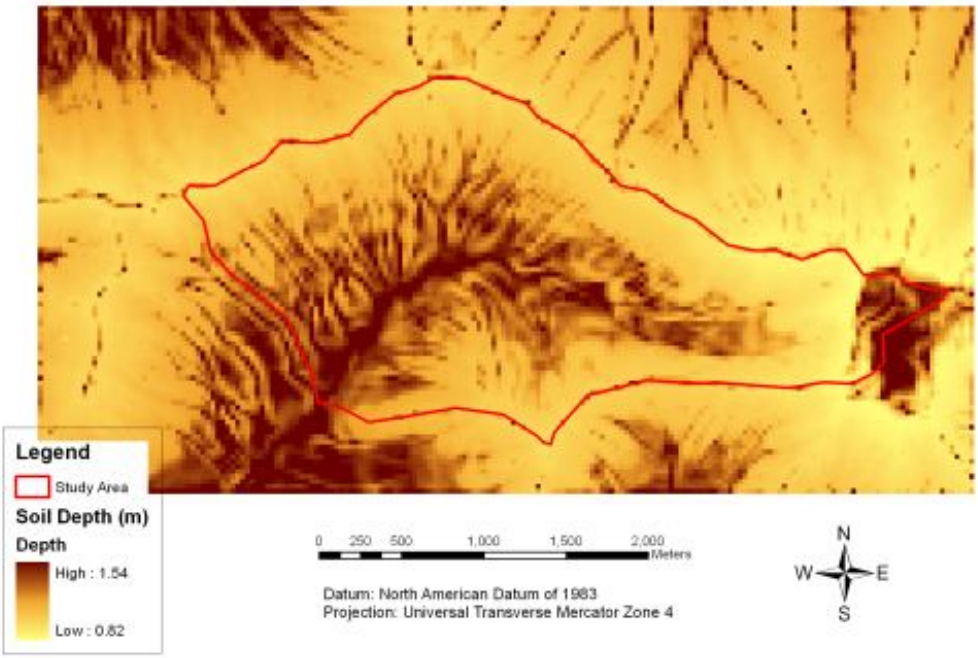

F. DHSVM default parameter settings

Constant parameters
Ground Roughness (m) = 0.02
Snow Roughness (m) = 0.01
Rain Threshold (^{o}C) = -1.5
Snow Threshold (^{o}C) = 1.0
Snow Water Capacity (-) = 0.008
Reference Height (m) = 50.0
Rain LAI Multiplier (-) = 0.0001
Snow LAI Multiplier (-) = 0.0005
Min Intercepted Snow (m)= 0.005
Outside Basin Value = 0

Soil Parameters	*Soil type*			
Soil Description	8 = SILTY CLAY LOAM	9 = CLAY LOAM	11 = SILTY CLAY	17 = MUCK
Lateral Conductivity (m/s)	8 = 0.01	9 = 0.01	11 = 0.01	17 = 0.01
Exponential Decrease (-)	8 = 3.0	9 = 3.0	11 = 3.0	17 = 3.0
Maximum Infiltration (m/s)	8 = 3e-5	9 = 1e-5	11 = 1e-5	17 = 1e-5
Surface Albedo (m/s)	8 = 0.1	9 = 0.1	11 = 0.1	17 = 0.23
Temperature Exponent (-)	8 = 3	9 = 3	11 = 3	17 = 6
Thermal Inertia (-)	8 = 0.8	9 = 0.8	11 = 0.8	17 = 0.5
Number of Soil Layers	8 = 3	9 = 3	11 = 3	17 = 3
Porosity (-)	8 = .48 .48 .48	9 = .46 .46 .46	11 = .49 .49 .49	17 = .47 .47 .47
Pore Size Distribution (-)	8 = .13 .13 .13	9 = .12 .12 .12	11 = .1 .1 .1	17 = .08 .08 .08
Bubbling Pressure (-)	8 = .34 .34 .34	9 = .26 .26 .26	11 = .34 .34 .34	17 = .37 .37 .37
Field Capacity (-)	8 = .36 .36 .36	9 = .31 .31 .31	11 = .37 .37 .37	17 = .36 .36 .36
Wilting Point (-)	8 = .21 .21 .21	9 = .23 .23 .23	11 = .25 .25 .25	17 = .27 .27 .27
Bulk Density (kg/m^3)	8 = 1381. 1381. 1381.	9 = 1600. 1600. 1600.	11 = 1346. 1346. 1346.	17 = 1600. 1600. 1600
Vertical Conductivity (m/s)	8 = 0.01 0.01 0.01	9 = 0.01 0.01 0.01	11 = 0.01 0.01 0.01	17 = 0.05 0.05 0.05
Thermal Conductivity W/m°C	8 = 7.114 6.923 7.0	9 = 7.114 6.923 7.0	11 = 7.114 6.923 7.0	17 = 7.114 6.923 7.0
Thermal Capacity J/m^3°C	8 = 1.4e6 1.4e6 1.4e6	9 = 1.4e6 1.4e6 1.4e6	11 = 1.4e6 1.4e6 1.4e6	17 = 1.4e6 1.4e6 1.4e6

Geological parameters	*Geology Type*		
Geology Description	1 = Alluvium	3 = Basalt Flows	4 = Breccia and Tuff
Groundwater Conductivity (m/s)	1 = 5e-6	3 = 1e-6	4 = 1e-7
Groundwater Conductivity Lateral (m/s)	1 = 1e-6	3 = 1e-6	4 = 1e-6
Groundwater Effective Porosity (-)	1 = 0.7	3 = 0.65	4 = 0.2
Aquifer Thickness (m)	1 = 5.0	3 = 5.0	4 = 5.0
Baseflow Gwater Temperature (oC)	1 = 4.0	3 = 10.0	4 = 10.0
Base Layer Conductivity (m/s)	1 = 1e-9	3 = 1e-10	4 = 1e-12
GeoWeathering Rate (m/s)	1 = 1e-7	3 = 1e-7	4 = 1e-7

Vegetation Parameters (1)	*Vegetation Type*	
Vegetation Description	2 = Evergreen Broadleaf *	4 = Deciduous Broadleaf
Impervious Fraction (-)	2 = 0.0	4 = 0.0
Overstory Present	2 = TRUE	4 = TRUE
Understory Present	2 = TRUE	4 = TRUE
Fractional Coverage (-)	2 = 0.9	4 = 0.9
Trunk Space (-)	2 = .5	4 = 0.9
Aerodynamic Attenuation (-)	2 = 1.5	4 = 0.5
Radiation Attenuation (-)	2 = 0.2	4 = 1.5
Max Snow Int Capacity (-)	2 = 0.003	4 = 0.2
Snow Interception Eff (-)	2 = 0.6	4 = 0.003
Mass Release Drip Ratio (-)	2 = 0.4	4 = 0.6
Height (m)	2 = 30.0 0.5	4 = 0.4
Impervious Fraction (-)	2 = 0.0	4 = 30.0 0.5
Overstory Monthly LAI (-)	2 = 10.0	4 = 2.0
Understory Monthly LAI (-)	2 = 3.0	4 = 2.0
Overstory Monthly alb (-)	2 = 0.2	4 = 5000. 3000.
Understory Monthly alb (-)	2 = 0.2	4 = 666.6 666.6
Maximum Resistance (s/m)	2 = 5000. 3000.	4 = 0.33 0.13
Minimum Resistance (s/m)	2 = 666.6 666.6	4 = 4000 4000
Moisture Threshold (-)	2 = 0.33 0.13	4 = .108 0.108
Vapor Pressure Deficit (Pa)	2 = 4000 4000	4 = 0.20
Rpc (-)	2 = .108 0.108	4 = 0.20
Number of Root Zones	2 = 3	4 = 3
Root Zone Depths (m)	2 = 0.10 0.25 0.40	4 = 0.10 0.25 0.40
Overstory Root Fraction (-)	2 = 0.20 0.40 0.40	4 = 0.20 0.40 0.40
Understory Root Fraction (-)	2 = 0.40 0.60 0.00	4 = 0.40 0.60 0.00

Vegetation Parameters (2)		*Vegetation Type*	
Vegetation Description	8 = Closed Shrub *	10 = Grassland	12 = Bare
Impervious Fraction (-)	8 = 0.0	10 = 0.0	12 = 0
Overstory Present	8 = FALSE	10 = FALSE	12 = FALSE
Understory Present	8 = TRUE	10 = TRUE	12 = FALSE
Fractional Coverage (-)	8 =	10 =	12 =
Trunk Space (-)	8 =	10 =	12 =
Aerodynamic Attenuation (-)	8 =	10 =	12 =
Radiation Attenuation (-)	8 =	10 =	12 =
Max Snow Int Capacity (-)	8 =	10 =	12 =
Snow Interception Eff (-)	8 =	10 =	12 =
Mass Release Drip Ratio (-)	8 =	10 =	12 =
Height (m)	8 =	10 =	12 =
Impervious Fraction (-)	8 = 2.0	10 = 0.5	12 =
Overstory Monthly LAI (-)	8 = 2.0	10 = 0.5	12 = 0
Understory Monthly LAI (-)	8 = 2.0	10 = 0.5	12 = 0
Overstory Monthly alb (-)	8 = 600	10 = 600	12 =
Understory Monthly alb (-)	8 = 200	10 = 200	12 =
Maximum Resistance (s/m)	8 = 0.33	10 = 0.33	12 =
Minimum Resistance (s/m)	8 = 4000	10 = 4000	12 =
Moisture Threshold (-)	8 = .108	10 = .108	12 =
Vapor Pressure Deficit (Pa)	8 = 0.14	10 = 0.19	12 = 0
Rpc (-)	8 = 0.14	10 = 0.19	12 = 0
Number of Root Zones	8 = 3	10 = 3	12 = 3
Root Zone Depths (m)	8 = 0.10 0.25 0.40	10 = 0.10 0.25 0.40	12 = 0.1 0.25 0.4
Overstory Root Fraction (-)	8 =	10 =	12 =
Understory Root Fraction (-)	8 = 0.40 0.60 0.00	10 = 0.40 0.60 0.00	12 = 0

G. Groundwater pumping data from Honolulu Board of Water Supply

		Mak II-IV Pumping rate (mm)[1]
2005	January	0.03
	February	0.39
	March	0.66
	April	2.85
	May	4.03
	June	2.26
	July	5.57
	August	5.61
	September	1.57
	October	1.79
	November	0.47
	December	0.76
2006	January	0.37
	February	0.33
	March	0.08
	April	1.15
	May	3.41
	June	4.68
	July	6.83
	August	3.15
	September	1.56
	October	0.90

[1]Equivalent depth over the subwatershed